ROE'S SCHEME, EULER EQUATIONS, CARTESIAN GRIDS, NON-CARTESIAN GEOMETRIES, RIGID WALLS AND ALL THAT

A. Priestley

Numerical Analysis Report 14/87

The work reported here forms part of the research programme of the Reading/Oxford Institute for Computational Fluid Dynamics. The funding of the S.E.R.C. is gratefully acknowledged under contract no GR/D/29529.

Abstract

In this report a method of enforcing rigid wall boundary conditions is presented that uses a cartesian grid and thus avoids the need for body fitted meshes. Roe's scheme is used on the regular grid with a special technique for boundary conditions.

A number of test problems are tackled which show the approach to be reliable. The test problems presented are steady state problems and Roe's scheme, which is time-accurate, is used to converge to steady state. There is a brief discussion on time-acceleration techniques to improve the convergence.

1. INTRODUCTION

In this report we shall consider the application of Roe's scheme to the Euler equations in more than one dimension. We shall not bore the reader here with details of the scheme, other than recalling that it is an upwind scheme based on characteristics, safe in the knowledge that this is done elsewhere, see Roe (1981), Glaister (1986) and for a recent account Priestley (1987). Of prime concern here will be the imposition of rigid wall boundary conditions along, for example, a curving aerofoil or perhaps an irregular stretch of coastline in the case of the shallow water equations.

Roe's scheme is essentially one-dimensional in nature in that it is based on an approximate one-dimensional Riemann solver. Attempts to solve two-dimensional problems with these methods have relied upon regarding the two-dimensional problem as two one-dimensional problems and then using the 1-D scheme individually on both problems using some form of splitting, see e.g. Strang (1968), Barley (1987). Whichever of the procedures is preferred, a rectangular 2-D mesh of grid points is required. It is also possible to consider 'genuine' 2-D upwind schemes, see Smolarkiewicz (1984) for example, but with the extra calculation and housekeeping needed when an irregular mesh is needed it is debatable whether the modest increase in flexibility that this allows is worth the cost.

In the next section the possible approaches to the problem of creating and using a mesh in this context will be discussed. The fors and againsts of working in transformed space, using a body fitted mesh in physical space or using a cartesian grid in physical space will be considered. In Section 3 the difficulty of having curved boundaries while trying to use the latter type of mesh will be attacked. In the next section, Section 4, two test problems will be discussed and results presented that indicate that the solution has not been sabotaged by our unfashionable choice of mesh.

Methods of speeding up the convergence to steady state will also be discussed. Finally in Section 5 some tentative conclusions will be drawn and some suggestions made for further work.

2. THE ALTERNATIVES

2.1 Transformed Space

2.1e Conformal Mappings

Schwarz - Christoffel transformations and the hodograph transformations are very nice when they work, but are limited to 2-D. Three-dimensions can, however, be tackled by slicing the domain into a series of two-dimensional problems with the transformation being applied to each separately. This is not an entirely satisfactory procedure, though, and can lead to a lack of smoothness in the resulting grid, see Thompson et al (1985).

2.1b Body Fitted Co-ordinates

Perhaps, in some ways, this is the most satisfying of the three methods considered here, The whole domain is transformed, although not necessarily with a single transformation, so that the irregular body is now very much a regular body in (ξ,η) space, the transormed co-ordinates. That is, in (ξ,η) the rigid wall boundary lies along lines of constant ξ and/or constant η . The imposition of the reflecting boundary condition is now a simple affair being purely one-dimensional in nature, see Figure 1.

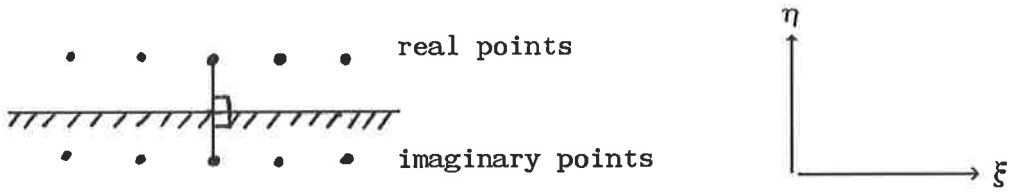

Figure 1.

In this particular case the ξ component of velocity would be taken equal at the imaginary point and the η component equal and opposite.

Transormations have been used since time immemorial but more recently Sells (1980) used transformations to calculate flows around the NACA0012 aerofoil that we shall discuss later, although he did use slightly different schemes. Glaister (1987a) transformed a circular cylinder using in fact precisely the schemes we shall use here for calculating the flow.

Unfortunately, as with most things in life, there is a price to pay. Apart from the two one-off calcuations required at the start to generate the transformations and at the end to transfer the results back to physical space, which can largely be overlooked, at each time-step at every point new equations will need to be solved, and it is fair to say that these will be considerably more complicated and in some cases may involve the introduction of source terms. Roe (1986), Glaister (1987), Priestley (1987) have shown that these source/forcing terms can be adequately dealt with within the framework of the method but again it

introduces extra computation throughout the calculation. There is, of course, more 'houskeeping' involved in storing the details of the transformation, although this is in part negated by the fact that we can use a perfectly uniform square mesh.

We could use the same grid generation techniques but work with them in physical space as in 2.2a.

2.2 Physical Space

2.2a Body Fitted Co-ordinates

Apart from being aesthetically very pleasing this approach has little to recommend it if a characteristic based scheme has been chosen. The fluxes across cell interfaces can be calculated fairly straightforwardly but the real problem is in determining where to send the updates. To gain any accuracy from the effort involved it would also be necessary to feature fit the grid. This has been done very successfully by Paisley (1986), with a rather different method, for a 2-D aerofoil with a single attached shock. However, for a 3-D calculation around a complex body it is hard to see that a body plus feature fitted grid would have much of a saving over one of the fully adaptive mesh techniques. It would also be very difficult to produce a mesh that adequately matched all the conflicting requirements on a complex geometry. The real advantage of a body fitted grid would come at the rigid wall type boundary of the body.

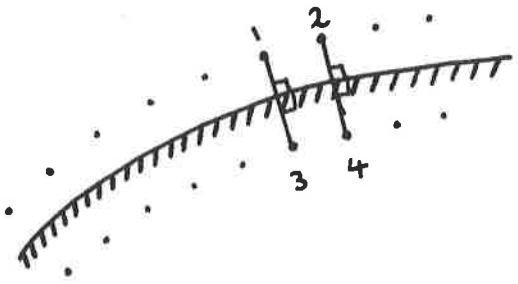

Figure 2.

Due to the use of the body fitted mesh it would be relatively straightforward to arrange our 'imaginary' points as shown and hence the updating of the values at these imaginary points is simply $\underline{u}_3 = \underline{u}_1$ and $\underline{u}_4 = \underline{u}_2$, except of course for velocities which have to be resolved into normal and tangential components, with the normal component being equal and opposite across the boundary while the tangential component is the same across the rigid wall.

2.2b Cartesian Grids

The benefits of a cartesian grid are obvious:- our scheme can be used per se on the unmolested equations and housekeeping is kept to a minimum. The grid can also be packed in close to the body if desired by using an irregular mesh. Also using a 3-D cartesian grid is only marginally more difficult than the 2-D version whereas the other methods have special problems when moving to three dimensions.

The benefits are obvious, but so are the snags. The difficulty

with cartesian grids, for a fairly general body is how to cope with a rigid wall boundary that does not align itself with either of the co-ordinate directions, as in Figure 3.

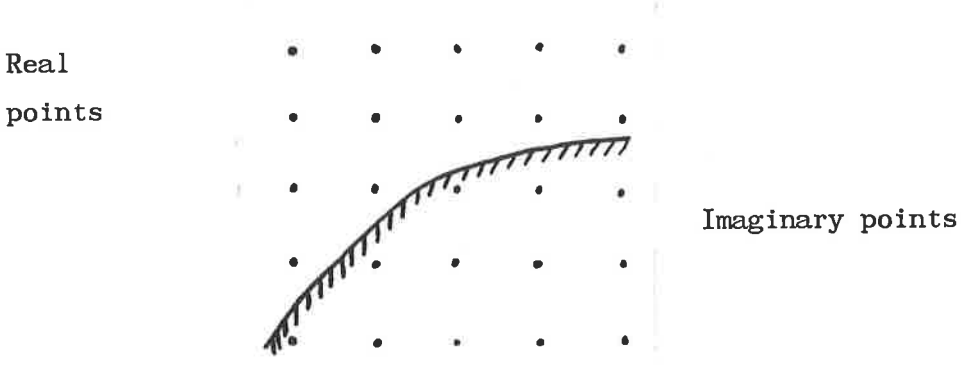

Figure 3.

Here the boundary is curved and the problem lies in how to update the 'imaginary' points (in this case below the line) after each time-step in order to be able to apply the scheme throughout the grid.

In the next few sections a simple way of overcoming the problems at the boundary will be discussed that is easily extendable to three dimensions, and proved on some test problems. At the moment the procedure limits us to the use of the basic first order Roe's scheme at the boundary but this is shown not to degrade the solution on the test problem even though one of the second order Roe type methods is being used away from the boundary.

3. Rigid Wall Boundary Conditions

Consider a patch of the grid, much as in Figure 3, through which the rigid wall cuts.

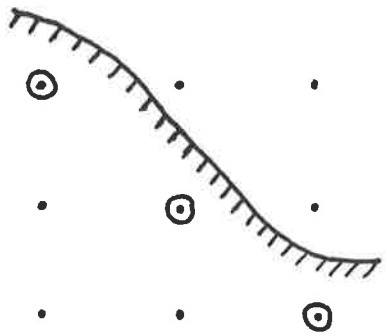

Figure 4.

It is the circled points that we are considering now. Since we are restricting ourselves to a first order scheme around the boundary, other points below the surface can only affect points like themselves, and are hence of equally little interest, or circled points which will be overwritten with values from the external flow at the end of the time-step. Hence these points do not need updating and can be ignored.

Figure 5 represents an enlargement of the top righthand part of the grid in Figure 4. The rigid wall has been replaced locally by a straight line.

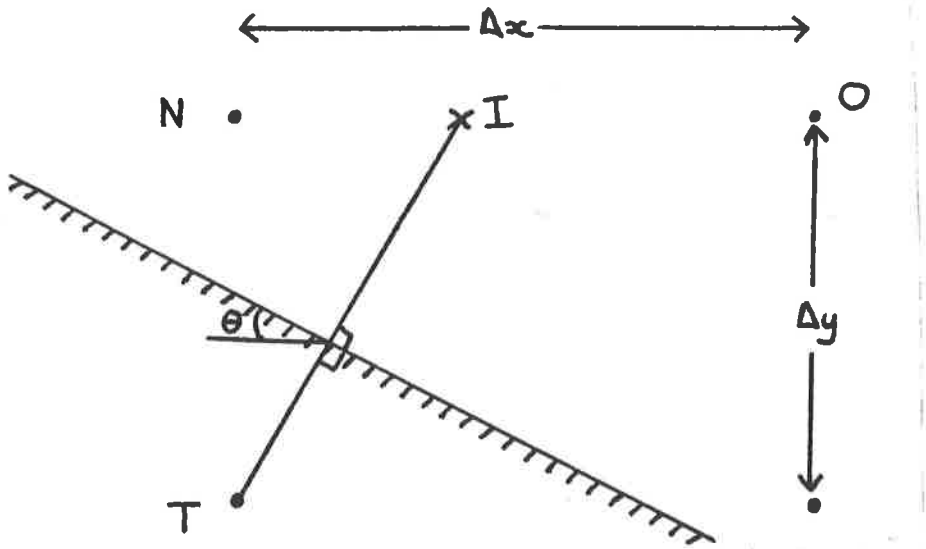

Figure 5.

Given the intercept of the rigid wall, the line joining T and N and the angle θ, a point I on the line NO can be defined. Since the values of all the variables are known at both points N and O then we can obtain values for the variables at I just by using linear extrapolation. This gives us the values (u_I, v_I, ρ_I, p_I) where the obvious notation has been used. Assuming no curvature at the boundary we can quickly obtain the values of density and pressure at T as $\rho_T = \rho_I$ and $p_T = p_I$. If there is curvature, or we wish to imply a curvature, the value of the pressure must be modified.

The velocities need to be converted to normal and tangential components and this is done by multiplying $\begin{bmatrix} u_I \\ v_I \end{bmatrix}$ by the rotation matrix

$$R(Q) = \begin{bmatrix} \sin\theta & \cos\theta \\ \cos\theta & -\sin\theta \end{bmatrix}, \qquad (3.1)$$

hence

$$\begin{bmatrix} q_{normal} \\ q_{tang} \end{bmatrix}_I = R(\theta) \begin{bmatrix} u \\ v \end{bmatrix}_I . \tag{3.2}$$

The tangential component at T equals the tangential component at I . The normal component at T must be chosen so that if the variable is linearly extrapolated between T and I it vanishes at the rigid wall. If we define another matrix $V(x,\theta)$, where x is the intercept on TN , then

$$\begin{bmatrix} q_{\ Norm} \\ q_{\ Tang} \end{bmatrix}_T = V(x,\theta)R(\theta) \begin{bmatrix} u \\ v \end{bmatrix}_I , \tag{3.3}$$

with

$$V = \begin{bmatrix} \alpha(x,\theta) & 0 \\ 0 & 1 \end{bmatrix} .$$

The function $\alpha(x,\theta)$ is the formula for calculating q_{norm} , T to accomplish the vanishing at the boundary.

To return to cartesian co-ordinates just requires the multiplication of (3.3) by $R(\theta)^{-1}$, and so we finally have

$$\begin{bmatrix} u \\ v \end{bmatrix}_N = R(\theta)^{-1} V(x,\theta) R(\theta) \begin{bmatrix} u \\ v \end{bmatrix}_I . \qquad (3.4)$$

If the positioning of points in Figure 5 is altered by a rotation of ψ degrees ($\psi = 0^o, 90^o, 180^o, 270^o$) then the formula just becomes

$$\begin{bmatrix} u \\ v \end{bmatrix}_N = R(360-\psi) R(\theta)^{-1} V R(\theta) R(\psi) \begin{bmatrix} u \\ v \end{bmatrix}_I . \qquad (3.5)$$

This is the final formula and we have now obtained values of the four variables u,v, $Gr.\rho$ and p at the imaginary point. Energy, momentums and enthalpy can then also be derived as required.

The only other variation is if the point 0 and the unmarked point lie to the left of TN instead of the right. This cannot be considered just as a reflection because the senses of u and v remain unaltered. However, an equation entirely similar to (3.5) can be derived for this case.

In practice it has been found advisable to overwrite the value of the intercept, x , with 0.5 . This does not affect the position of the point I and hence does not affect the density, pressure or tangential velocity. However, if the intercept is close to either end point (i.e. 0 or 1) then a modest value of the normal velocity at I can be translated into an enormous (and of the opposite sign) value at T . This leads to much larger momentums and energy values than would be expected and leads to problems at the boundaries. Assuming the

intercept to be at 0.5 does not appear to degrade the solution even when the grid has not been especially refined around the body.

We can see the problems involved by considering the model inviscid Burgers' equation

$$u_t + uu_x = 0 \tag{3.6}$$

on $[0,\infty)$. The boundary at $x = 0$ is a rigid wall. The initial conditions are

$$\left.\begin{aligned} u(x) &= 1 \quad \text{if} \quad x > 0 \\ u(x) &= 0 \quad \text{if} \quad x = 0 \end{aligned}\right\} . \tag{3.7}$$

If we assume a uniform mesh and our wall cuts the mesh a distance $\alpha\Delta x$, $\alpha\epsilon(0,1)$, from the first internal point then the value at the imaginary point will be $(\alpha-1)/\alpha$. Calculating the update due to the boundary between the cells centred on the imaginary point and the first internal point leads to a flux of

$$0 \quad \text{or} \quad -\frac{\Delta t}{\Delta x}\left[1 - \frac{1}{4\alpha}\right]$$

according to whether

$$\min\left[-1\ ,\ 1-\frac{1}{2\alpha}\right] = 1-\frac{1}{2\alpha} \text{ or } -1\ .$$

$\left[1-\frac{1}{2\alpha}\right.$ is the eigenvalue at the discontinuity at $x = 0$ i.e.

$1-\frac{1}{2\alpha} = \frac{1}{2}\left[1+(1-\frac{1}{\alpha})\right]\Big]$. The correct flux should be $\frac{-\Delta t}{2\Delta x}$. If

$1-\frac{1}{2\alpha} < -1$ i.e. $\alpha < \frac{1}{4}$ then nothing happens. If $\frac{1}{4} < \alpha < \frac{1}{2}$ then we do not subtract enough from the internal cell and hence it has too high a value. For $\frac{1}{2} < \alpha < 1$ we subtract too much and it takes on a value too low. Only for $\alpha = \frac{1}{2}$ do we make the correct contribution.

4. TEST PROBLEMS

In this section two problems are considered that show the flexibility and robustness of the approach that has been suggested in the previous sections and highlight one or two possible difficulties and how they may be overcome. The first consists of a Mach 3 flow in a wind tunnel around a blunt, shuttle-like, body. The geometry can be seen in any of the figures 6-19. This problem was chosen because the supersonic inflow/outflow means that all/no variables are prescribed. The rigid walls of the wind tunnels are aligned with the mesh and hence present no problems. The only possible difficulty from the imposition of boundary conditions will occur around the body in the interior.

A square mesh is used of (70 x 100). A good many of these fall inside the body of course and hence we do not need to calculate updates at all 7000 points. The grid has been deliberately kept uniform to show that the rigid wall boundary conditions along the non-aligned section cope well even if the boundary is not that well defined. Indeed, along the whole of the 45^{o} slope and the semi-circle there are just 23 image points used. The solutions given are for angles of attack of -15^{o} , -10^{o} , -5^{o} , 0^{o} , 5^{o} , 10^{o} & 15^{o} with both the first order scheme and with the use of the second order minmod limiter. As can be seen, from

Figures 6-19 the solution is essentially the same for both methods. The strong bow shock is captured very successfully by both of the methods, with very little smearing even with the first order scheme. Apologies are made for the misplaced text on these pictures. The second order method does sharpen the shock slightly more than the first order method and the resolution of the Mach stem on the wind tunnel boundary is superior. The first order scheme has also been tried on a slightly different domain shown in Figures 20-26. The extra part of the non-aligned boundary is a 68^{o} slope which requires a further 5 boundary points to be defined.

Armed with this vindication of our approach a rather more down to earth example was then tried. That is flow around the NACA0012 aerofoil. The formula describing this aerofoil is given in the GAMM workshop paper (1986) together with results for certain farfield values. In the specifications for the problems involving this aerofoil it was suggested thart a grid of approximately 4000 points should be used so that results could be fairly compared. Although we have not been attempting the same test problems here we have tried to work within the same guidelines. Unfortunately, due to a slight miscalculation, just over 5000 points were actually used. If the reader can bring himself or herself to look at Figures 27 and 28 he/she will see that for simplicity a tensor product grid has been used. This leads to rather more work being done away from the body than is actually needed and it is

reasonably fair to say that all the results presented here could be reproduced on a 4000 point grid with no loss of accuracy.

From Figures 27 and 28 it can be seen that the mesh has been refined around the aerofoil so that its shape can be more accurately modelled and because the area immediately around the body is where the solution might be expected to be at its most interesting. There is however a problem with aerofoil type shapes that cannot be overcome by refinement. This occurs at the trailing edge. In Figure 29 the difficulty is depicted.

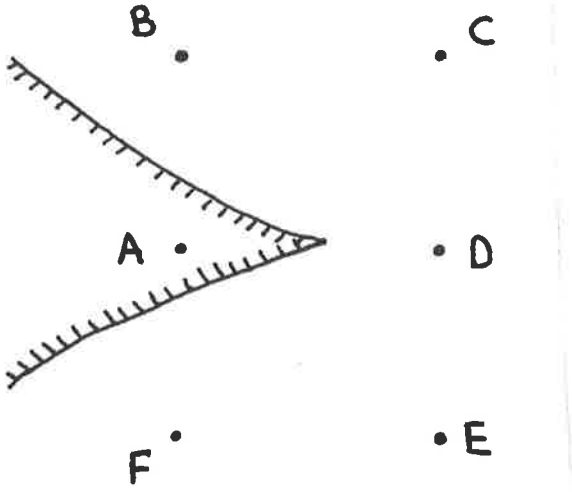

Figure 29.

Here the point A is an image point of both point B and point F . (In some situations it can also be regarded as an image point of D) . In general the points B and F will prescribe differing values upon A and hence defining A to have some sort of average value may be quite an approximation. The answer though is quite simple. Point A is given two values, one prescribed by point B the other by point F . When the updates between the cells F and A are being calculated the values $\underline{u}_F$ and $\underline{u}_{A_F}$ are used. When the updates due to the interface between the cells of point A and point B the values of $\underline{u}_{A_B}$ and $\underline{u}_B$ are used. For calculating the update between D and A we have simply used $\underline{u}_D$ and $\frac{1}{2}(\underline{u}_{A_F} + \underline{u}_{A_B})$.

Although this proved adequate for the use in our test problems here a rather more sophisticated approach would be to calculate analytically where the shear line from the trailing edge fell. If it fell below the shear line then we would take $\underline{u}_D = \underline{u}_{A_F}$ and if it fell above then we would use $\underline{u}_{A_B}$.

Figures 30-49 are results for a Mach 3 incident flow around our aerofoil with attack angles of 0^o , 5^o , 10^o , 15^o and 20^o respectively. The plots are density and entropy deviation contours and surface plots of pressure and entropy deviation. These problems are steady state (we assume!) and the solutions have been obtained in a time-accurate manner which is not the most efficient way of reaching the steady state. Hence, due to the restricted computing facilities

available to us, the solutions presented are not yet at the steady state, although they are hopefully well on the way. We note with satisfaction the sharp bow shocks on all the pictures and the zero lift with the 0^{o} angle of attack. The entropy along the body should be a constant, assuming no attached shocks, as the rigid wall of the aerofoil forms a streamline. As can be seen there is an increase in the entropy deviation at the leading face. This is not an unexpected phenomenon due to the sudden introduction of the body into a free flow and it is hoped that it may be controlled by using the 'leaky boundary' technique of Sells (1980). This may also provide a means for tackling problems with larger angles of attack where cavitation becomes a problem.

A Note on speeding up convergence

As has been mentioned, trying to reach a steady state flow in a time-accurate manner is not a particularly efficient means of going about it. One means of accelerating the convergence is to use a different time-step in each cell such that the maximum CFL number in that cell is equal to some predetermined maximum premitable value. Reading Sells (1980) one gets the impression that this procedure is somewhat delicate. This author tried a similar arrangement but allowed each wave in each cell to have a different time-step so that its CFL number took on the maximum value allowed. This was found to be exceedingly delicate; indeed no more than 6 time-steps were ever satisfactorily performed using this acceleration method. It is believed

that the problem is caused by having widely varying Δt's between cells (or in cells in the latter case).

To obtain a smoother variation of Δt it was therefore decided to use a different Δt for each of the u-a , u u+a characteristics. Typically a Δt was chosen for the u+a characteristics and then $3\Delta t/2$ and $2\Delta t$ were taken for the u , u-a characteristics. This procedure was found to work quite reliably. A second idea used here was based on the philosophy that much work is done, particularly with the meshes shown in Figures 27 and 28, in the farfield where very little is happening. Hence, a much smaller interior region just surrounding the aerofoil was chosen in which more 'time'-steps were done. As the solution in this inner region converged it was systematically enlarged.

Solutions obtained using both these techniques are shown in Figures 50-59. These show density and entropy deviation contours for varying numbers of 'time'-steps. The angle of attack was five degrees.

Another way in which it is hoped to speed up convergence and to improve the accuracy of the results is to use an adaptive mesh technique. The initial grid used is shown in Figure 60 for a brick type object. The grid has already been refined around the boundary. Figures 61 and 62 show the grid and density contours at a later time (obtained in a time-accurate fashion). The refinement of cells was based on the gradient of the density and obviously more than the one refinement used here would be done in practise. Figure 63 shows a possible initial grid generated for the NACA0012 aerofoil.

Unfortunately this work has now ceased due to the work of Roberts (1987) who has cast doubt on the use of Roe's scheme for steady state calculations, and not at all due to the fact that the present author had immense difficulty writing a boundary recognition routine sufficiently general to cope with the NACA0012 aerofoil as shown in Figure 63.

5. CONCLUSIONS

We have introduced a new approach for applying Roe type schemes to problems in two-dimensions that have rigid wall boundaries not aligned with the mesh. This approach has proved to be versatile, robust, accurate and very efficient. Perhaps more importantly it is relatively straightforward to extend the method to three-dimensions. As calculations proceed into ever more complex 3-D geometries cartesian meshes are bound to find more adherents.

By way of further work the time-acceleration techniques need to become more refined while the grid that automatically refines itself in areas of interest c.f. Babuska and Rheinboldt (1979) needs to be developed more fully.

It is hoped that the combination of these two ideas will lead to a very efficient and accurate application of Roe's scheme to steady Euler flows.

Together with the work on source/forcing terms reported by Priestley (1987) it is hoped we shall soon have a very effective means for calculating steady/unsteady hypersonic flows.

6. ACKNOWLEDGEMENTS

Thanks to Dr M J Baines for encouraging me to pursue this work. Thanks are also due to Dr P K Sweby and Mr P Glaister for useful discussions. Also to S Davis for the excellent typing.

7. REFERENCES

1. Babuska, I., Rheinboldt, W.C. 1979: Adaptive Approaches and Reliablity Estimations in Finite Element Analysis. Comp. Meth. Appl. Mech. Engng., 17/18, 519-540.

2. Barley, J.J., 1987: A Survey of Operator Splitting Applied to Upwind Differencing. University of Reading Numerical Analysis Report (to appear).

3. GAMM-Workshop, 1986: 2nd Announcement of the GAMM-Workshop on the Numerical Simulation of Compressible Euler Flows. INRIA, France.

4. Glaister. P., 1986: An Approximate Linearised Riemann Solver for the Euler Equations in One-Dimension with a General Equation of State. University of Reading Numerical Analysis Report 7/86.

5. Glaister, P., 1987a: A 2-D Compressible Solver Incorporating Body Fitted Co-ordinates. University of Reading Numerical Analysis Report 11/87 (to appear).

6. Glaister, P., 1987b; An approximate Riemann Solver for Compressible Flows with Axial Symmetry. University of Reading Numerical Analysis Report 2/87.

7. Paisley, M.F., 1986: Cell Vertex Methods and Shock Fitting for the Steady Euler Equations. Numerical Analysis Report 9/86, Computing Laboratory, University of Oxford.

8. Priestley, A., 1987: Roe Type Schemes for the 2-D Shallow Water Equations, University of Reading, Numerical Analysis Report 8/87.

9. Roberts, T., 1987: Private Communication.

10. Roe, P.L., 1981: Approximate Riemann Solvers, Parameter Vectors, and Difference Schems, Journal of Computational Physics, 43, 1981.

11. Roe, P.L., 1986: Upwind Differencing Schemes for Hyperbolic conservation Laws with Source Terms. Proc. 1st Int. Congress on Hyperbolic Problems, St. Etienne.

12. Sells, C.C.L., 1980: Solution of the Euler Equations for Transonic Flow Past a Lifting Aerofoil, R.A.E. Technical Report 80065.

13. Smolarkiewicz, P.K., 1984: A Fully Multidimensional Positive Definite Advection Transport Algorithm with Small Implicit Diffusion. Journal of Computational Physics, 54, 325-362.

14. Strang, G., 1968: On the Construction and Comparison of Difference Schemes. SIAM J. Numer. Anal., Vol. 5, No. 3.

15. Thompson, J.F., Warsi, Z.U.A., Mastin, C. W., 1985: Numerical Grid Generation Foundations and Applications. North-Holland.

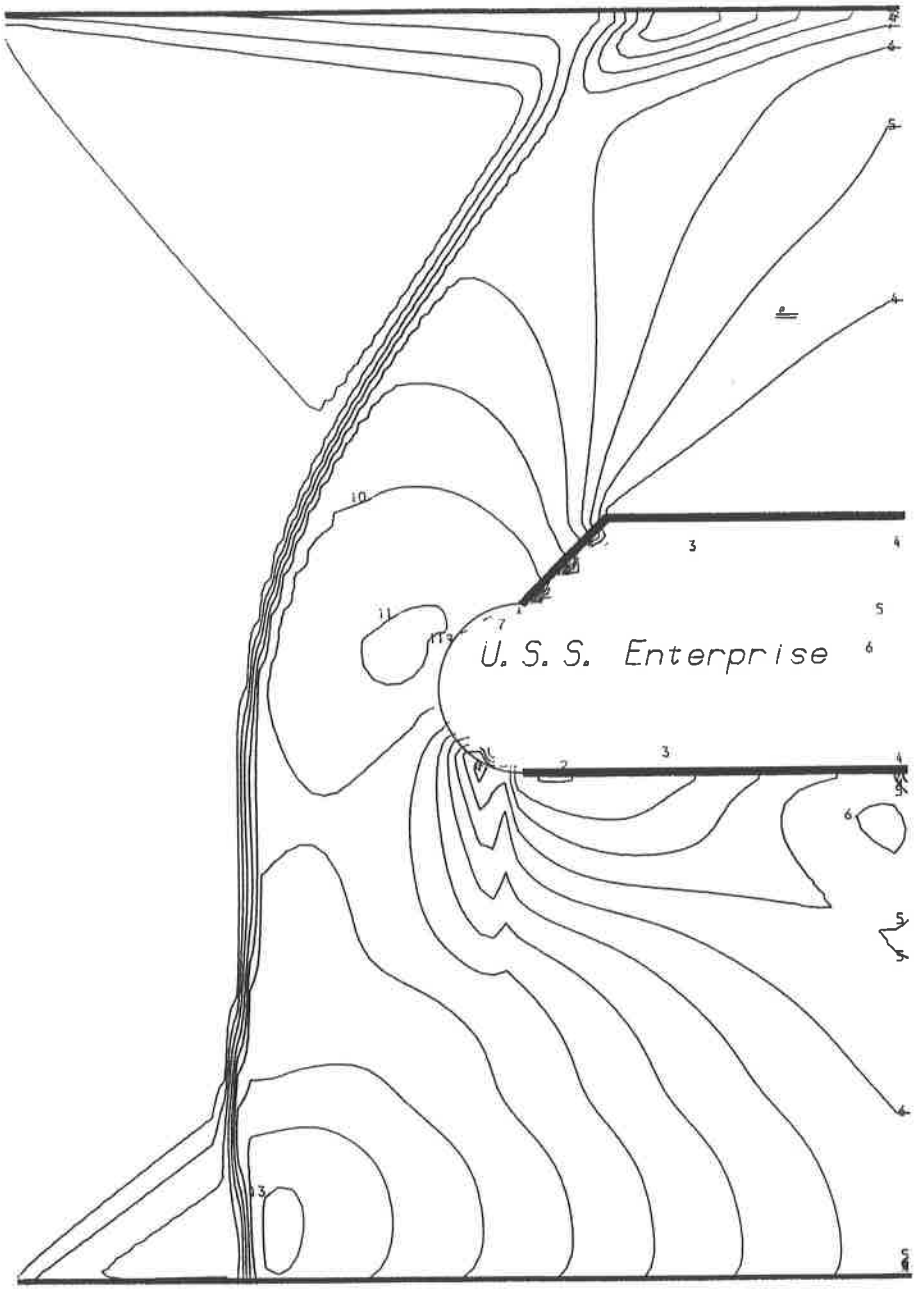

Mach 3 Flow Past a

Non-rectangular Body

Density at time T = 7.000.

Maximum density is 4.42.

Minimum density is 0.65.

First order method

Angle of attack is

-15.0 degrees.

Figure 6a

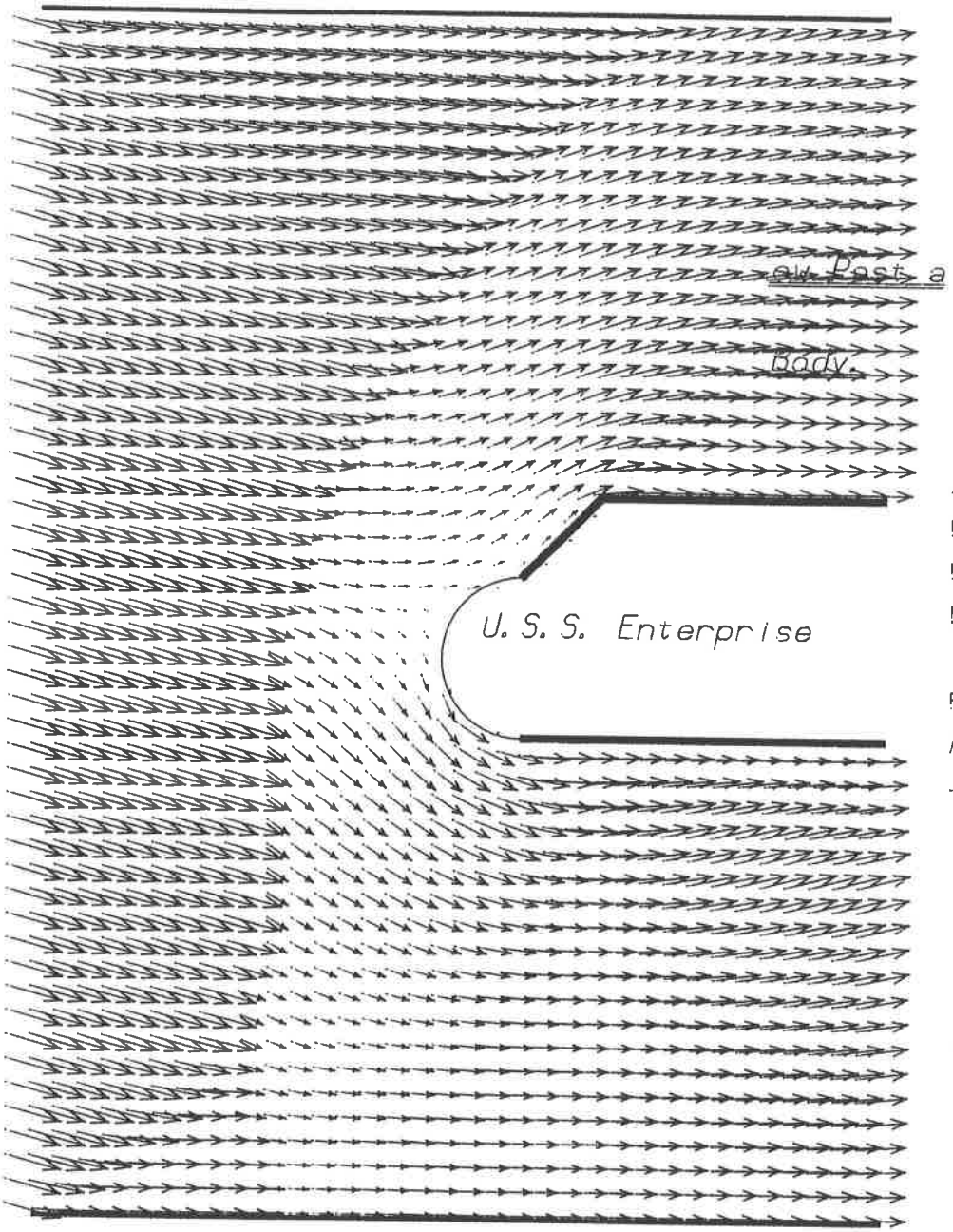
Mach 3 Fl
Non-rectangular
Body
U. S. S. Enterprise
Airflow at time T = 7.000.
Maximum flow velocity is 3.257.
Maximum CFL number is 0.480.
Dt/Dx = 0.10.
First order method
Angle of attack is
-15.0 degrees.

Figure 6b

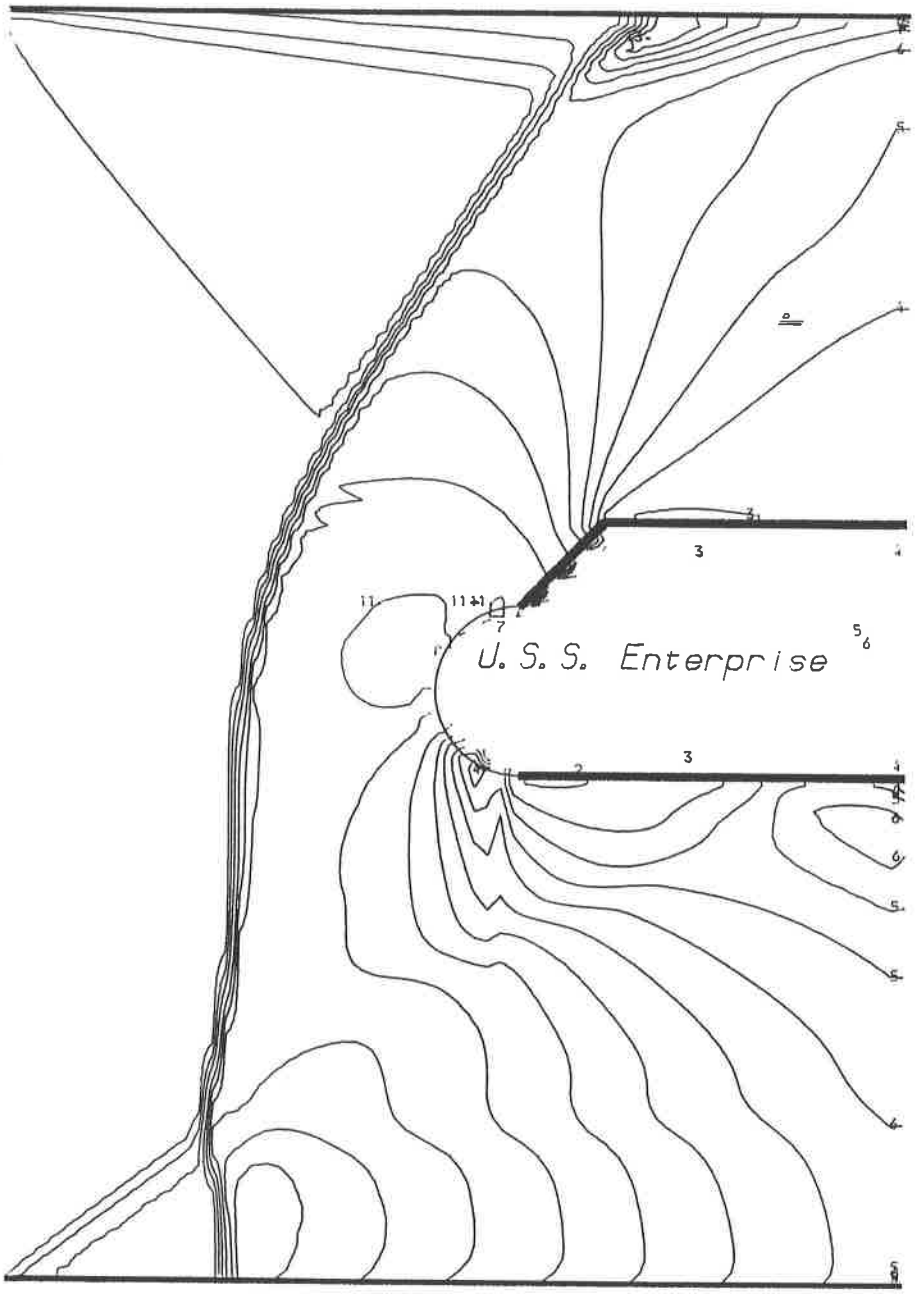

Mach 3 Flow Past a

Non-rectangular Body

Density at time T = 7.000.

Maximum density is 4.48.

Minimum density is 0.63.

Minmod

Angle of attack is

-15.0 degrees.

Figure 7a

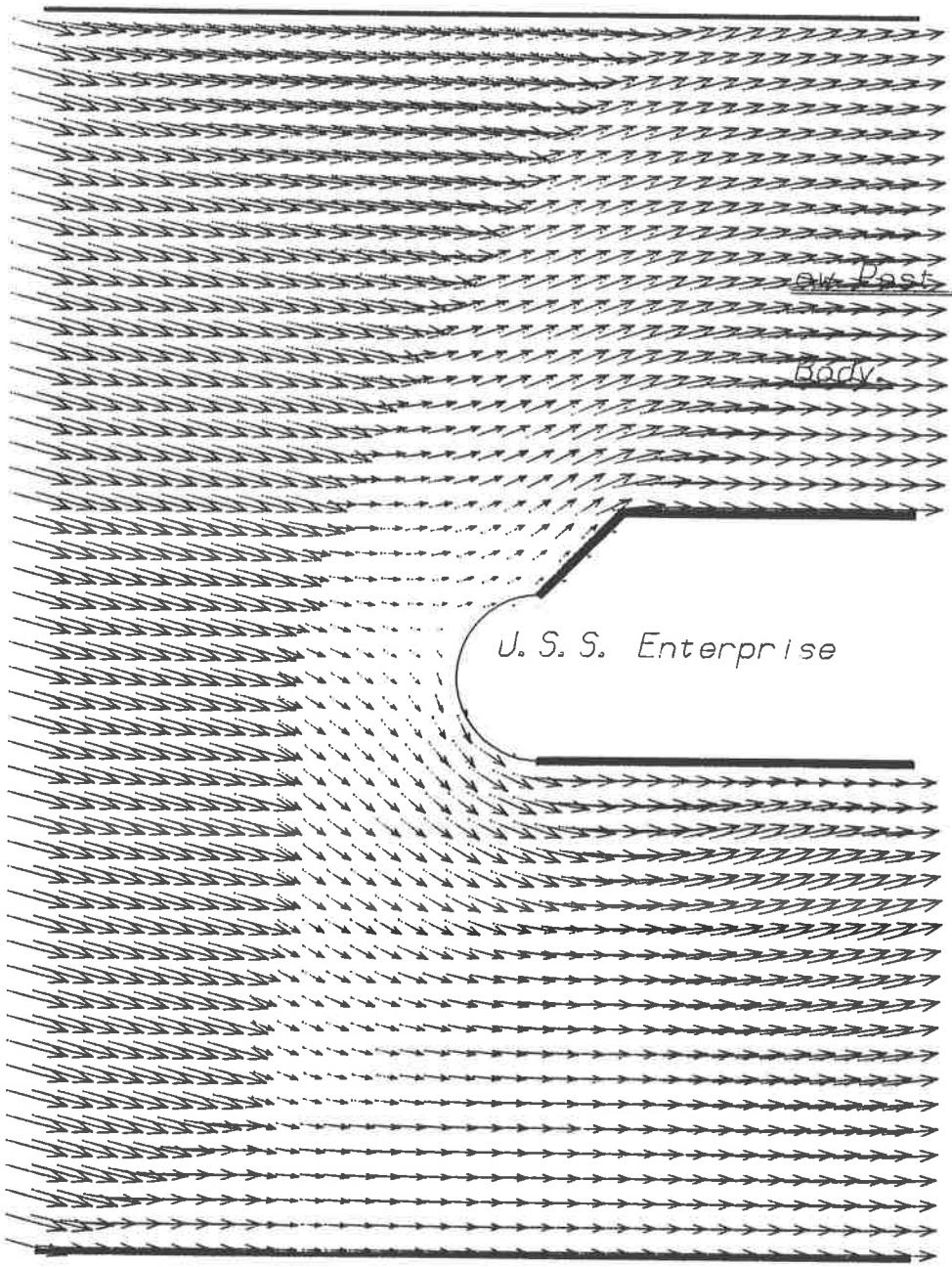

Mach 3 Fl

Non-rectangular

Airflow at time T = 7.000.
Maximum flow velocity is 3.258.
Maximum CFL number is 0.481.
Dt/Dx = 0.10.

Minmod
Angle of attack is
-15.0 degrees.

Figure 7b

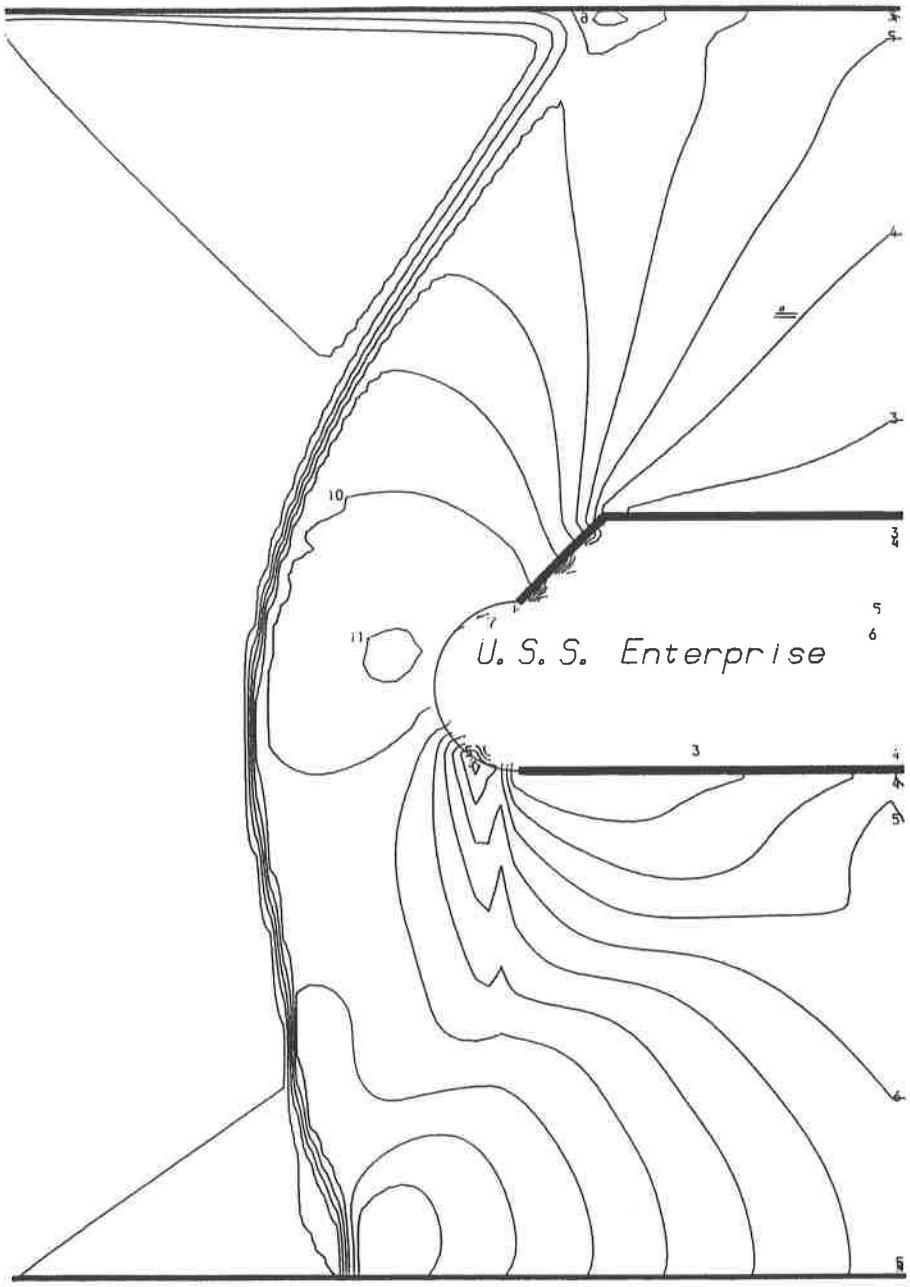

Mach 3 Flow Past a

Non-rectangular Body

Density at time T = 7.000.

Maximum density is 4.31.

Minimum density is 0.68.

First order method

Angle of attack is

-10.0 degrees.

Figure 8a

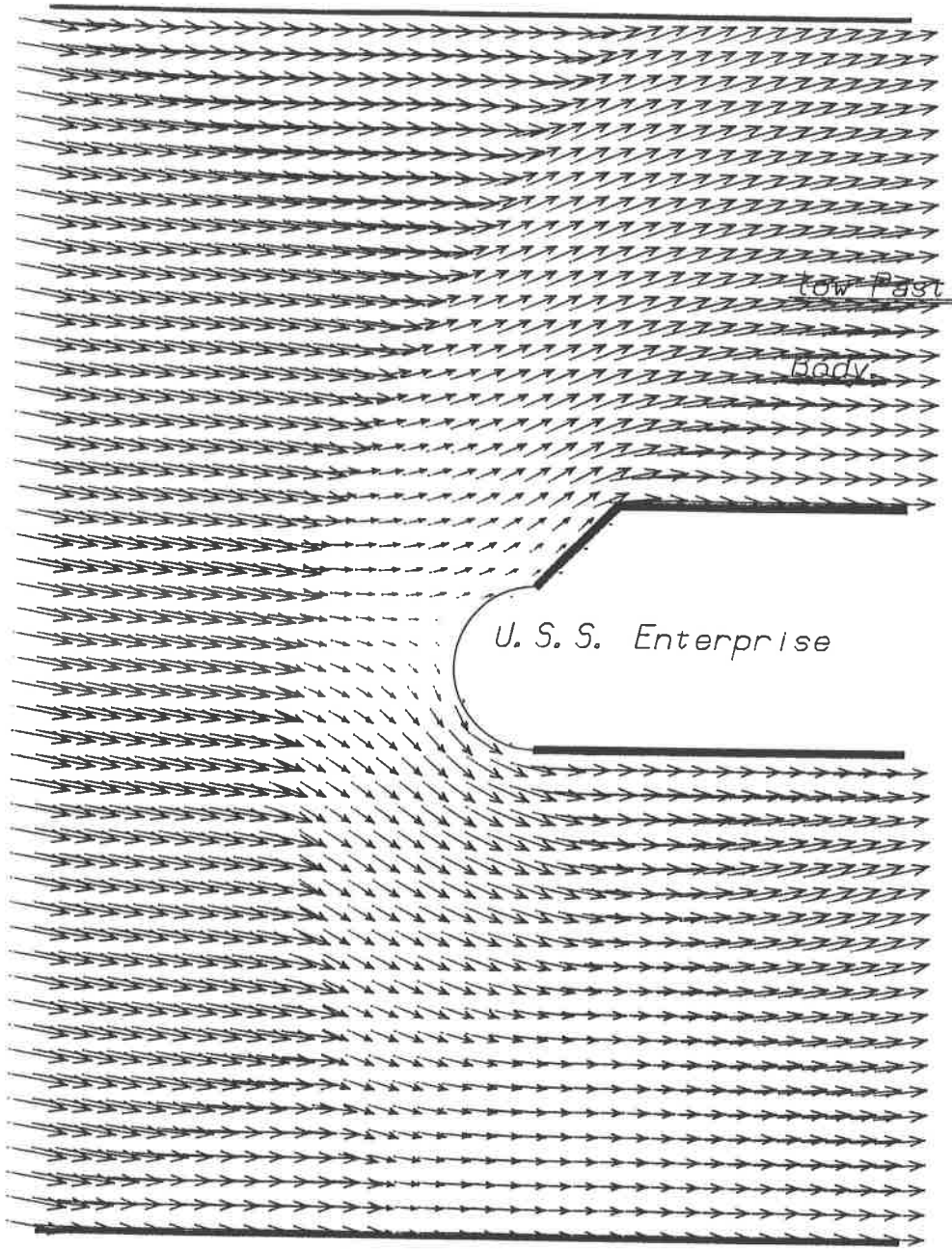

Mach 3 f

Non-rectangular

Airflow at time T = 7.000.
Maximum flow velocity is 3.259
Maximum CFL number is 0.483.
Dt/Dx = 0.10.

First order method
Angle of attack is
-10.0 degrees.

Figure 8b

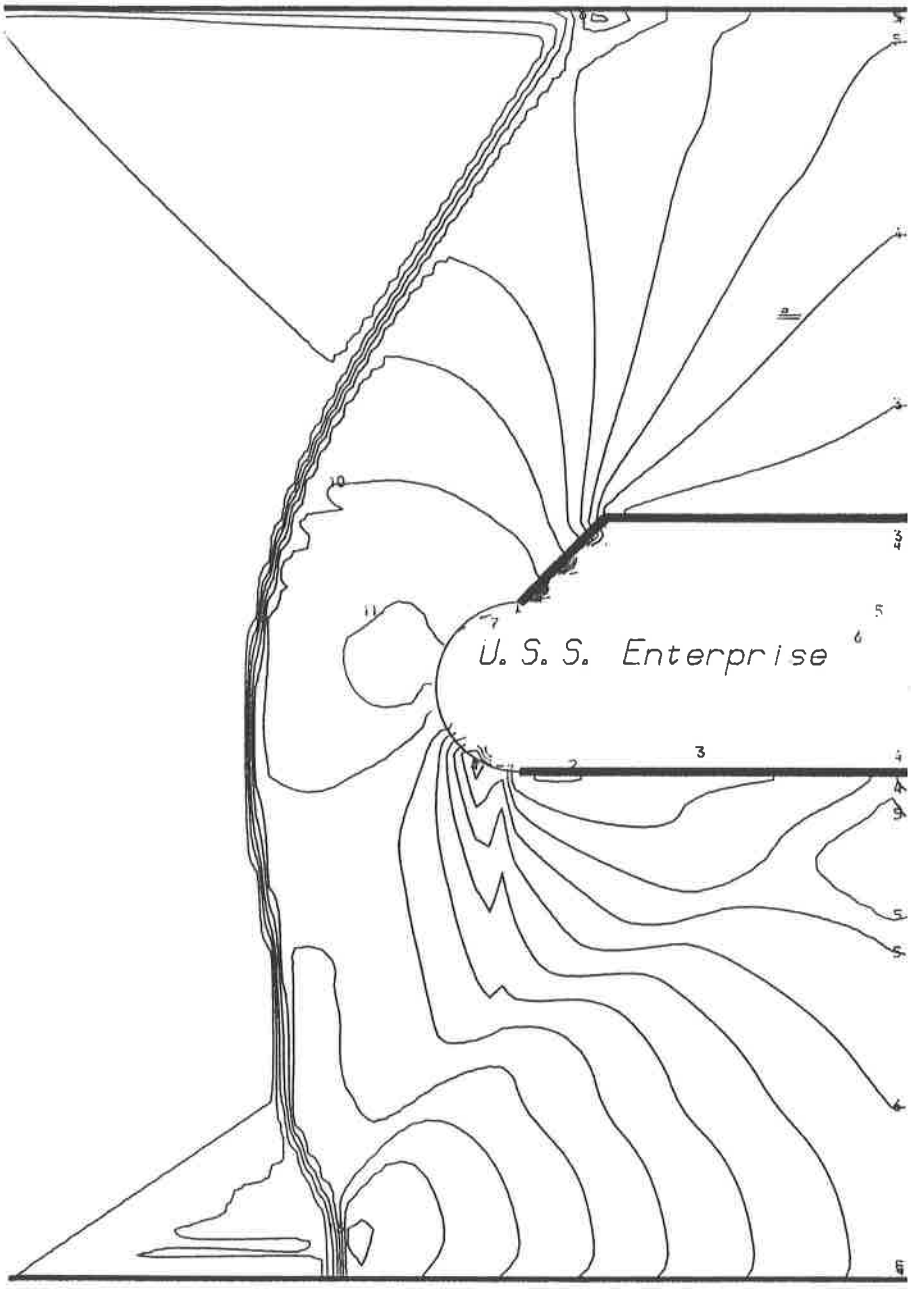

Mach 3 Flow Past a

Non-rectangular Body

Density at time T = 7.000.

Maximum density is 4.38.

Minimum density is 0.64.

Minmod

Angle of attack is

-10.0 degrees.

Figure 9a

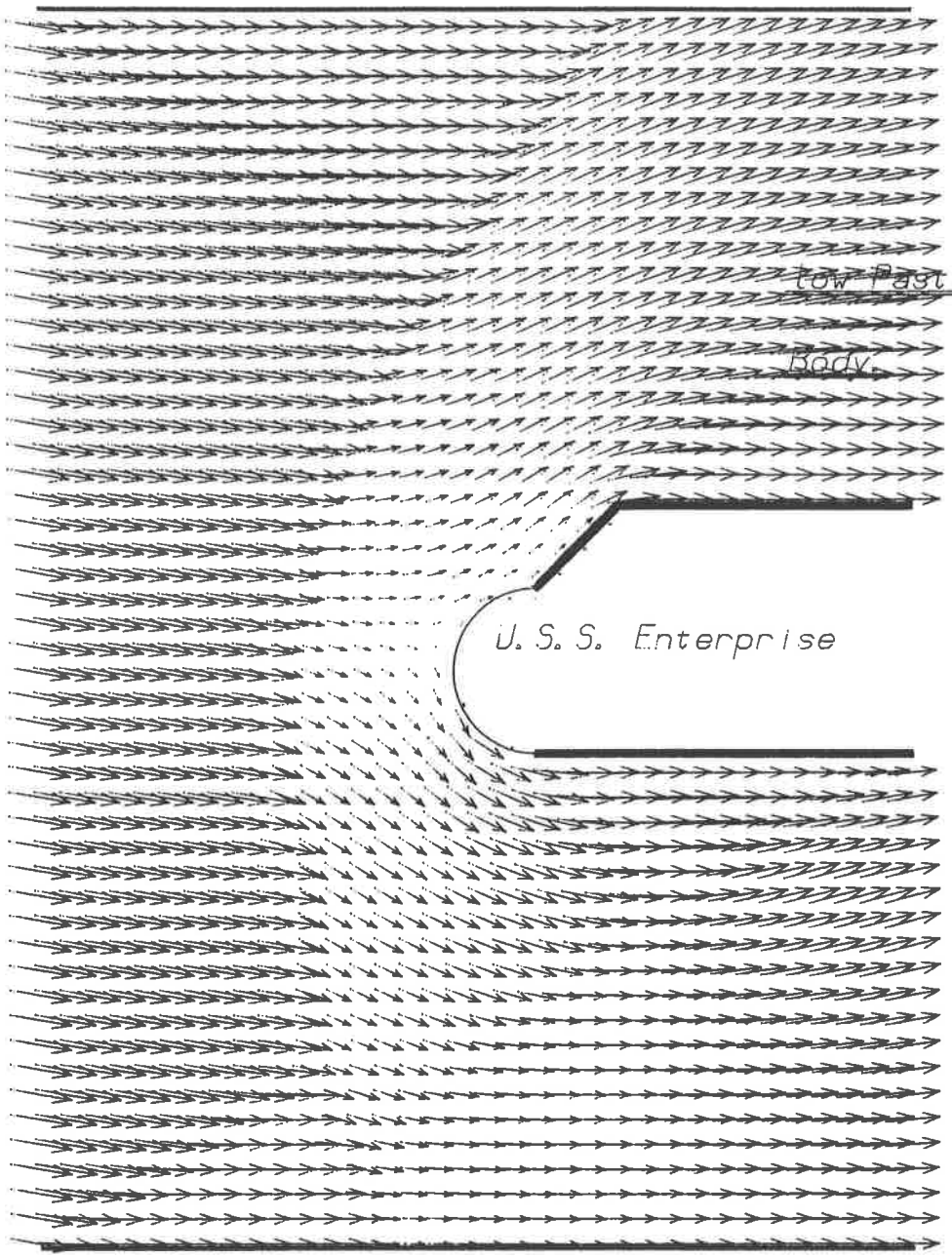
Mach 3 f
low Past a
Non-rectangular
Body
U. S. S. Enterprise
Airflow at time T = 7.000.
Maximum flow velocity is 3.269.
Maximum CFL number is 0.483.
Dt/Dx = 0.10.
Minmod
Angle of attack is
-10.0 degrees.

Figure 9b

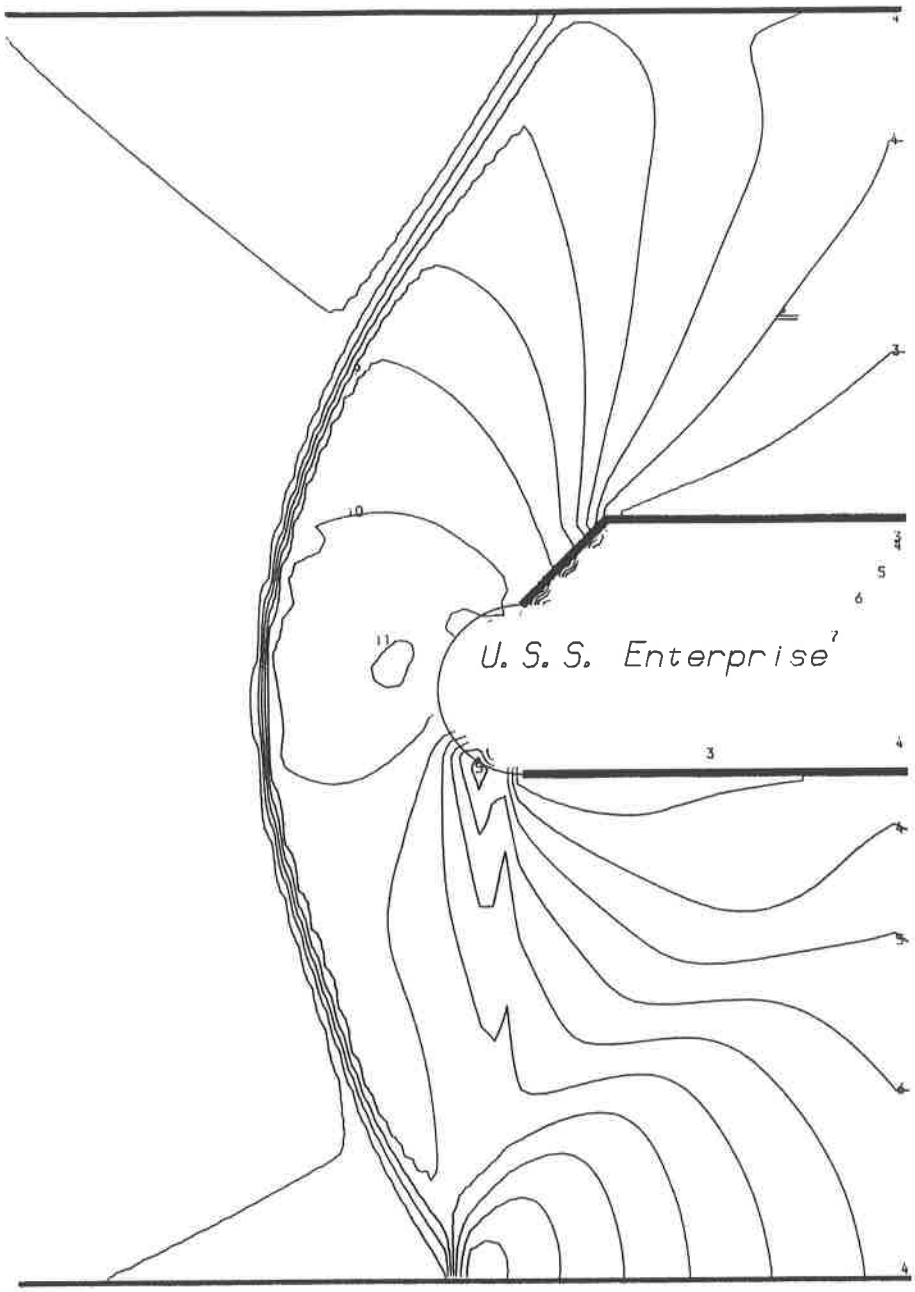

Mach 3 Flow Past a

Non-rectangular Body

Density at time T = 7.000.

Maximum density is 4.23.

Minimum density is 0.78.

First order method

Angle of attack is

-5.0 degrees.

Figure 10a

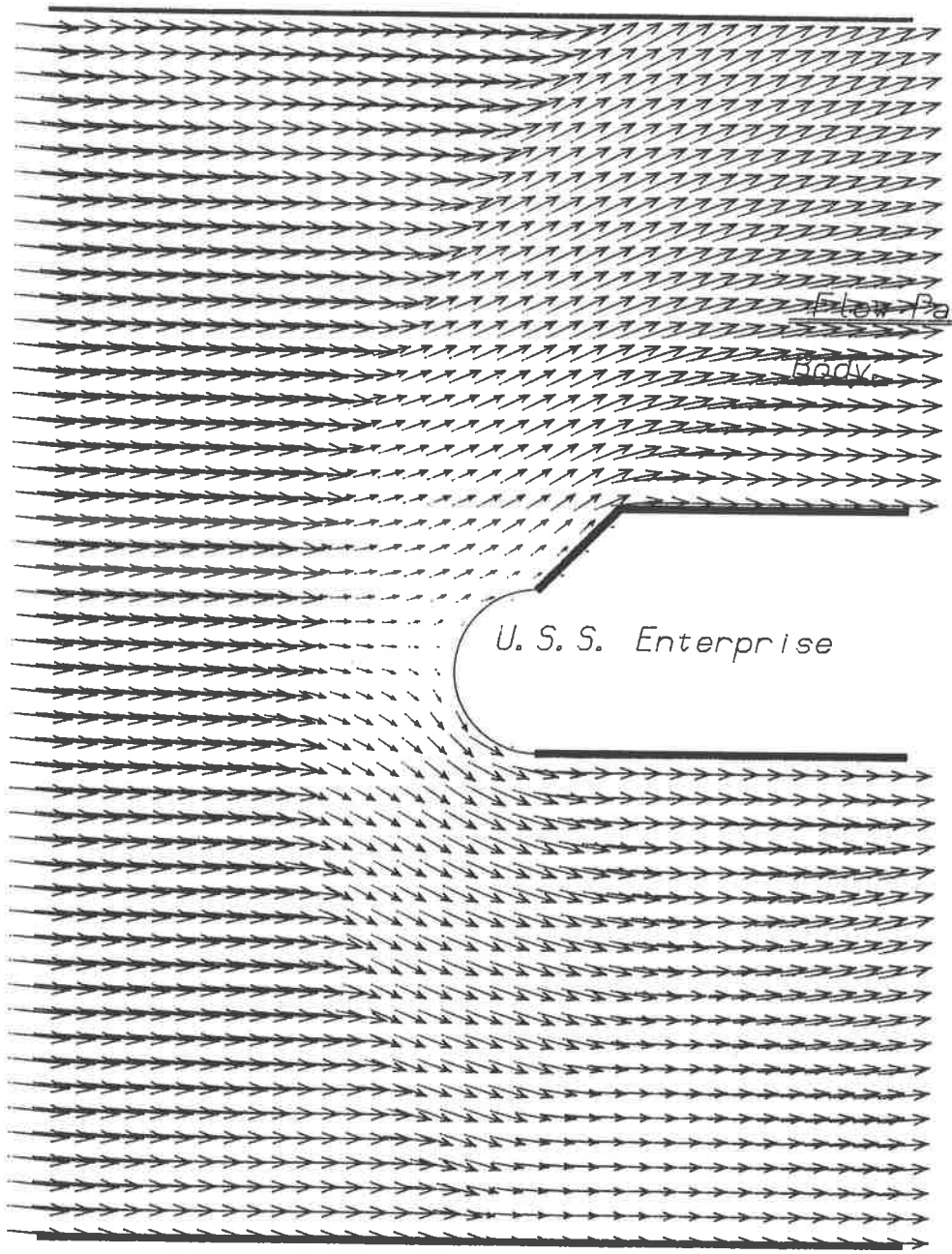
Flow Past a
Non-rectangular
Body.
Mach 3
U. S. S. Enterprise
Airflow at time T = 7.000.
Maximum flow velocity is 3.266.
Maximum CFL number is 0.483.
Dt/Dx = 0.10.
First order method
Angle of attack is
-5.0 degrees.

Figure 10b

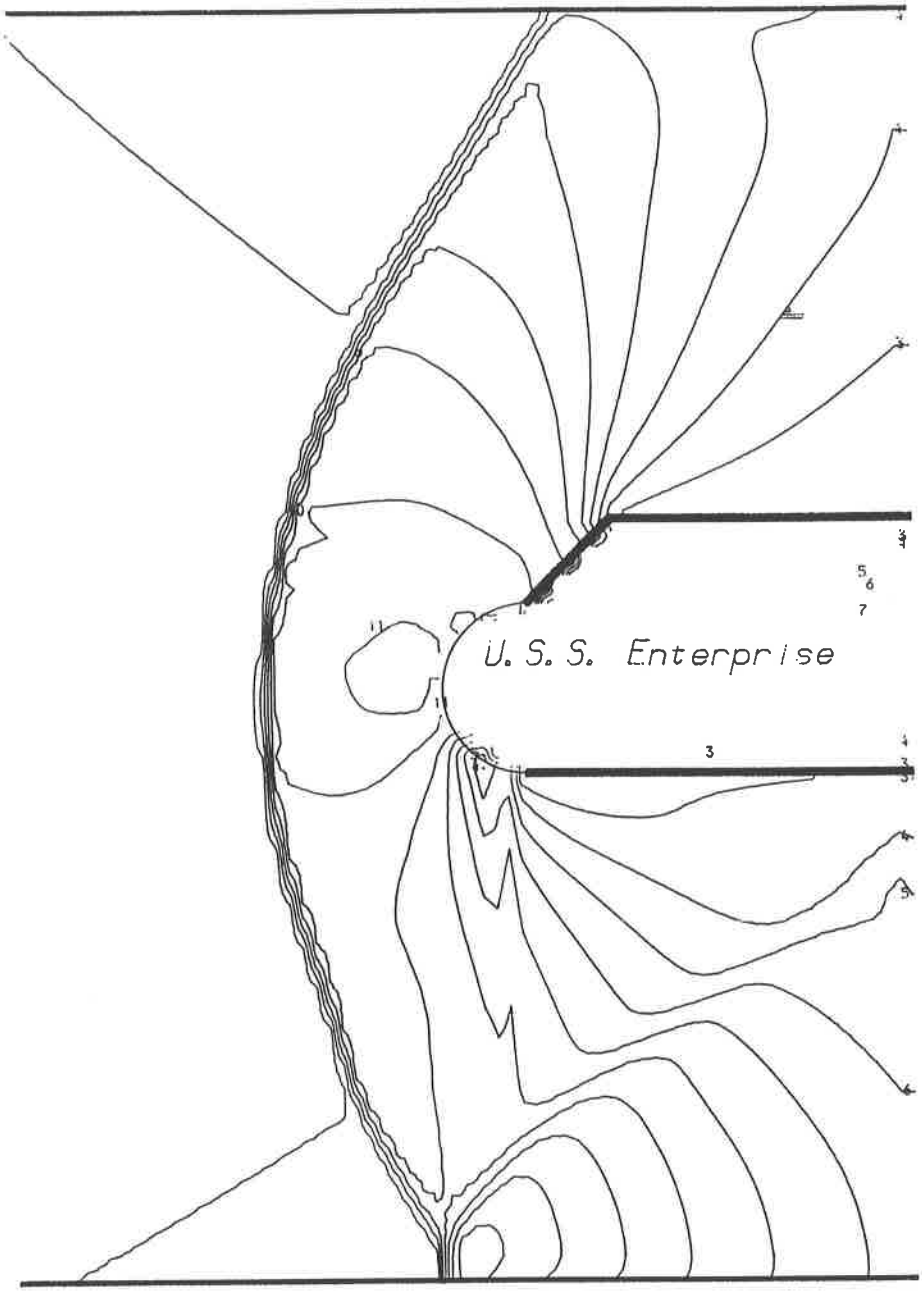

Mach 3 Flow Past a

Non-rectangular Body

Density at time T = 7.000.

Maximum density is 4.23.

Minimum density is 0.74.

Minmod

Angle of attack is

-5.0 degrees.

Figure IIa

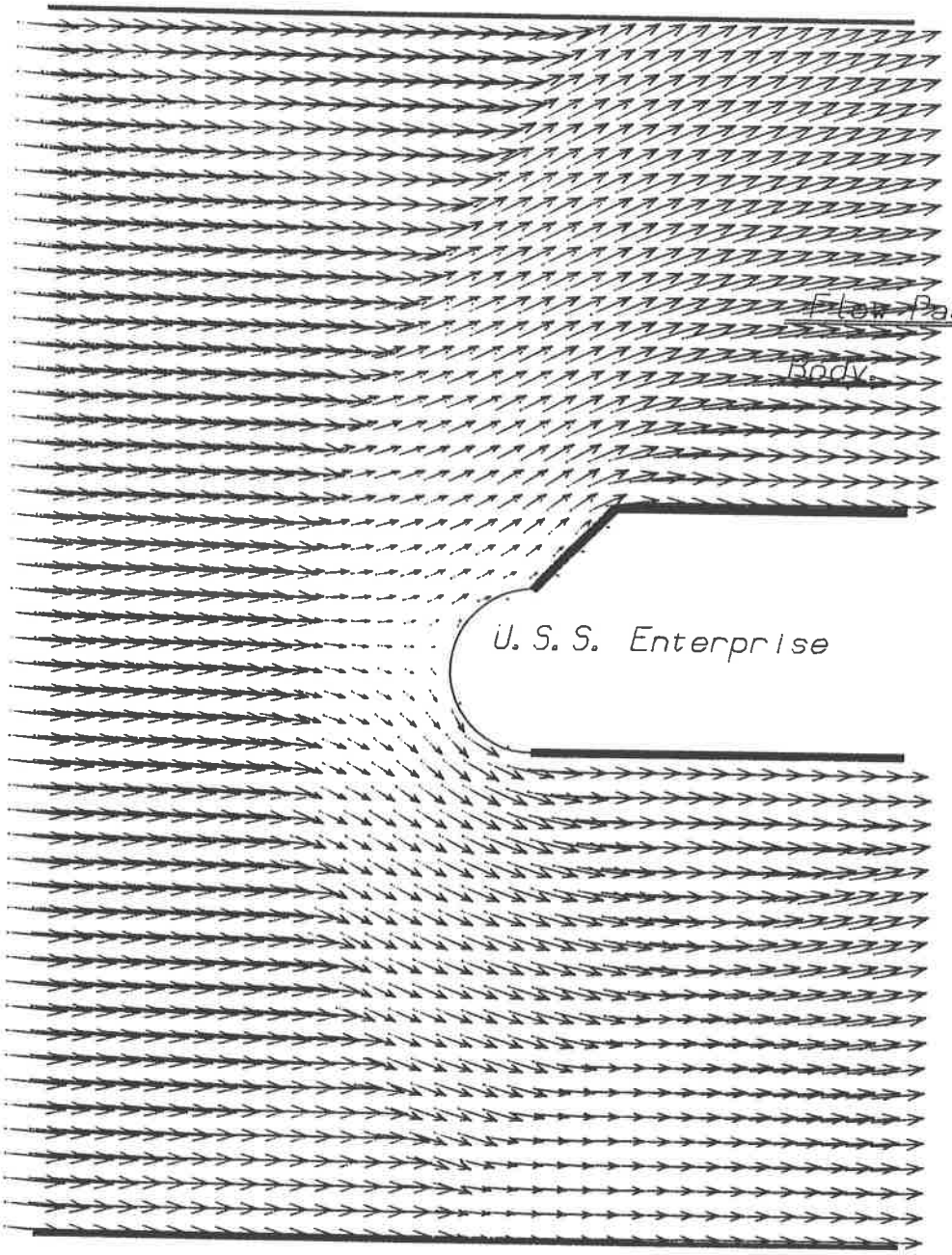
Mach 3
Flow Past a
Non-rectangular
Body
U. S. S. Enterprise
Airflow at time T = 7.000.
Maximum flow velocity is 3.268.
Maximum CFL number is 0.483.
Dt/Dx = 0.10.
Minmod
Angle of attack is
-5.0 degrees.

Figure 11b

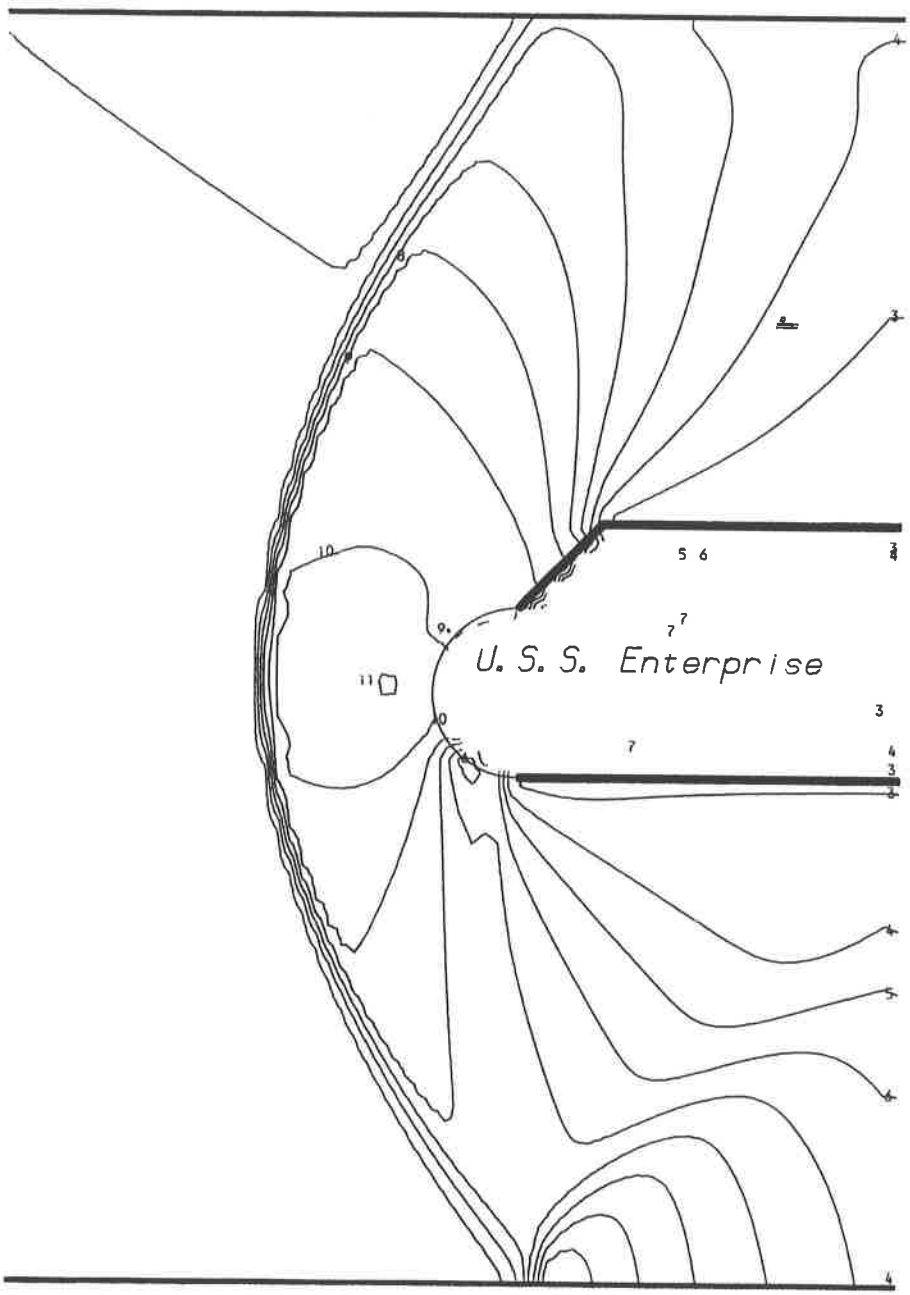

Mach 3 Flow Past a

Non-rectangular Body

Density at time T = 7.000.

Maximum density is 3.98.

Minimum density is 0.77.

First order method

Angle of attack is

0.0 degrees.

Figure 12a

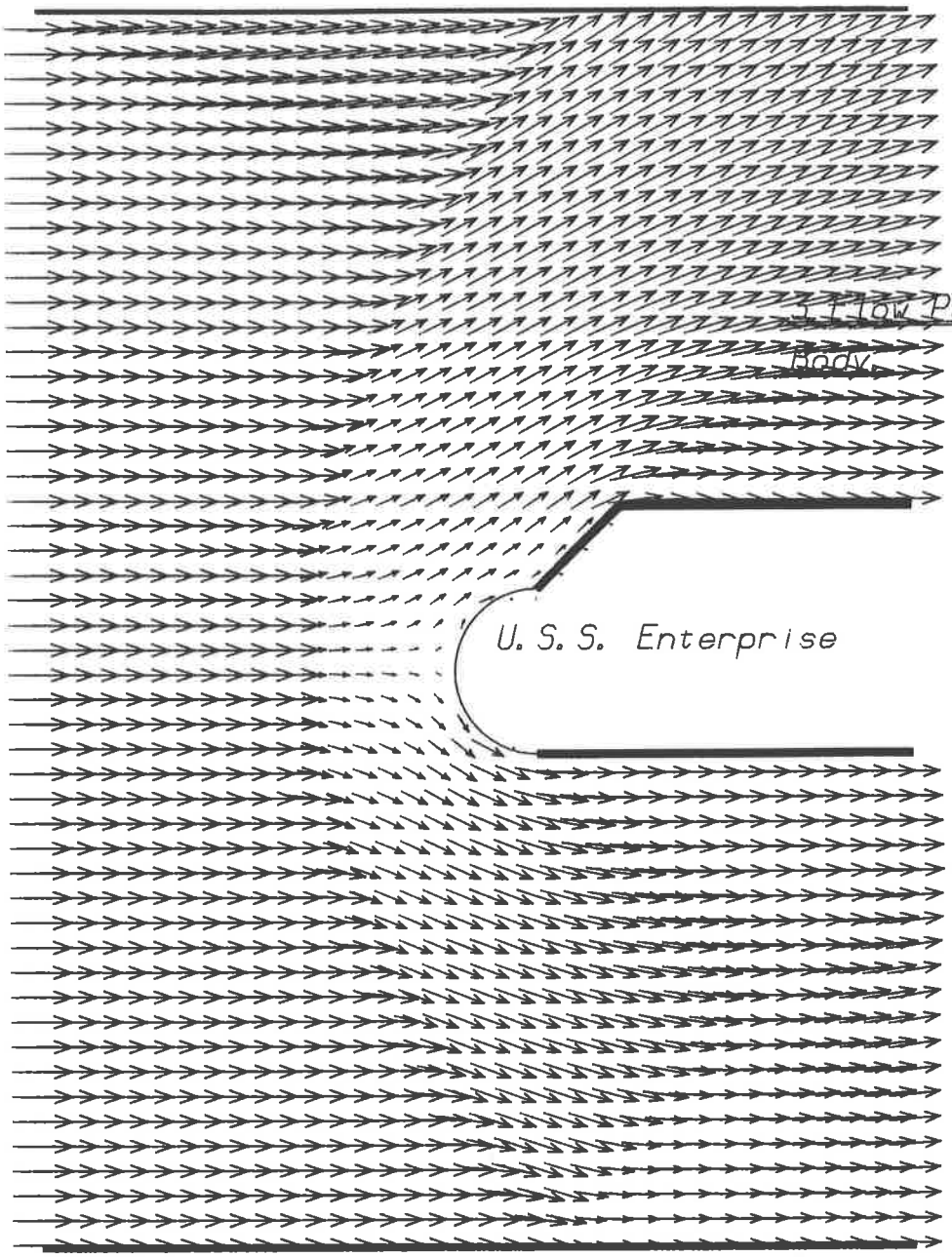
Mach
Flow Past a
Non-rectangular
Body.
Airflow at time T = 7.000.
Maximum flow velocity is 3.260.
Maximum CFL number is 0.482.
Dt/Dx = 0.10.
First order method
Angle of attack is
0.0 degrees.
U. S. S. Enterprise

Figure 12b

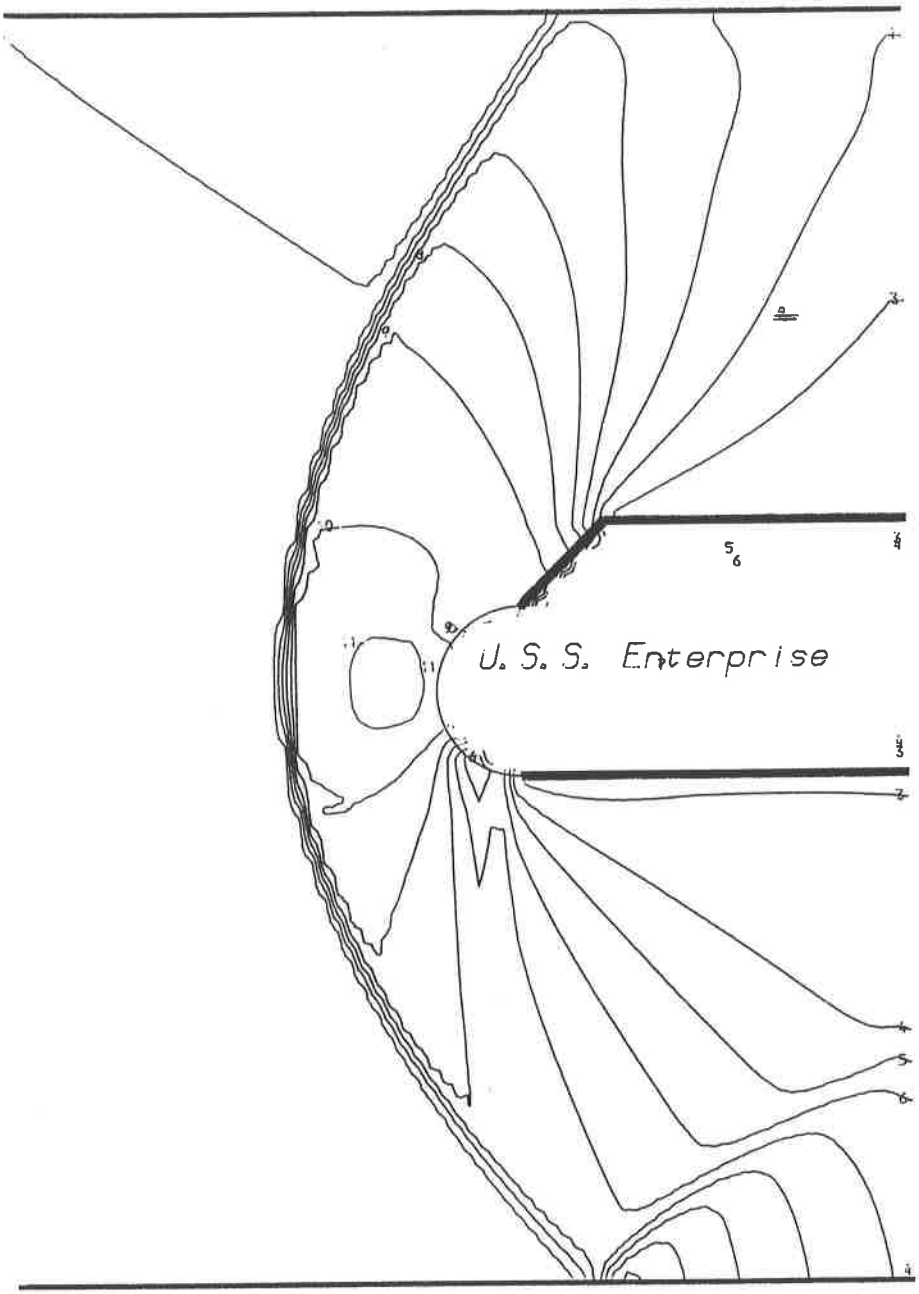

Mach 3 Flow Past a

Non-rectangular Body

Density at time T = 5.500.

Maximum density is 3.79.

Minimum density is 0.74.

Minmod

Angle of attack is

0.0 degrees.

Figure 13a

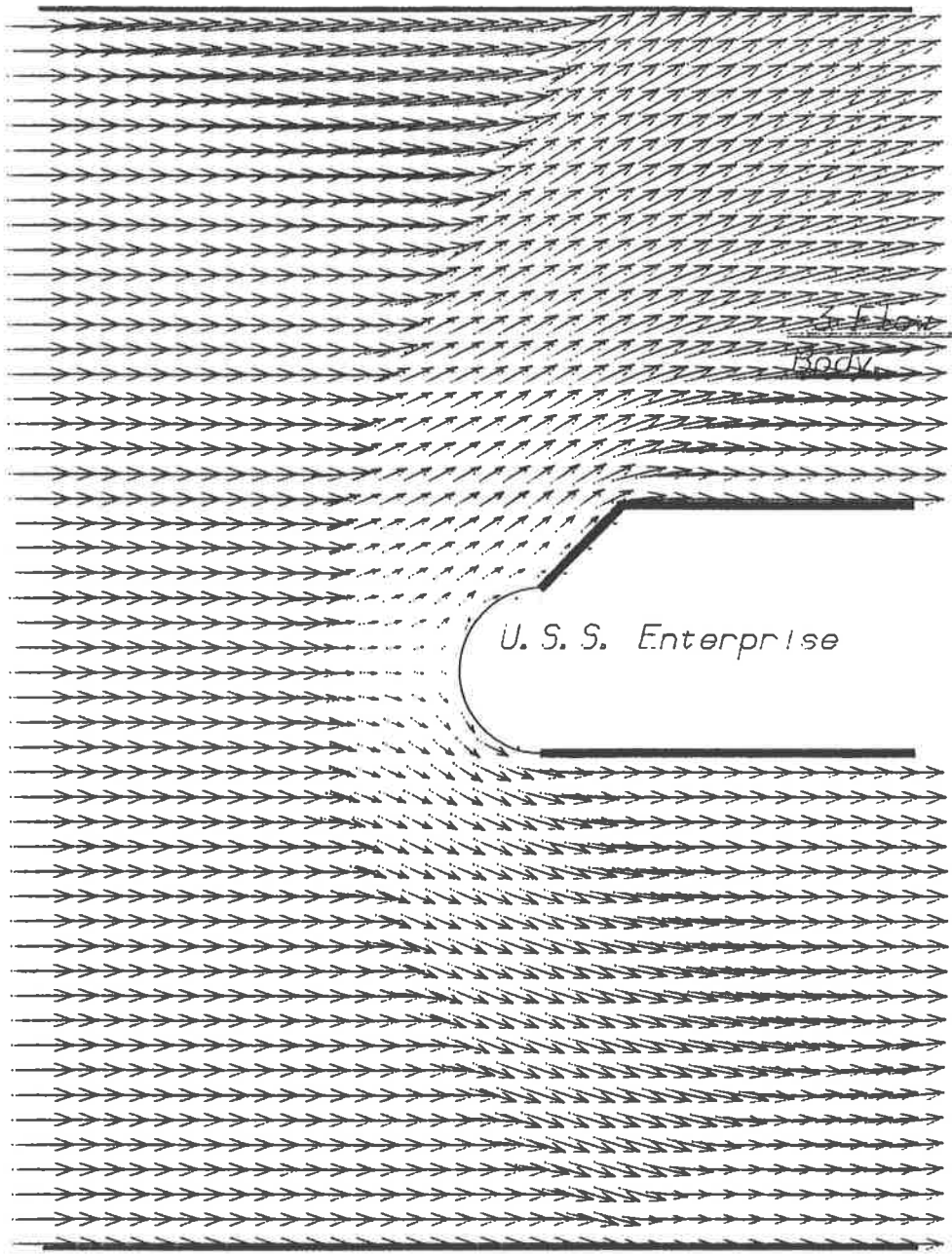

Mach

Flow Past a Non-rectangular Body

Airflow at time T = 5.500.

Maximum flow velocity is 3.262.

Maximum CFL number is 0.487.

Dt/Dx = 0.10.

Minmod

Angle of attack is

0.0 degrees.

Figure 13b

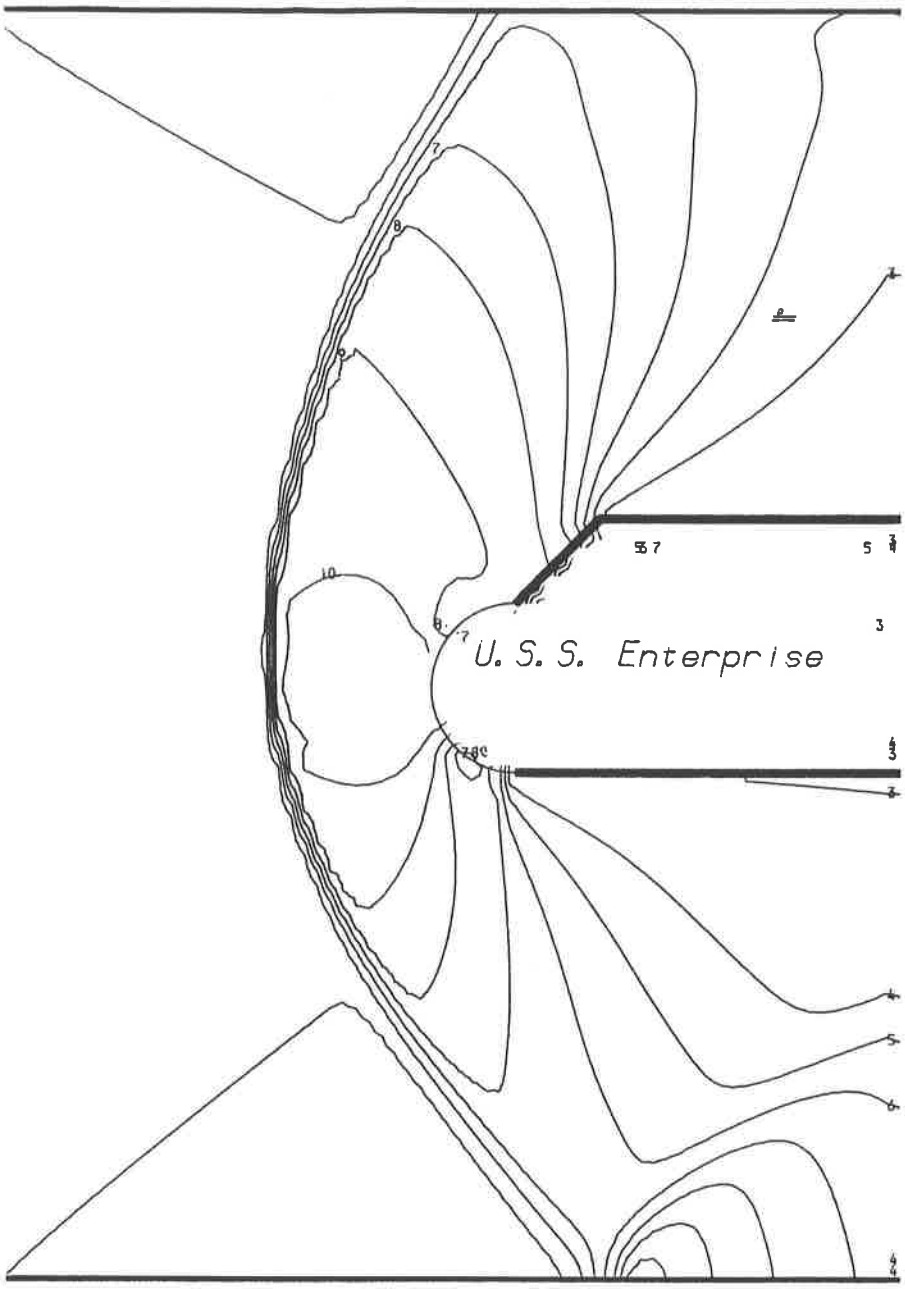

Mach 3 Flow Past a

Non-rectangular Body

Density at time T = 7.000.

Maximum density is 3.65.

Minimum density is 0.70.

First order method

Angle of attack is

5.0 degrees.

Figure 14a

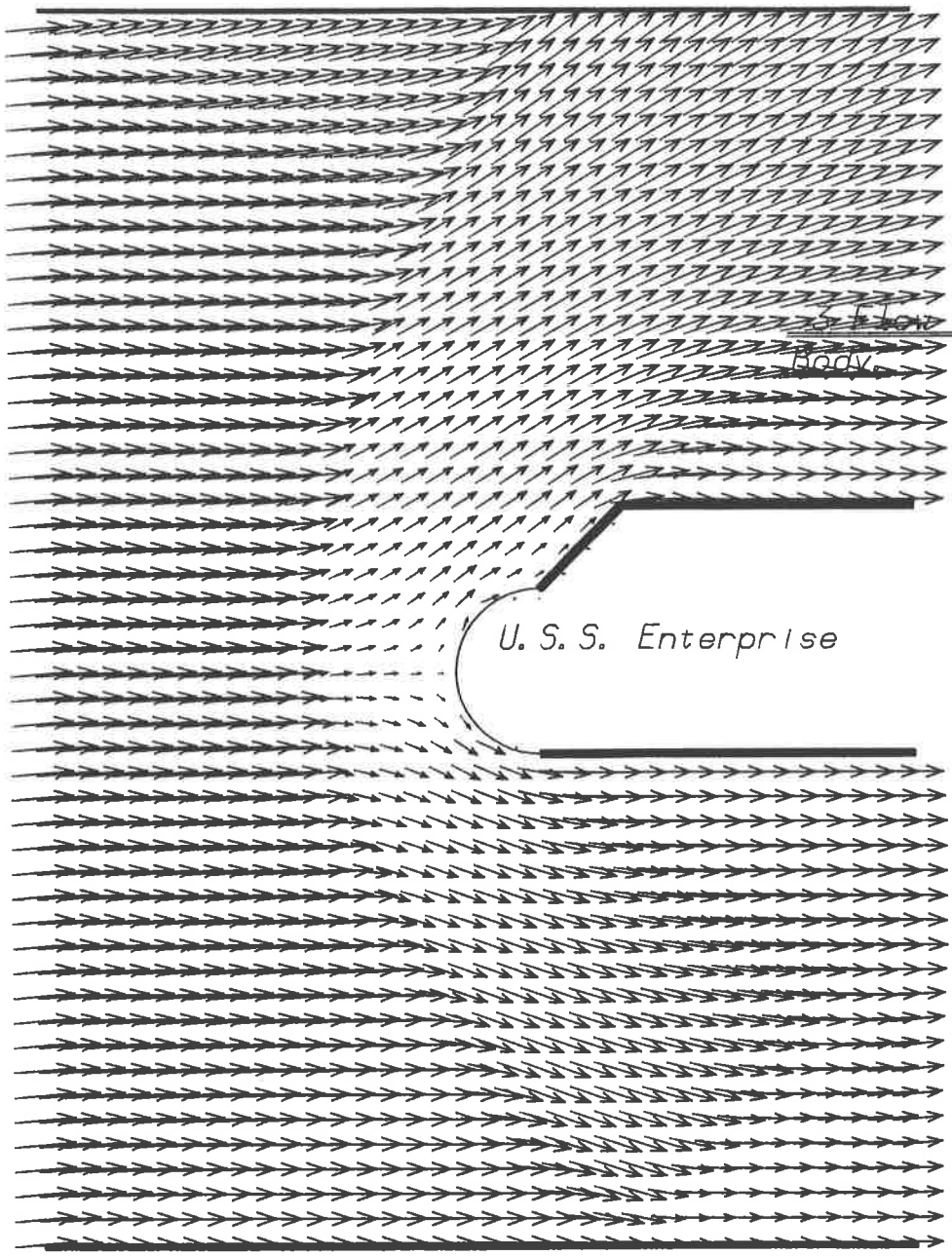

Mach Flow Past a Non-rectangular Body.

Airflow at time T = 7.000.

Maximum flow velocity is 3.262.

Maximum CFL number is 0.484.

Dt/Dx = 0.10.

First order method

Angle of attack is

5.0 degrees.

Figure 14b

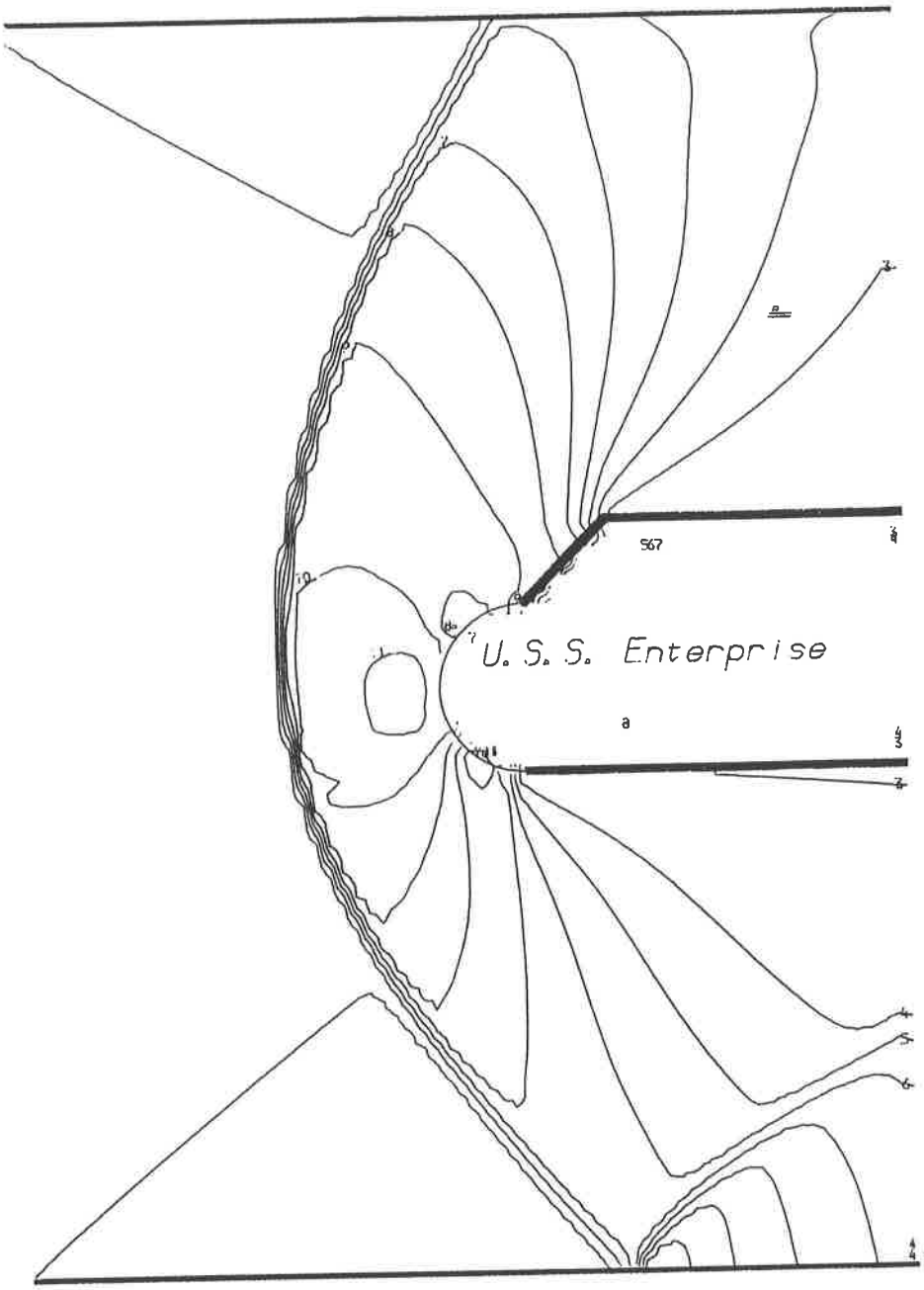

Mach 3 Flow Past a

Non-rectangular Body

Density at time T = 6.500.

Maximum density is 3.80.

Minimum density is 0.68.

Minmod

Angle of attack is

5.0 degrees.

Figure 15a

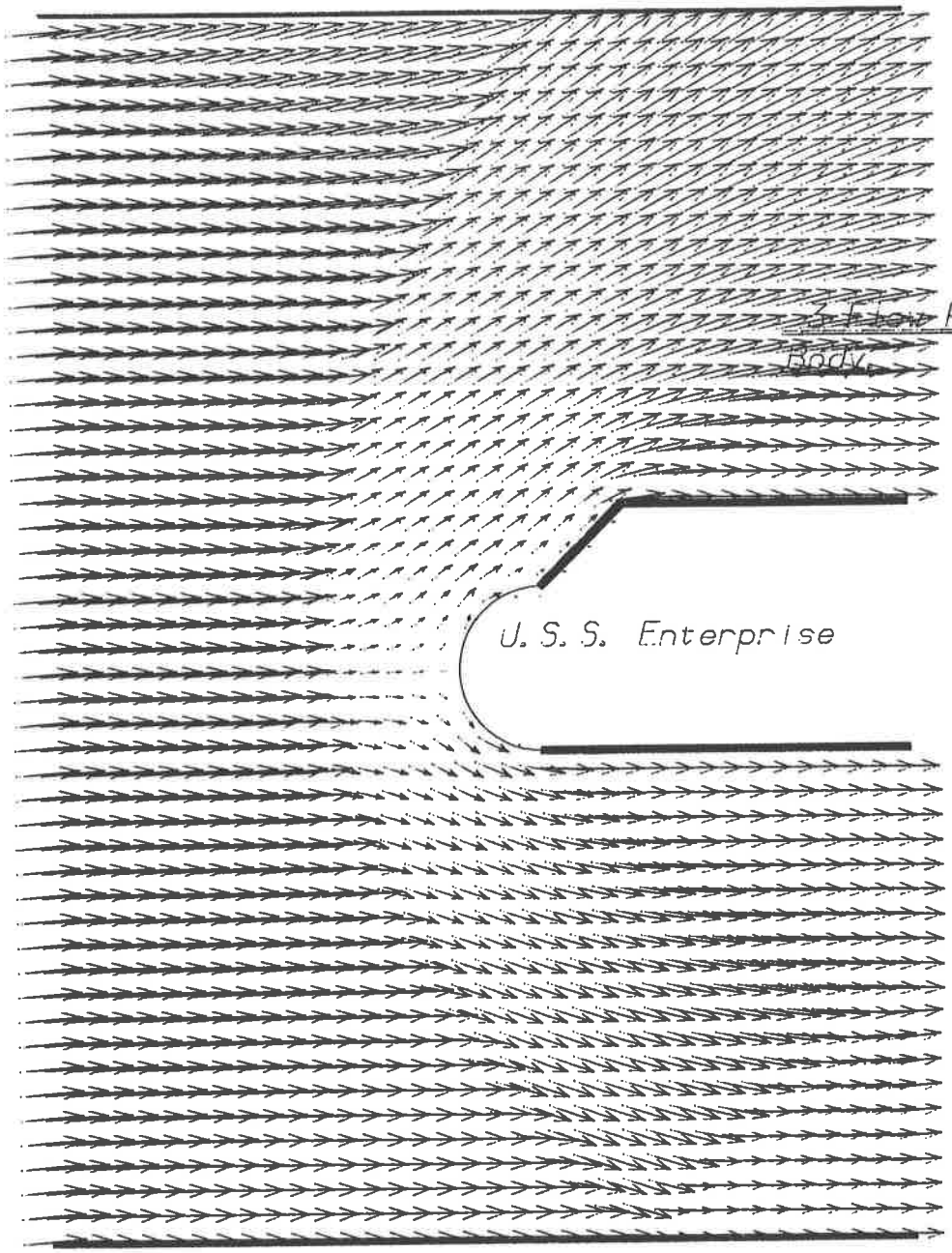

Mach

Flow Past a Non-rectangular Body

Airflow at time T = 6.500.

Maximum flow velocity is 3.262.

Maximum CFL number is 0.486.

Dt/Dx = 0.10.

Minmod

Angle of attack is

5.0 degrees.

Figure 15b

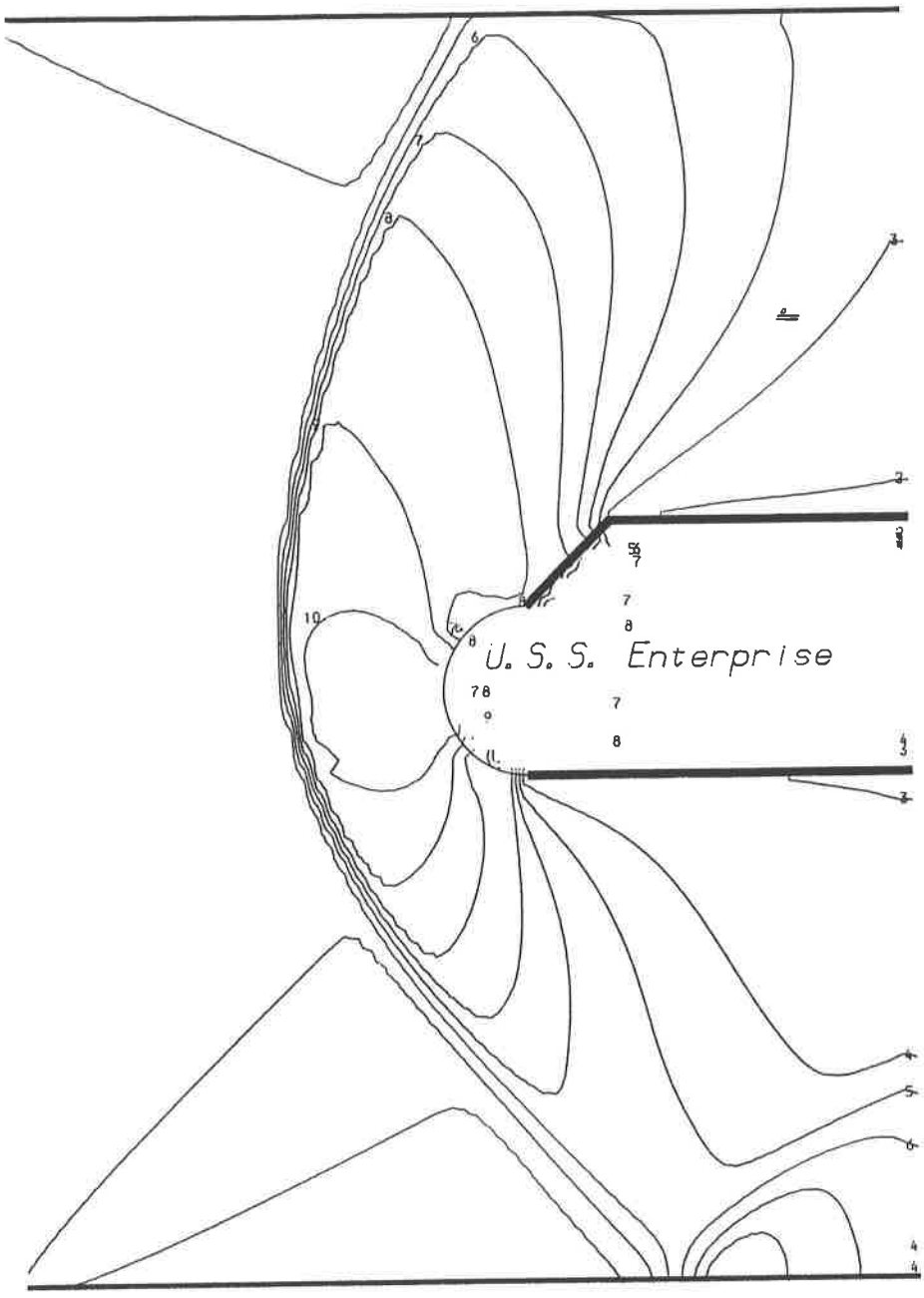

Mach 3 Flow Past a

Non-rectangular Body

Density at time T = 7.000.

Maximum density is 3.66.

Minimum density is 0.62.

First order method

Angle of attack is

10.0 degrees.

Figure 16a

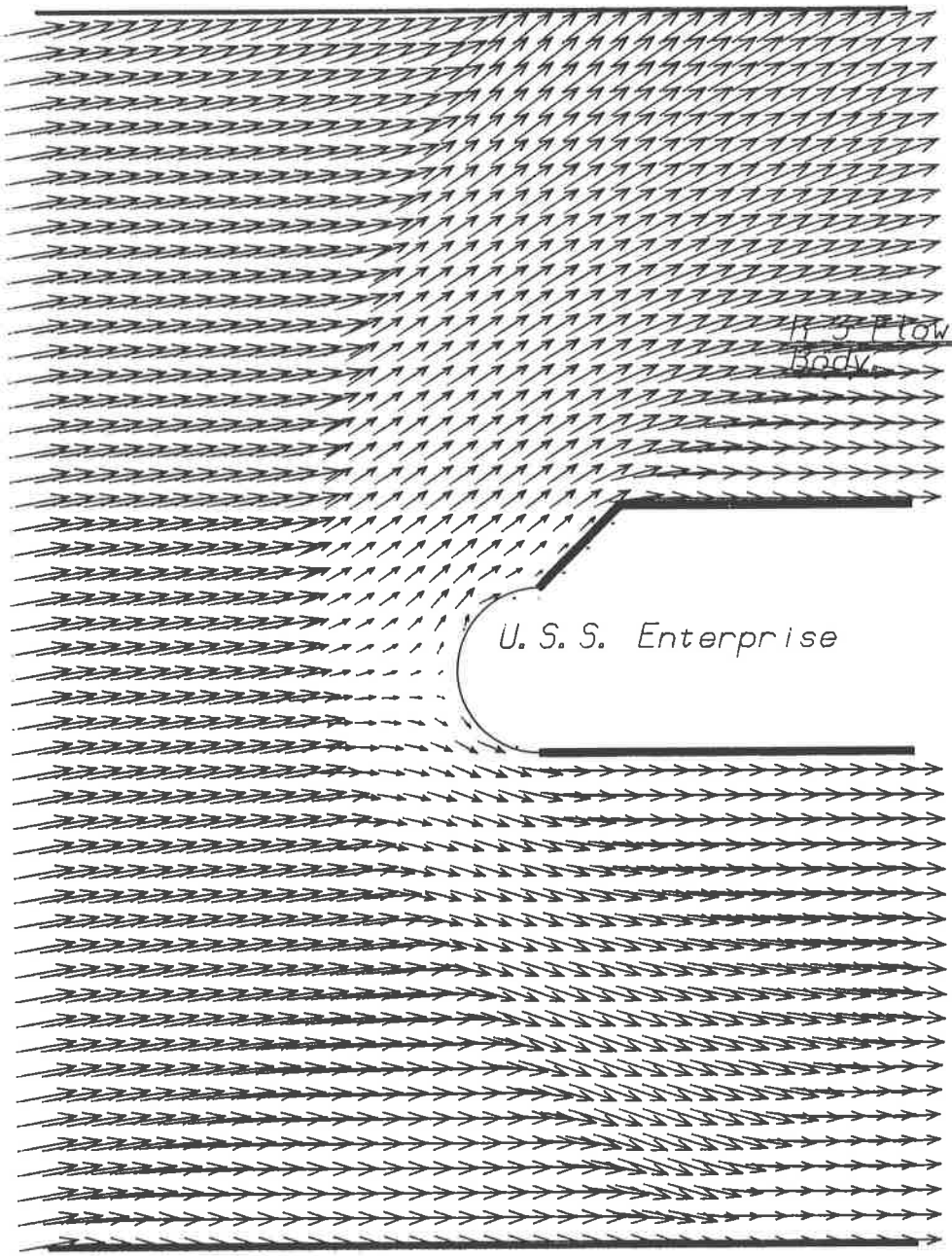

Mach 3 Flow Past Non-rectangular Body.

Airflow at time T = 7.000.

Maximum flow velocity is 3.314.

Maximum CFL number is 0.486.

Dt/Dx = 0.10.

First order method

Angle of attack is

10.0 degrees.

Figure 16b

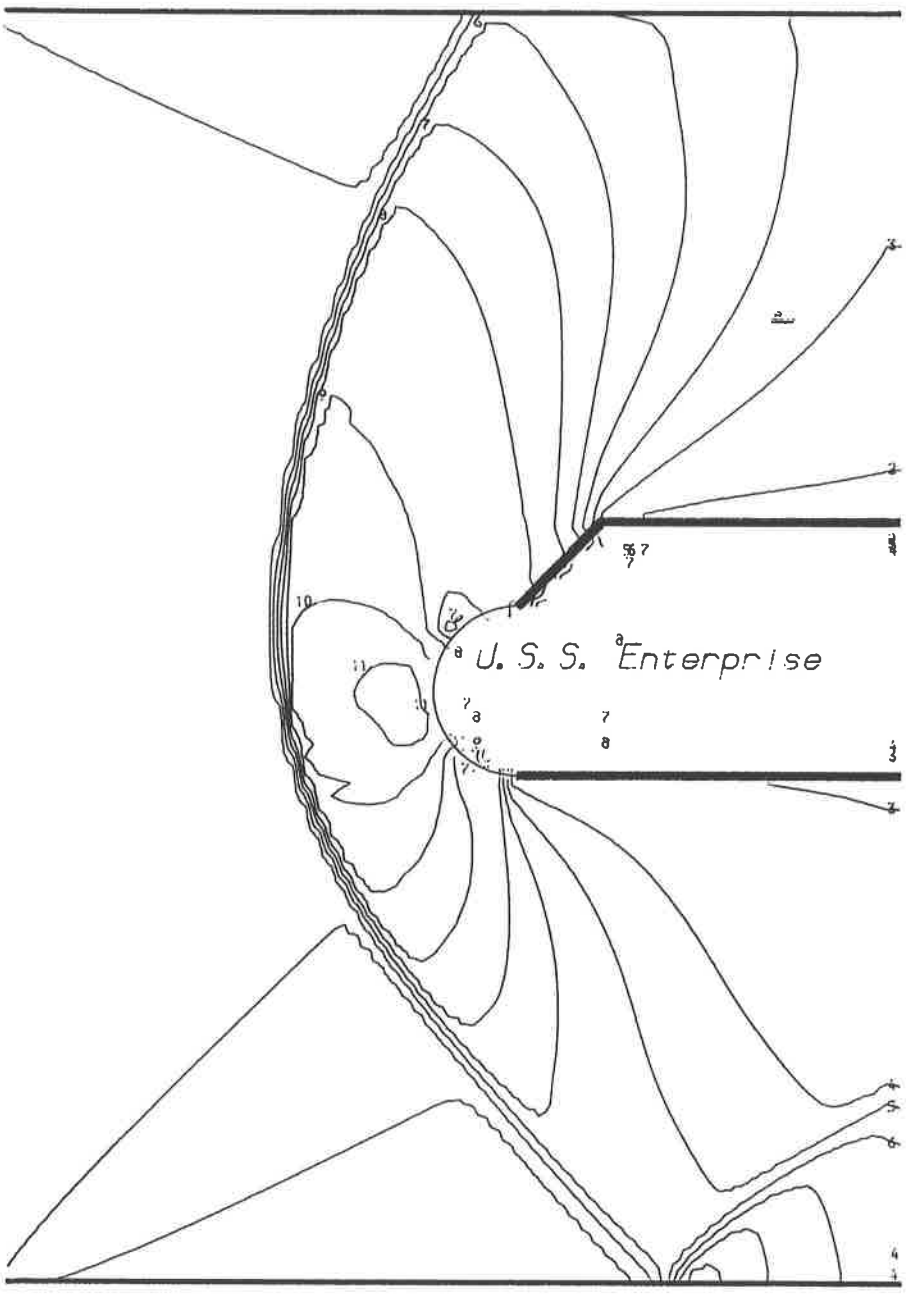

Mach 3 Flow Past a

Non-rectangular Body

Density at time T = 6.500.

Maximum density is 3.78.

Minimum density is 0.61.

Minmod

Angle of attack is

10.0 degrees.

Figure 17a

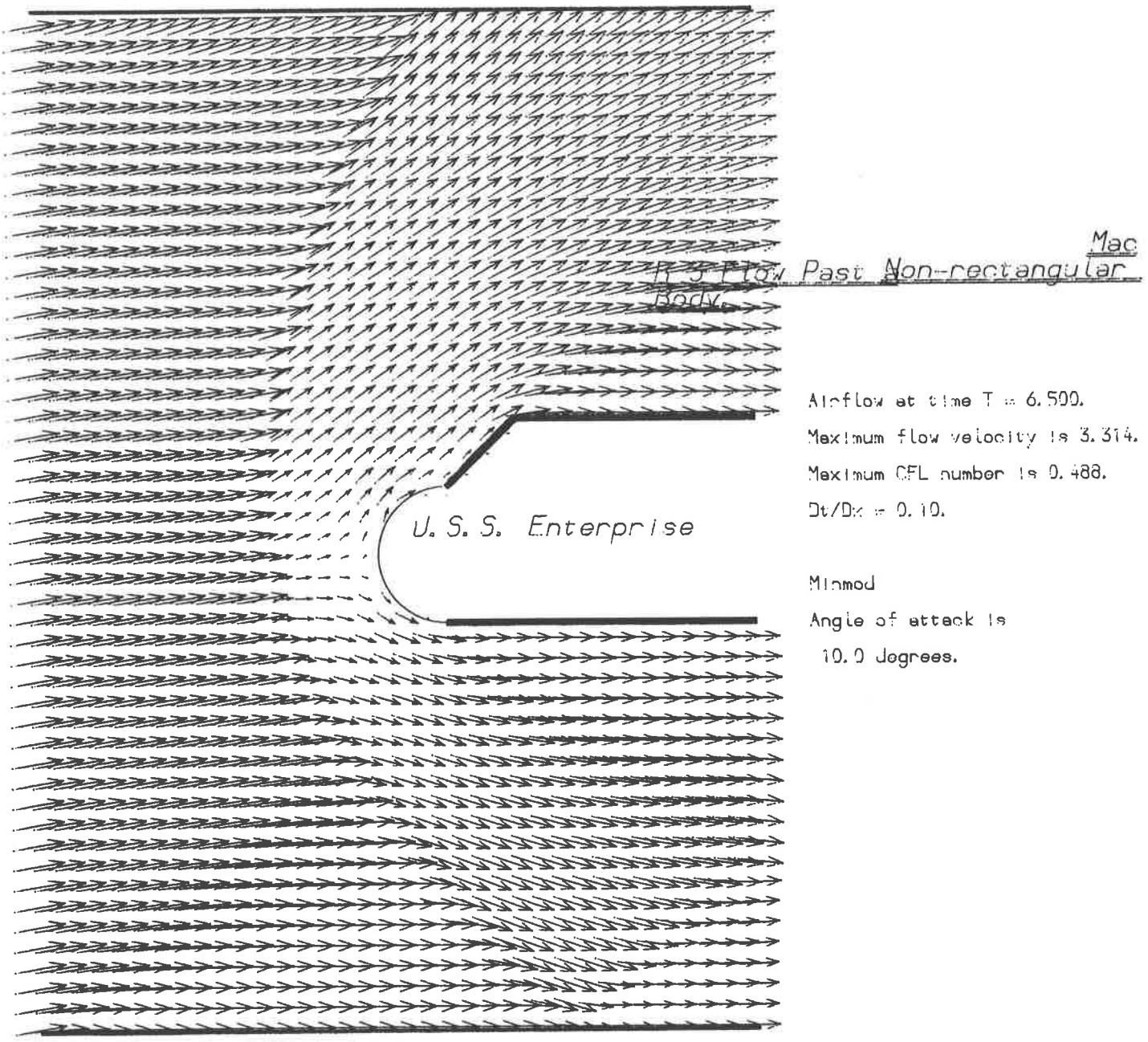
Mac
R-J Flow Past Non-rectangular Body.
Airflow at time T = 6.500.
Maximum flow velocity is 3.314.
Maximum CFL number is 0.488.
Dt/Dx = 0.10.
Minmod
Angle of attack is
10.0 degrees.
U. S. S. Enterprise

Figure 17b

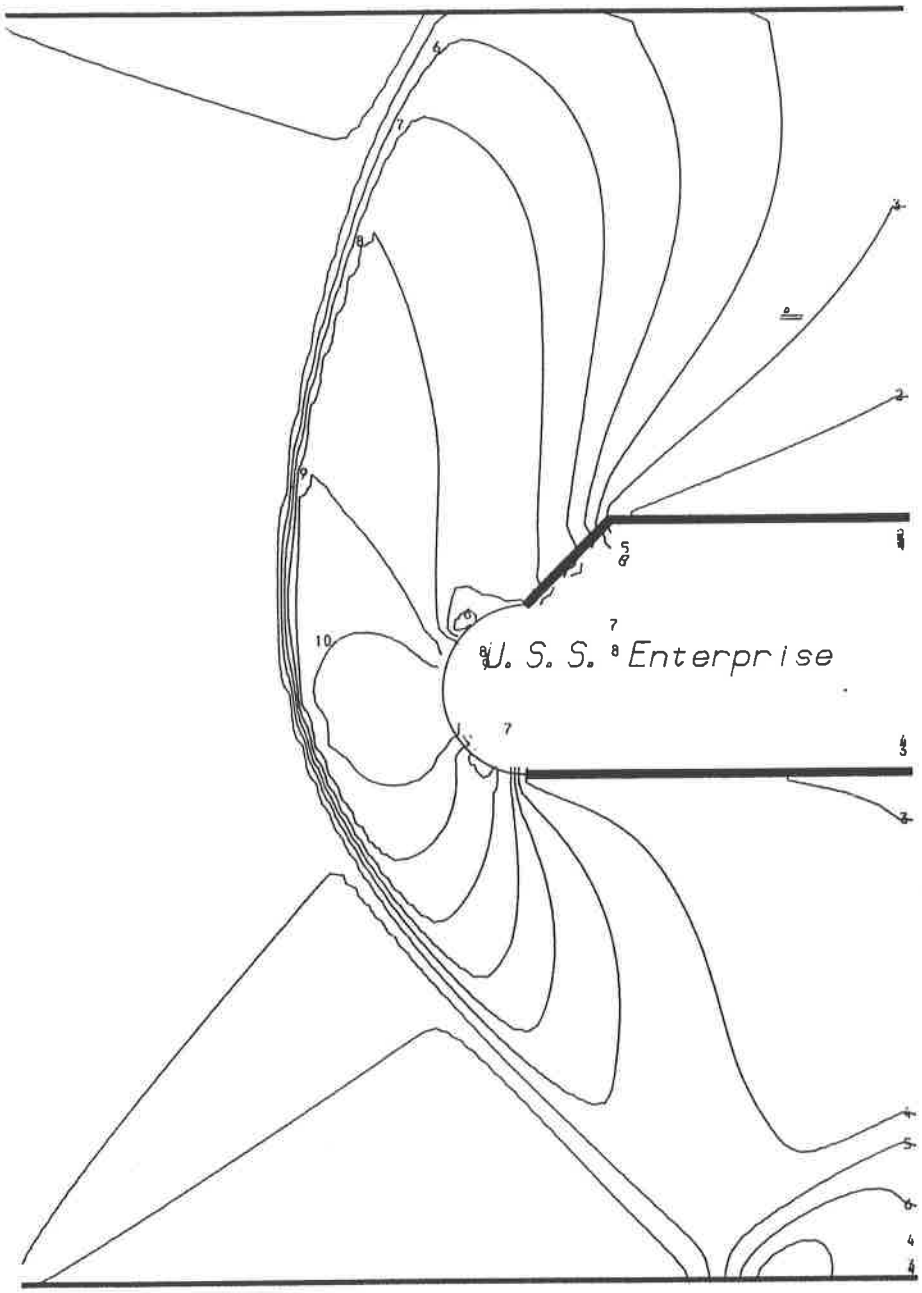

Mach 3 Flow Past a

Non-rectangular Body

Density at time T = 7.000.

Maximum density is 3.65.

Minimum density is 0.53.

First order method

Angle of attack is

15.0 degrees.

Figure 18a

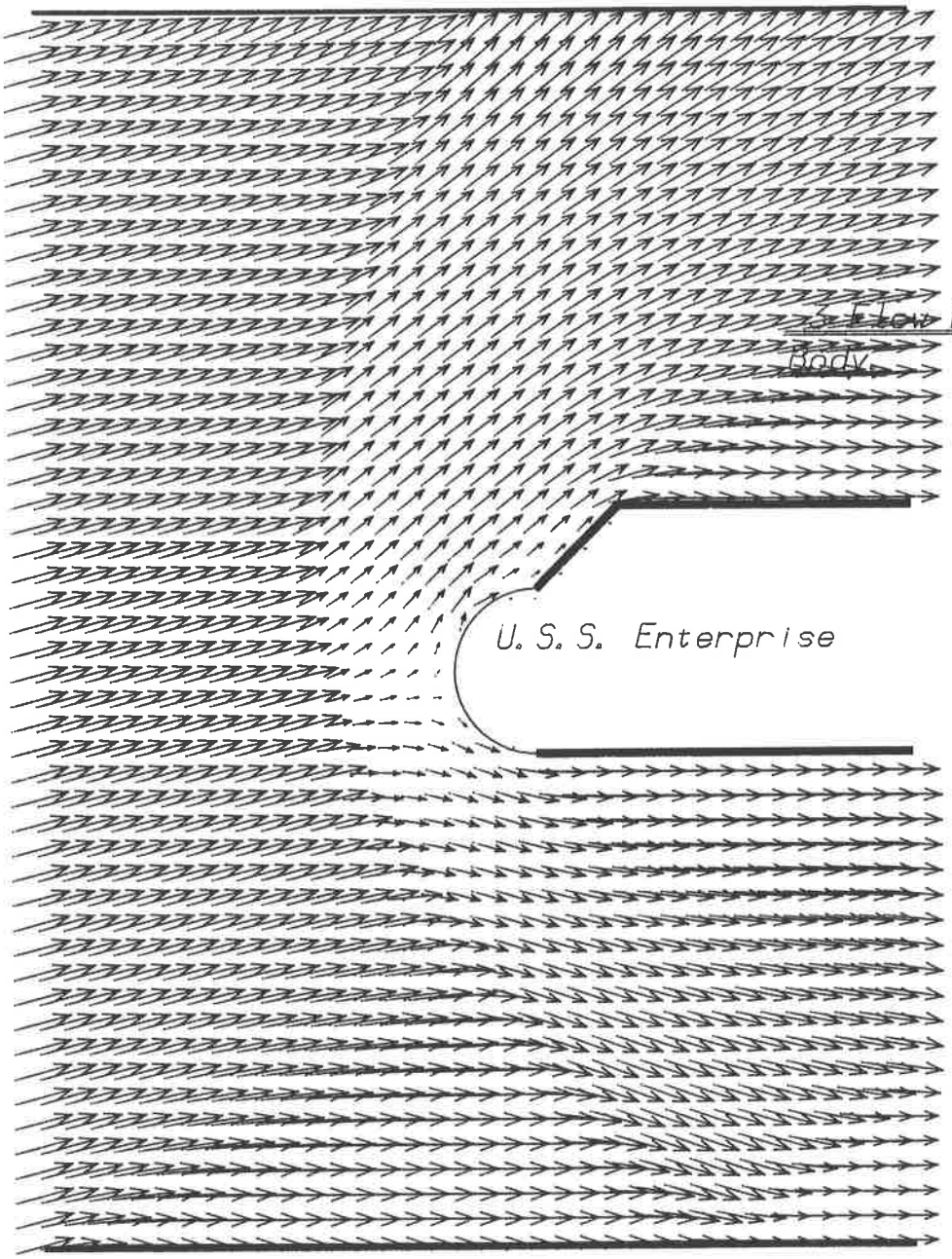

Mach

Flow Past a Non-rectangular Body

Airflow at time T = 7.000.

Maximum flow velocity is 3.447.

Maximum CFL number is 0.494.

Dt/Dx = 0.10.

First order method

Angle of attack is

15.0 degrees.

Figure 18b

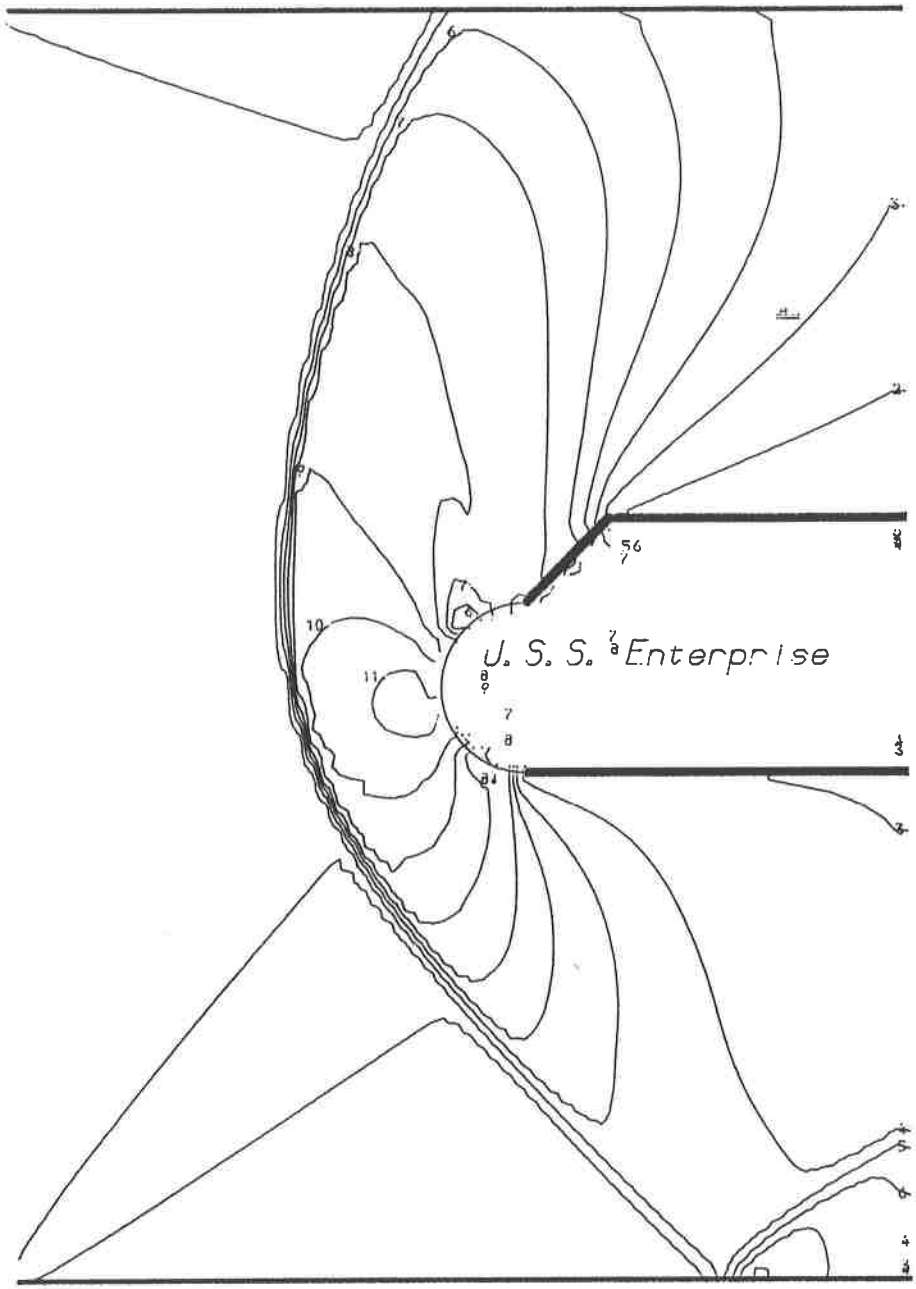

Mach 3 Flow Past a

Non-rectangular Body

Density at time T = 6.500.

Maximum density is 3.80.

Minimum density is 0.51.

Minmod

Angle of attack is

15.0 degrees.

Figure 19a

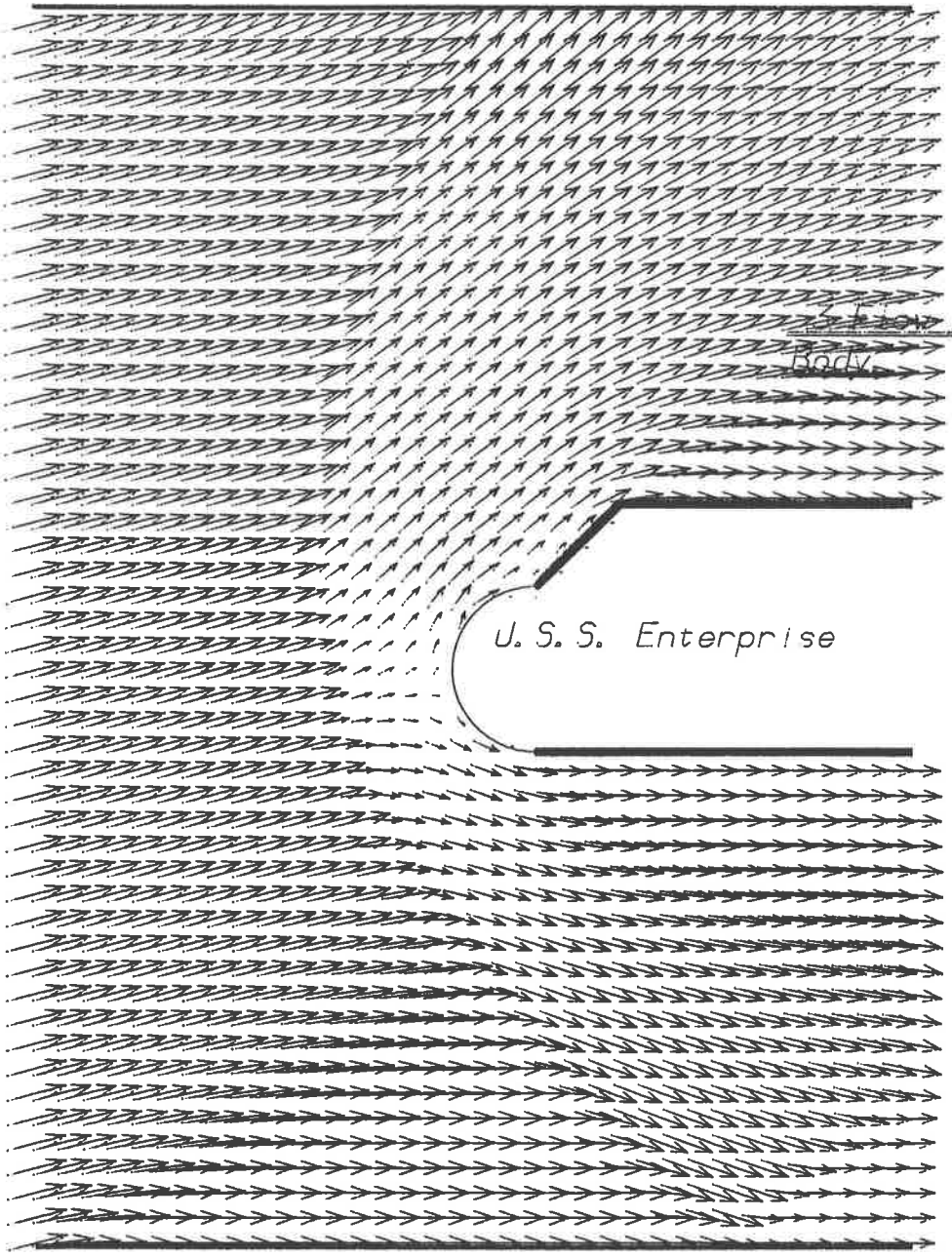
Mach
Past a Non-rectangular
Body
U. S. S. Enterprise
Airflow at time T = 6.500.
Maximum flow velocity is 3.448.
Maximum CFL number is 0.494.
Dt/Dx = 0.10.
Minmod
Angle of attack is
15.0 degrees.

Figure 19b

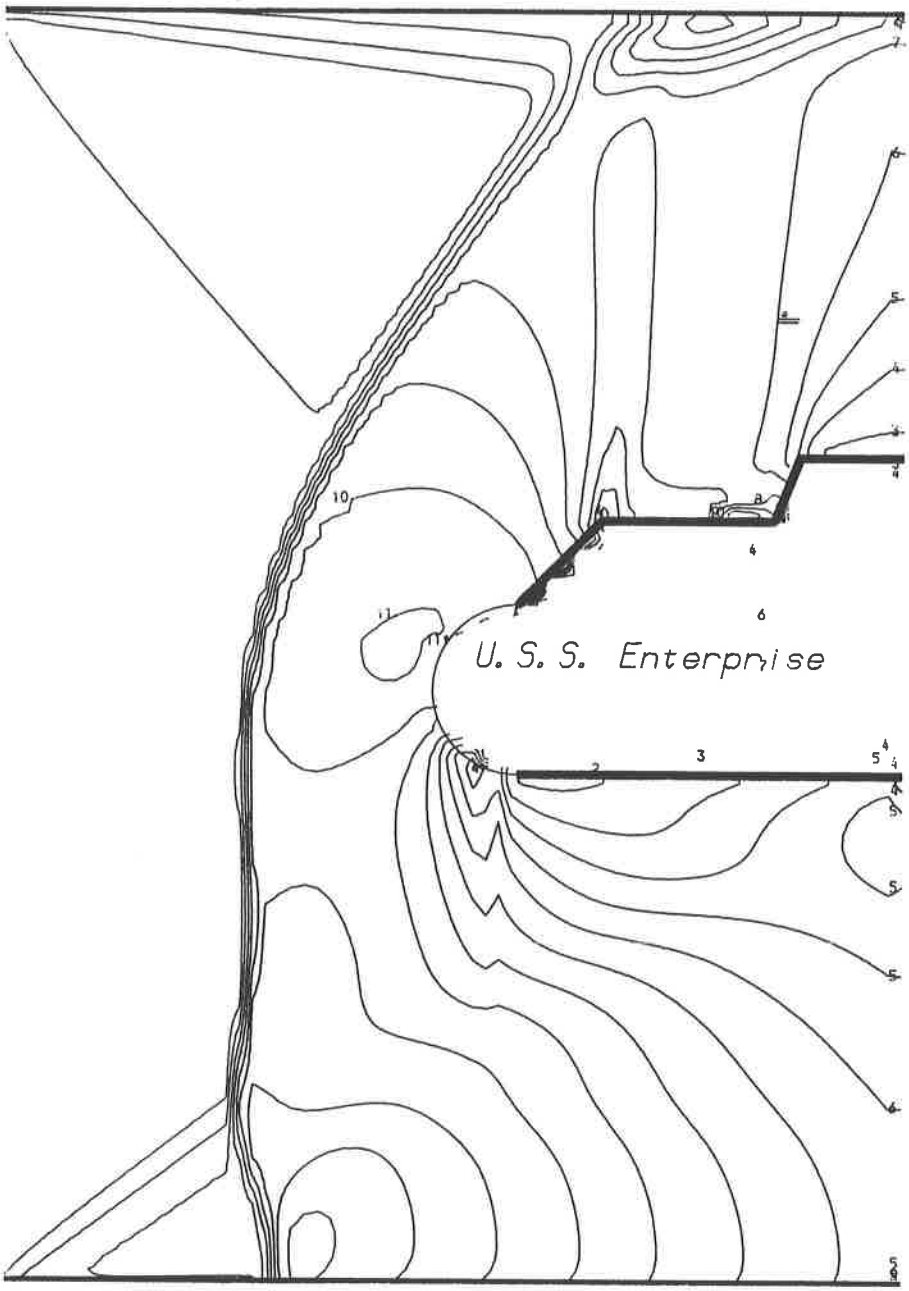

Mach 3 Flow Past a

Non-rectangular Body

Density at time T = 6.500.

Maximum density is 4.44.

Minimum density is 0.59.

First order method

Angle of attack is

-15.0 degrees.

Figure 20a

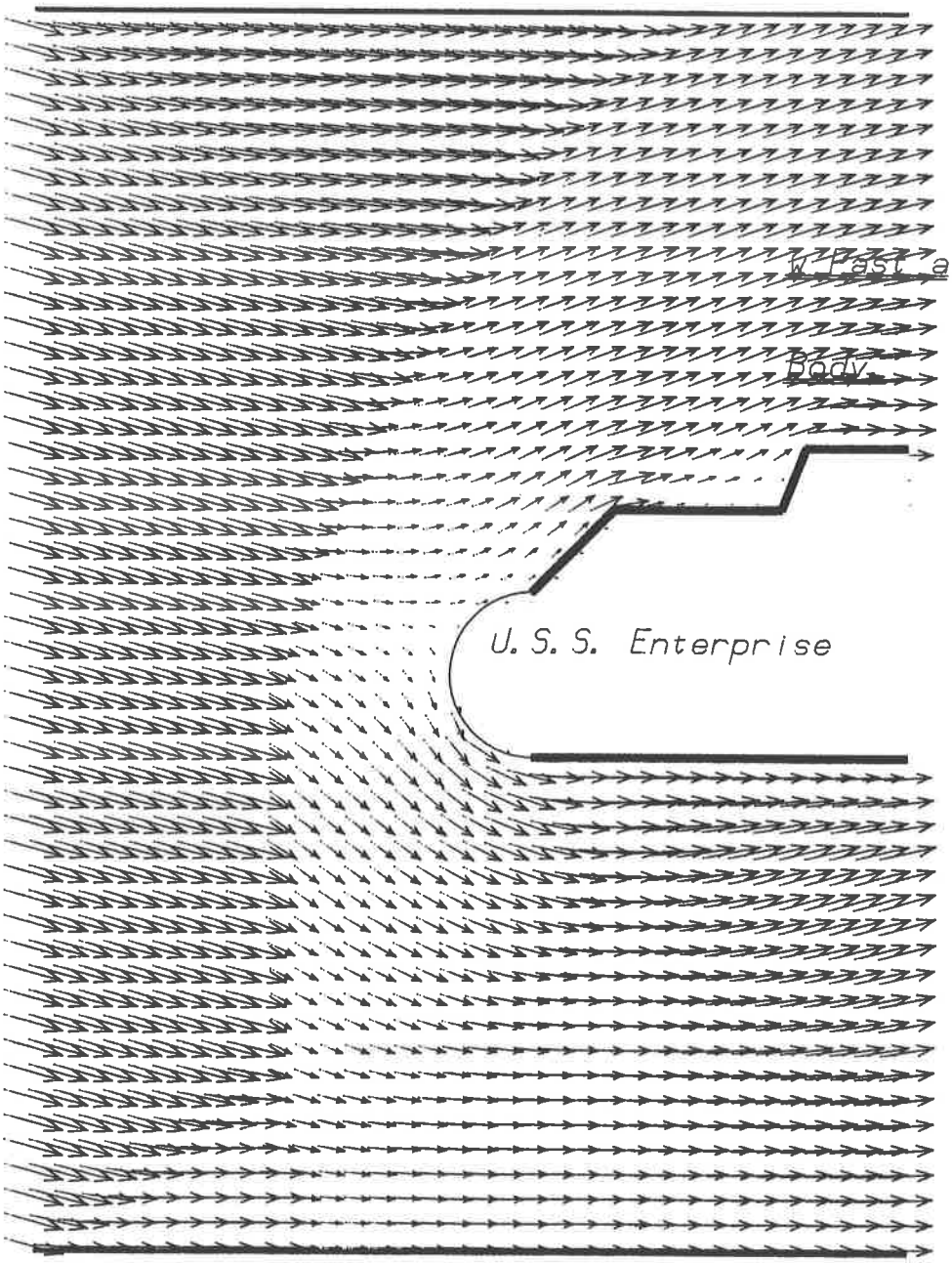

Mach 3 Flo

Non-rectangular

Airflow at time T = 6.500.
Maximum flow velocity is 3.257.
Maximum CFL number is 0.481.
Dt/Dx = 0.10.

First order method
Angle of attack is
-15.0 degrees.

Figure 20b

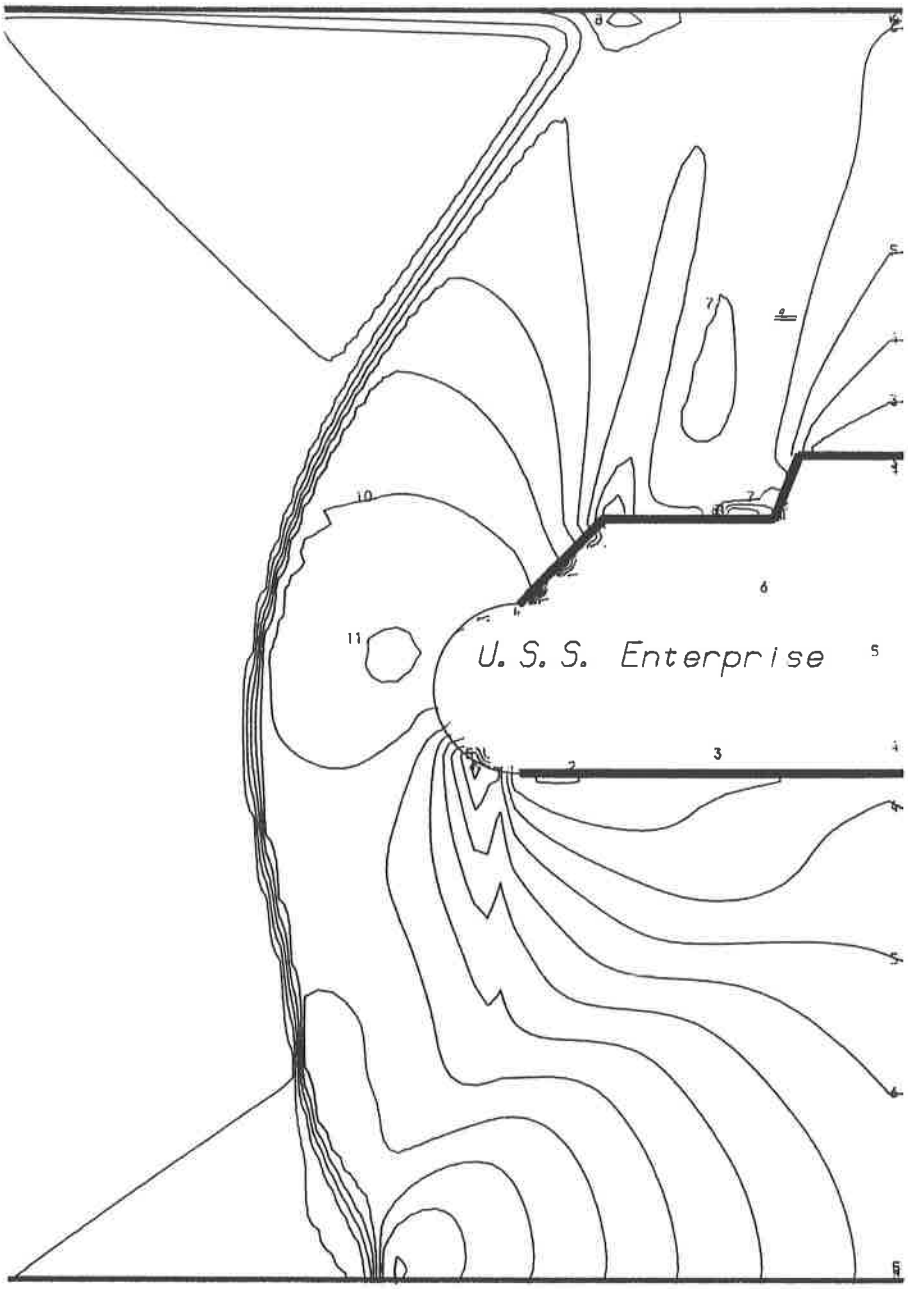

Mach 3 Flow Past a

Non-rectangular Body

Density at time T = 6.500.

Maximum density is 4.37.

Minimum density is 0.65.

First order method

Angle of attack is

-10.0 degrees.

Figure 21a

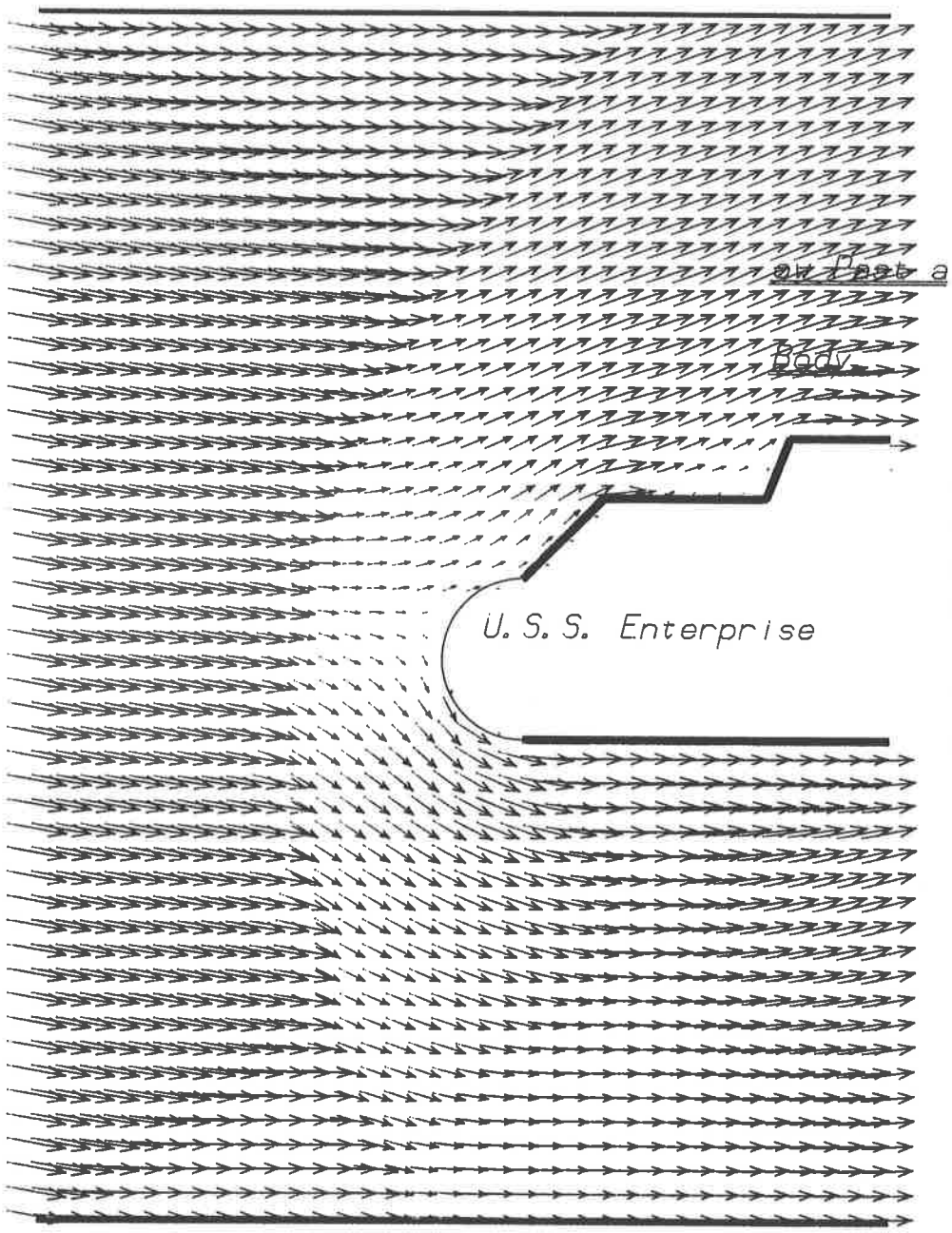

Mach 3 Fl

Non-rectangular

Airflow at time T = 6.500.

Maximum flow velocity is 3.259.

Maximum CFL number is 0.483.

Dt/Dx = 0.10.

First order method

Angle of attack is

-10.0 degrees.

Figure 21b

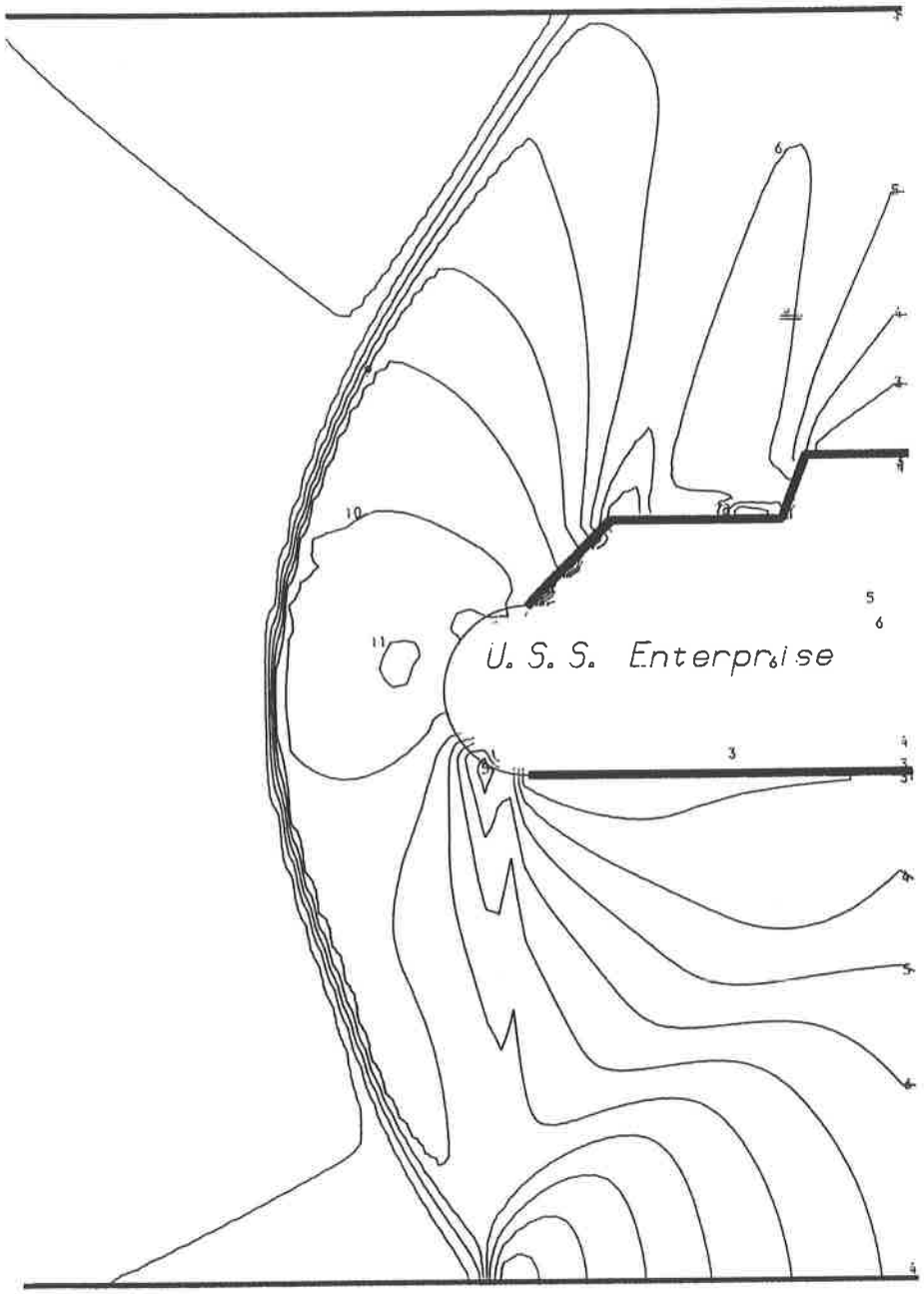

Mach 3 Flow Past a

Non-rectangular Body

Density at time T = 6.500.

Maximum density is 4.21.

Minimum density is 0.71.

First order method

Angle of attack is

-5.0 degrees.

Figure 22a

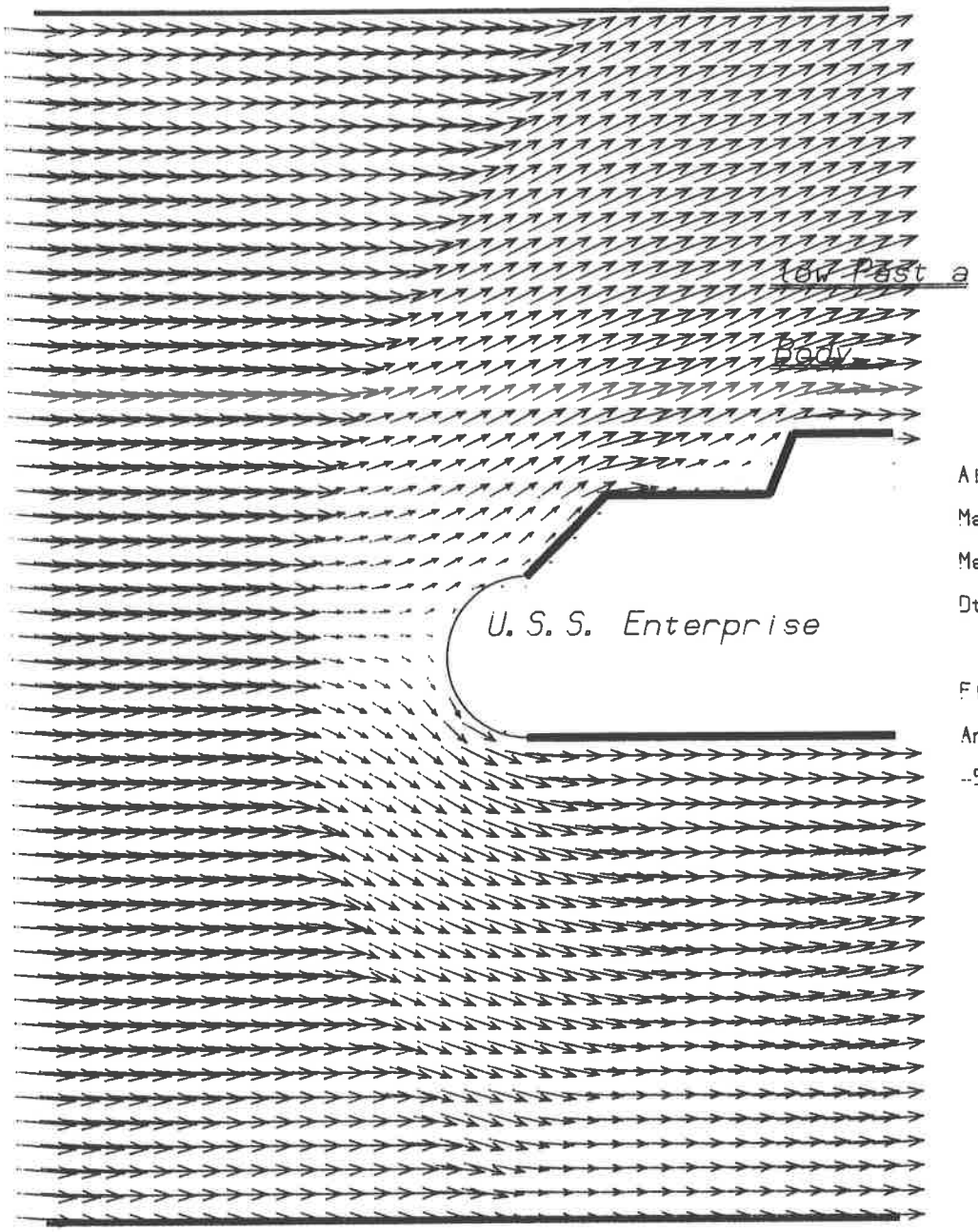

Mach 3 F

Non-rectangular

Airflow at time T = 6.500.
Maximum flow velocity is 3.266.
Maximum CFL number is 0.483.
Dt/Dx = 0.10.

First order method
Angle of attack is
-5.0 degrees.

Figure 22b

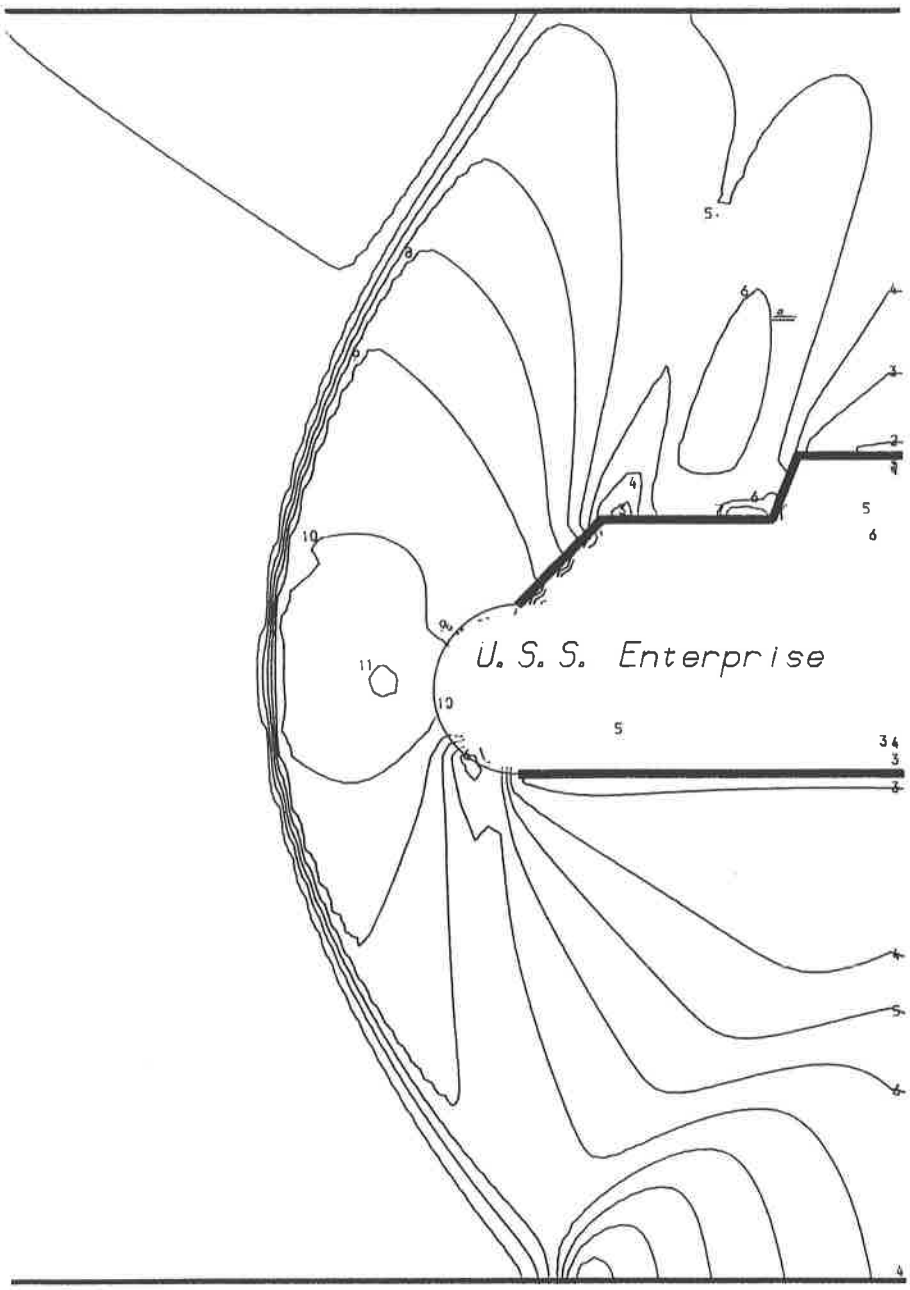

Mach 3 Flow Past a

Non-rectangular Body

Density at time T = 6.500.

Maximum density is 3.87.

Minimum density is 0.65.

First order method

Angle of attack is

0.0 degrees.

Figure 23a

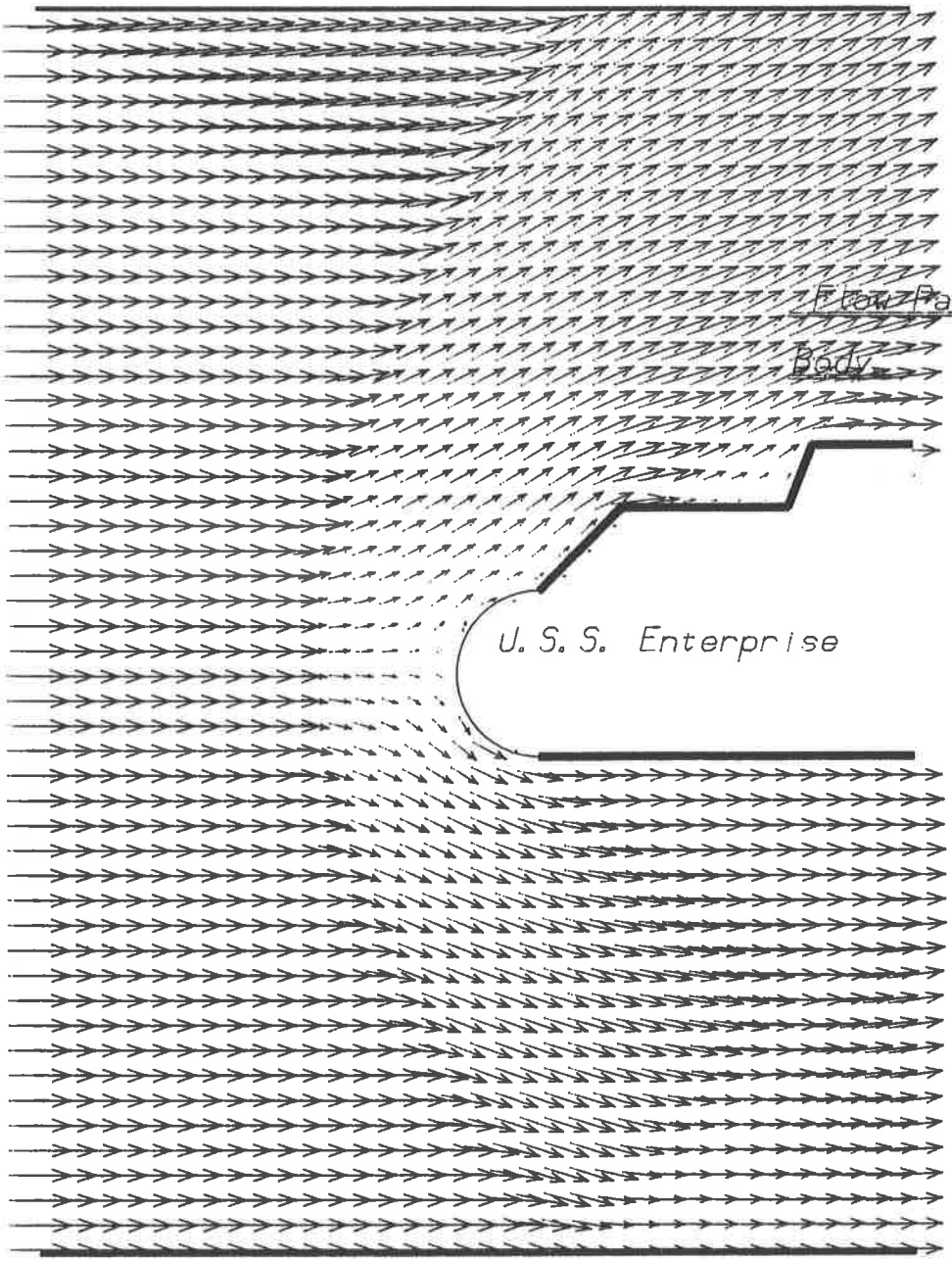

Mach 3

Flow Past a

Non-rectangular

Body

Airflow at time T = 6.500.

Maximum flow velocity is 3.260.

Maximum CFL number is 0.480.

Dt/Dx = 0.10.

First order method

Angle of attack is

0.0 degrees.

Figure 23b

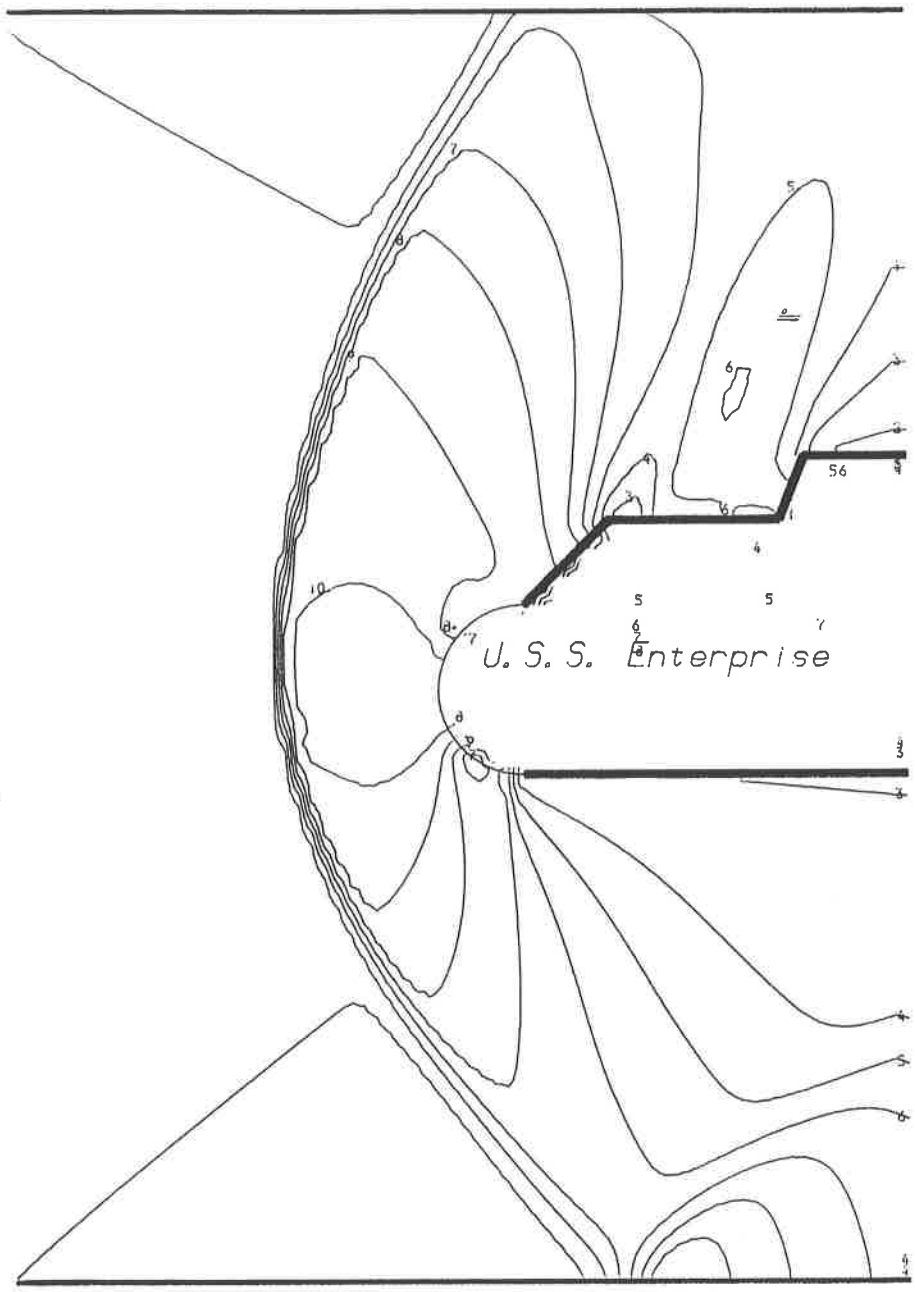

Mach 3 Flow Past a

Non-rectangular Body

Density at time T = 6.500.

Maximum density is 3.65.

Minimum density is 0.60.

First order method

Angle of attack is

5.0 degrees.

Figure 24a

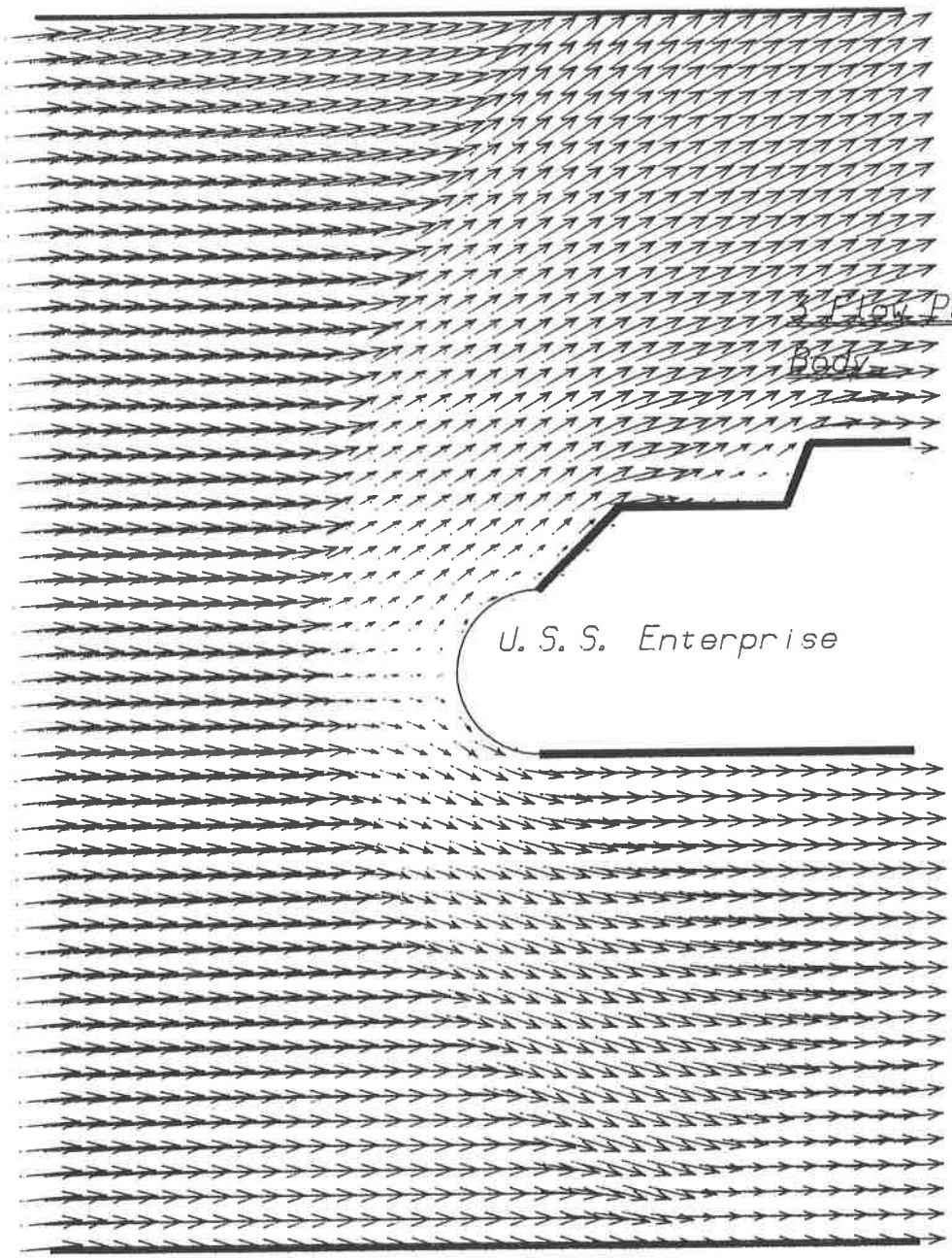
Mach
Flow Past a Non-rectangular
Body
U. S. S. Enterprise
Airflow at time T = 6.500.
Maximum flow velocity is 3.263.
Maximum CFL number is 0.478.
Dt/Dx = 0.10.
First order method
Angle of attack is
5.0 degrees.

Figure 24b

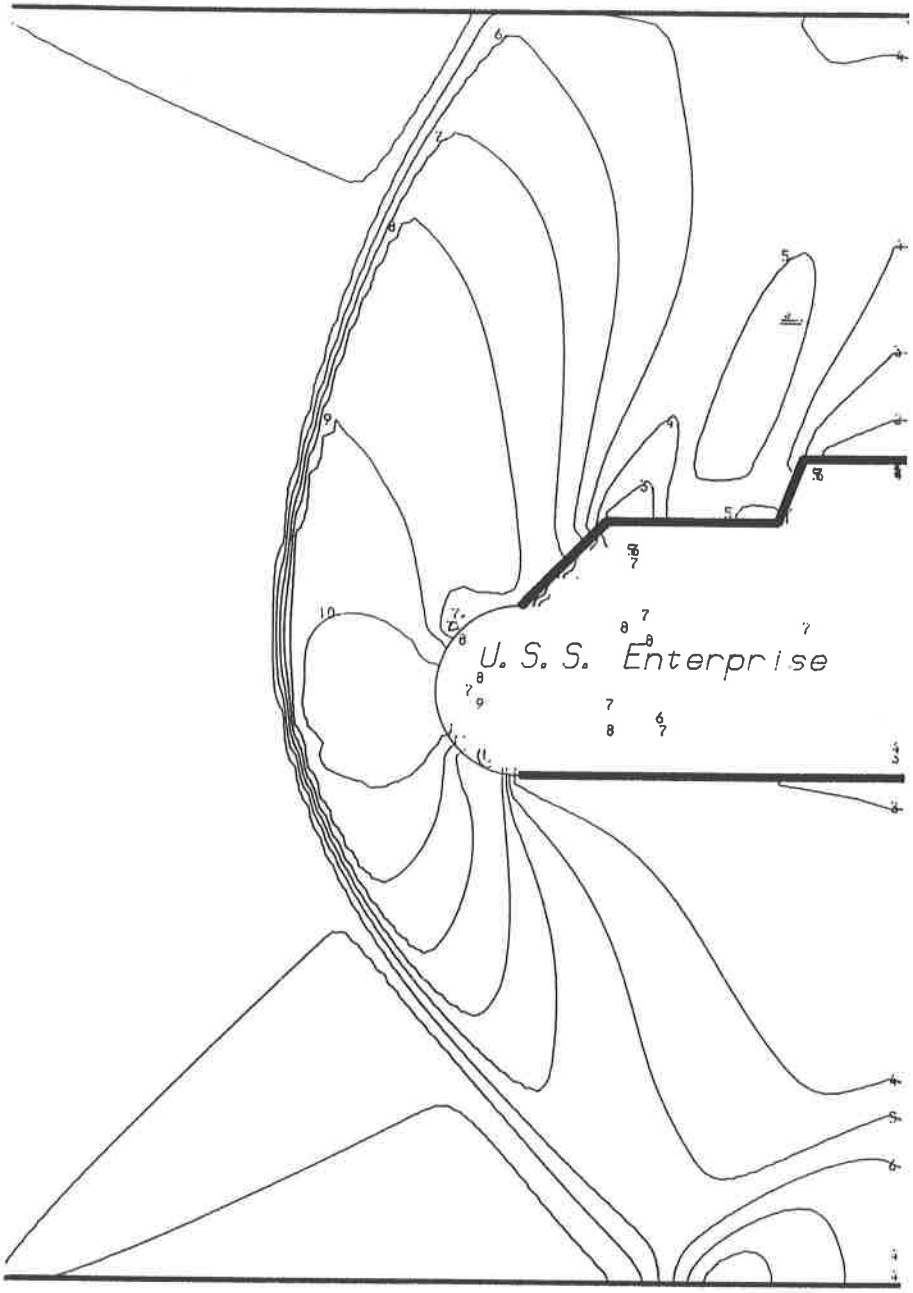

Mach 3 Flow Past a

Non-rectangular Body

Density at time T = 6.500.

Maximum density is 3.65.

Minimum density is 0.54.

First order method

Angle of attack is

10.0 degrees.

Figure 25a

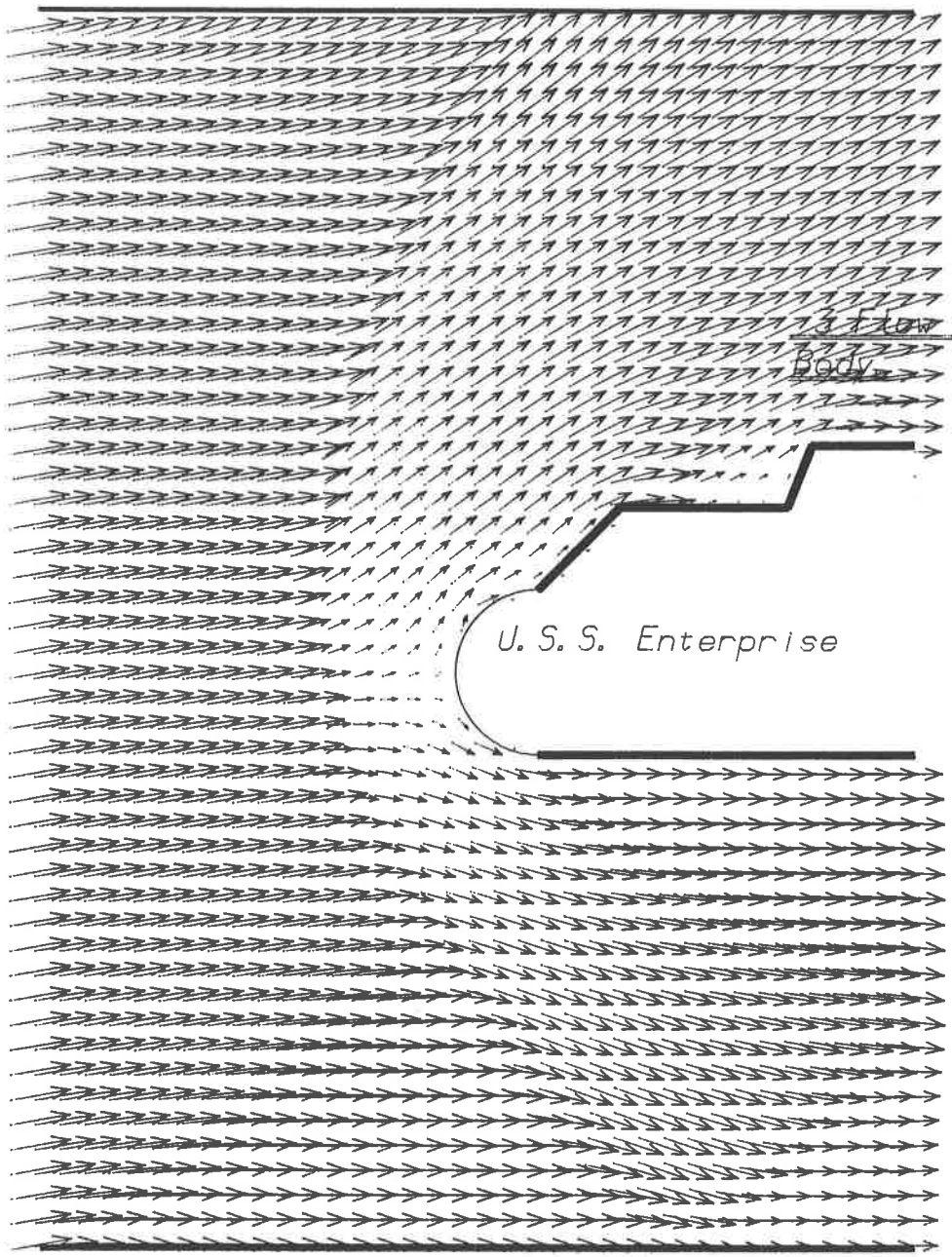
Mach
Flow Past a Non-rectangular
Body
U. S. S. Enterprise
Airflow at time T = 6.500.
Maximum flow velocity is 3.314.
Maximum CFL number is 0.486.
Dt/Dx = 0.10.
First order method
Angle of attack is
10.0 degrees.

Figure 25b

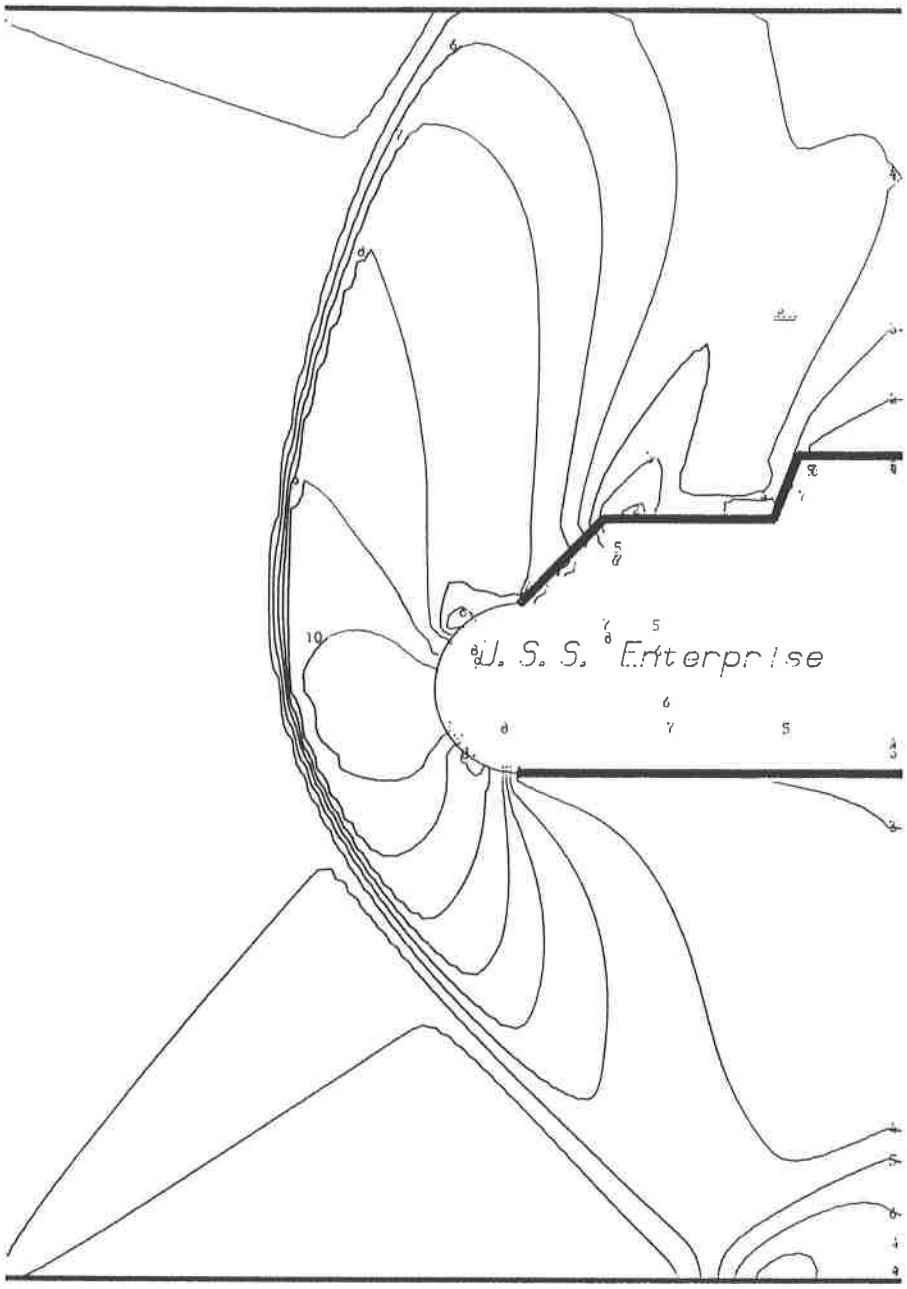

Mach 3 Flow Past a

Non-rectangular Body

Density at time T = 6.500.

Maximum density is 3.65.

Minimum density is 0.48.

First order method

Angle of attack is

15.0 degrees.

Figure 26a

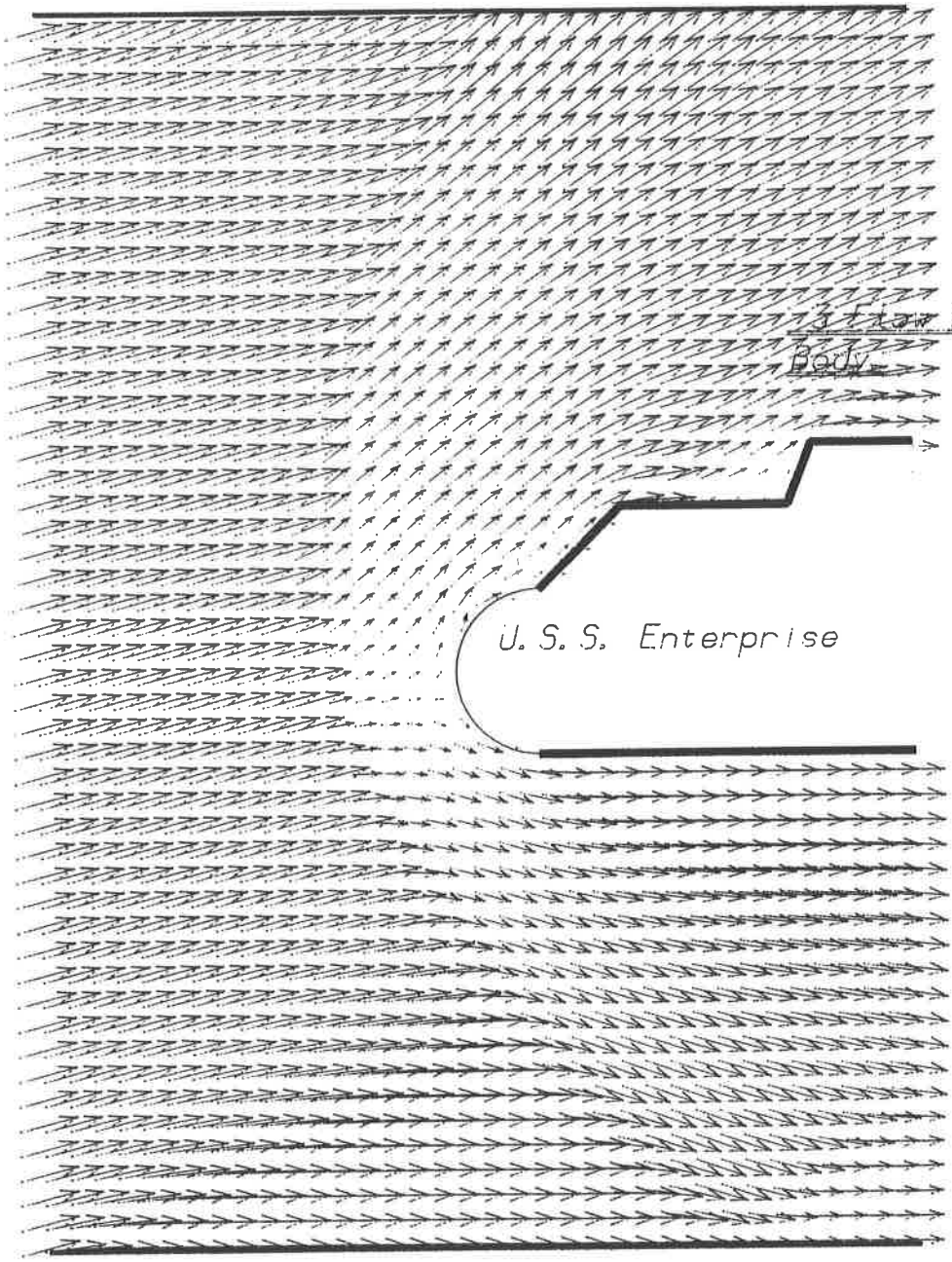

Mach 3 Flow Past a Non-rectangular Body

Airflow at time T = 6.500.
Maximum flow velocity is 3.447.
Maximum CFL number is 0.494.
Dt/Dx = 0.10.

First order method
Angle of attack is
15.0 degrees.

Figure 26b

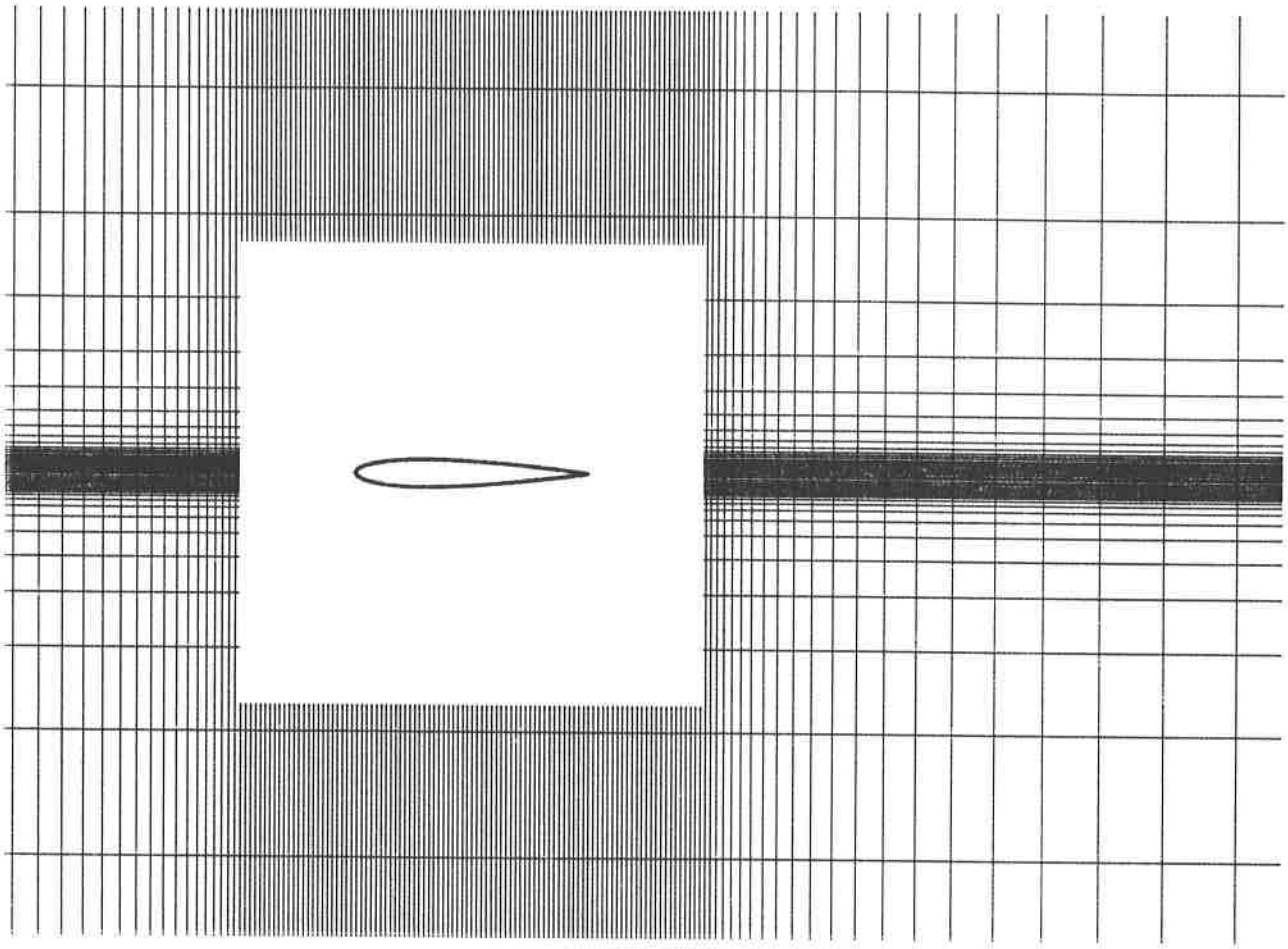

Figure 27

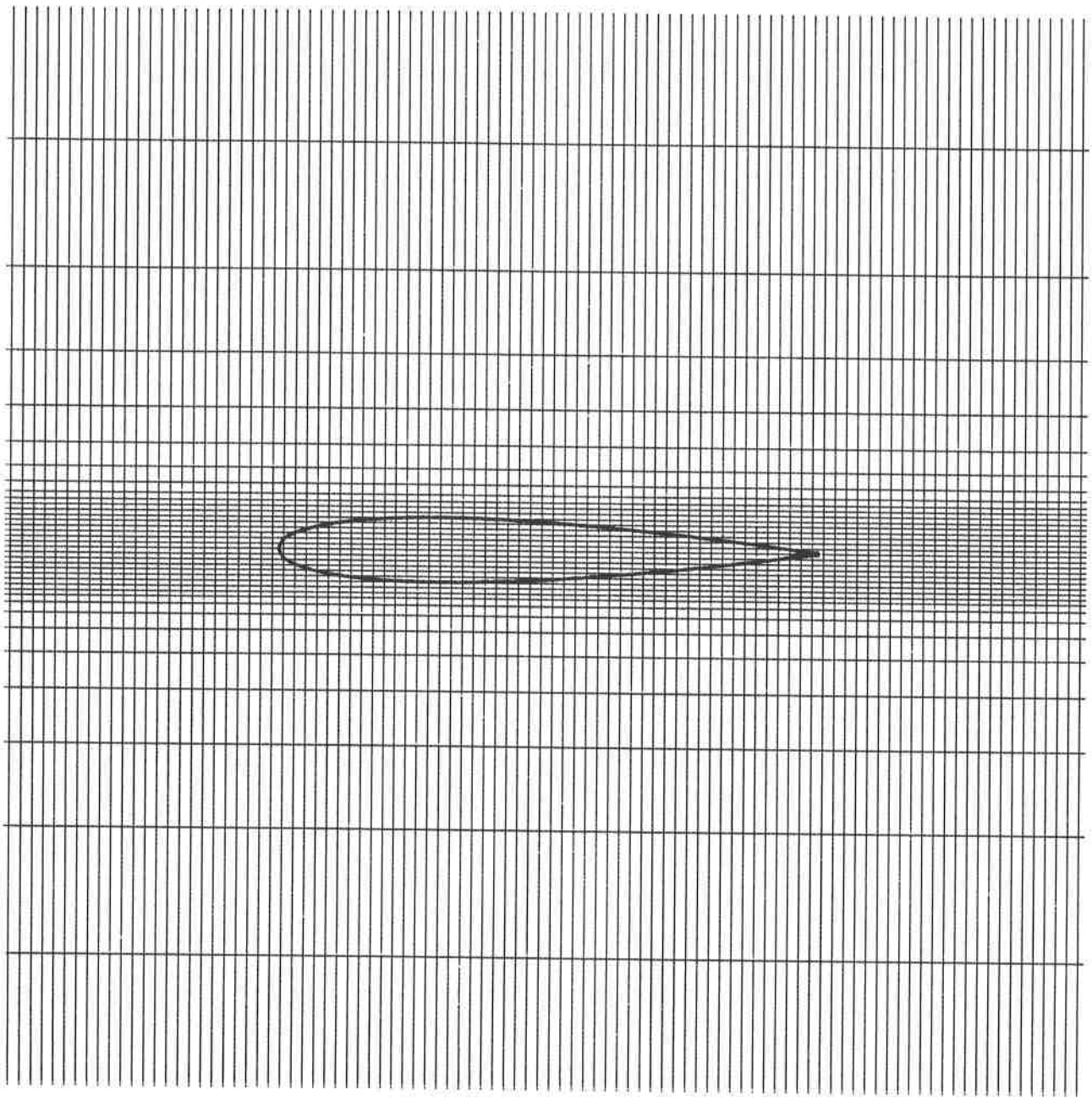

Figure 28

NACA0012 Aerofoil

Density contours for the NACA0012 aerofoil
in a Mach 3.00 flow. The angle of attack is 0.0 degrees.
Solution is shown after 400 time-steps and the maximum CFL no. is 0.349.
The maximum value of the density is 4.08.
The minimum value of the density is 0.86.
First order method

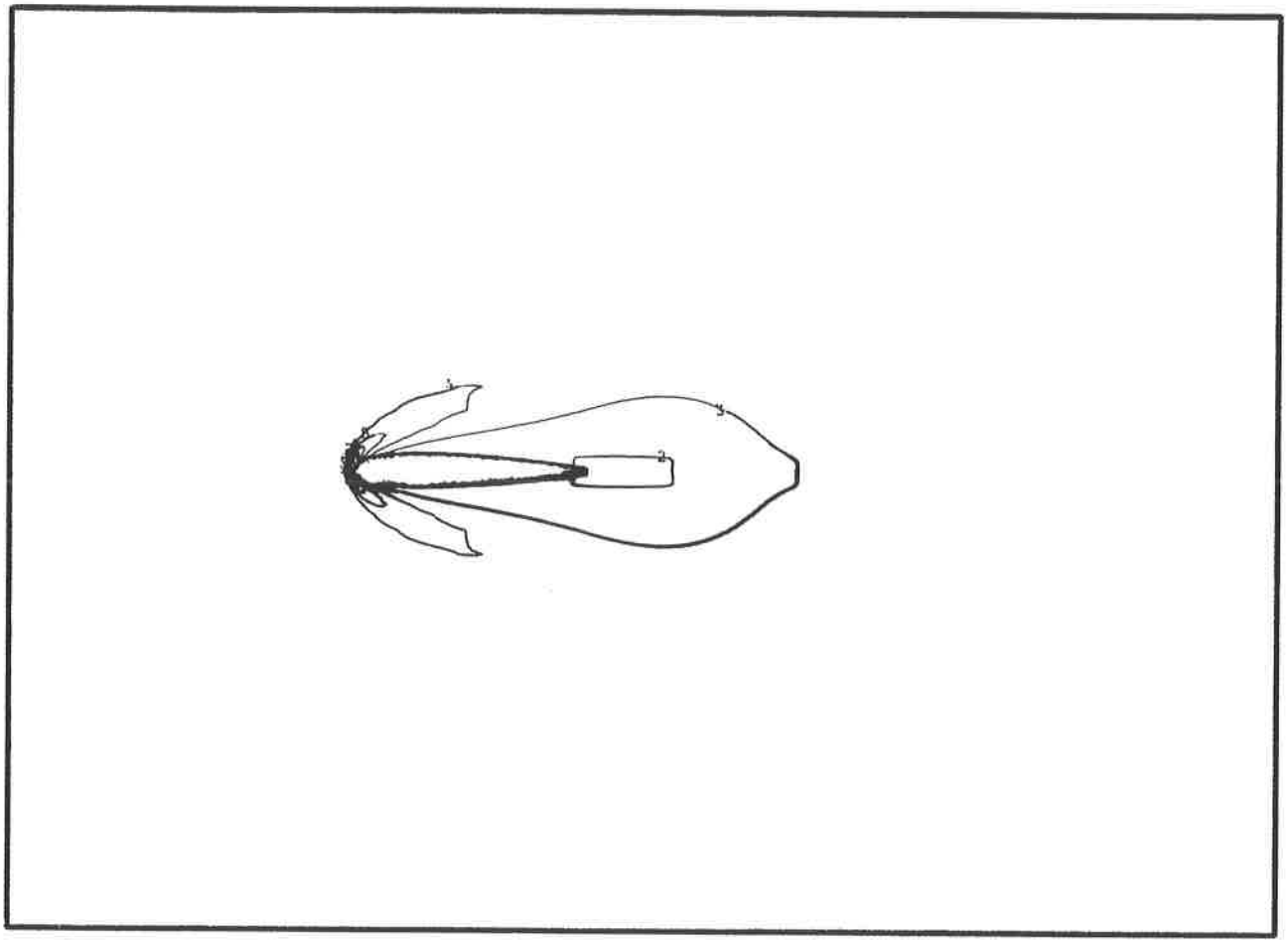

Figure 30

NACA0012 Aerofoil

Entropy deviation for the NACA0012 aerofoil
in a Mach 3.00 flow. The angle of attack is 0.0 degrees.
Solution is shown after 400 time-steps and the maximum CFL no. is 0.349.
The maximum value of the entropy deviation is 1.17.
The minimum value of the entropy deviation is 0.00.
First order method

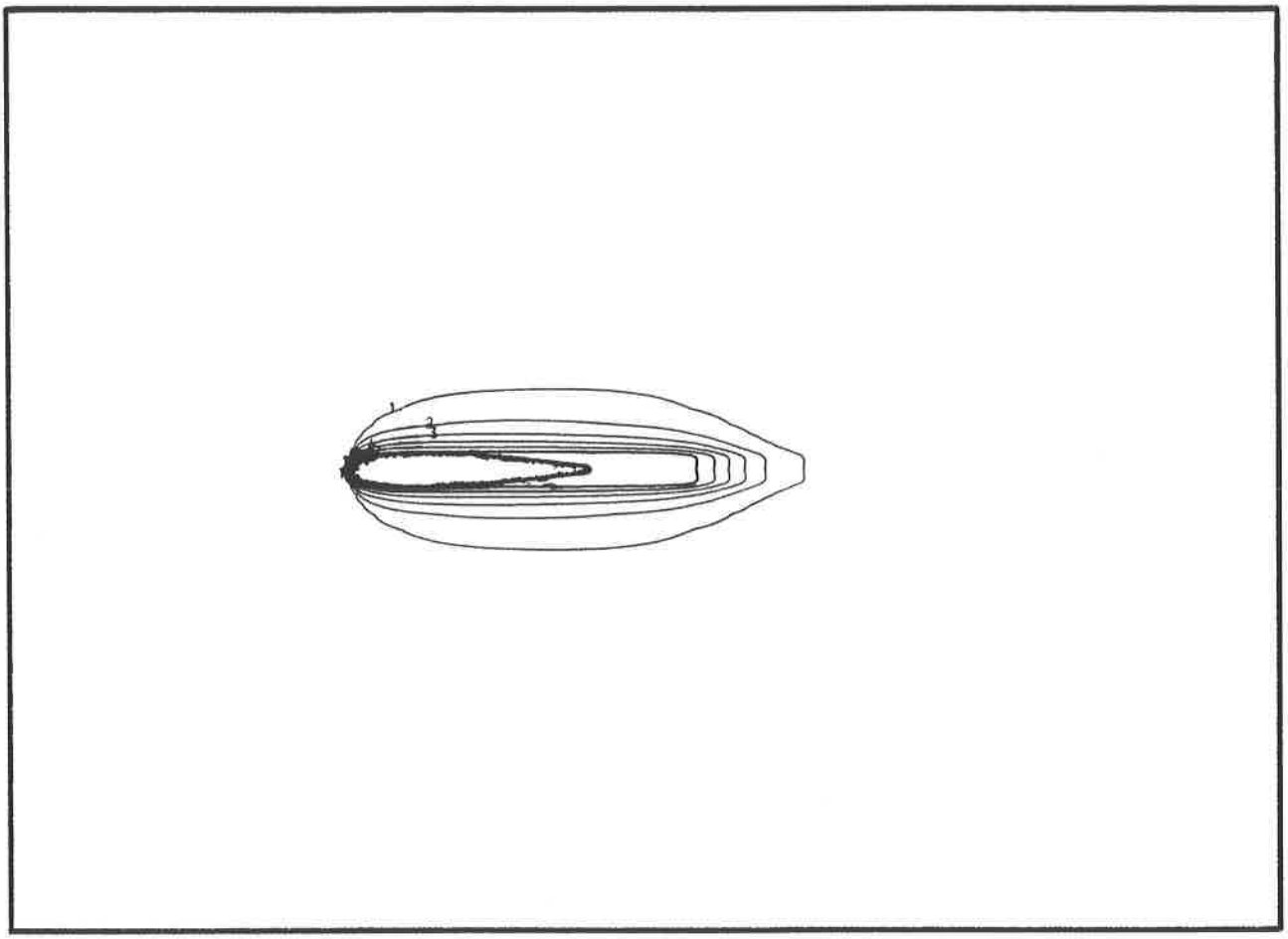

Figure 31

NACA0012 Aerofoil

Surface pressure deviation along NACA0012 aerofoil
in a Mach 3.00 flow. The angle of attack is 0.0 degrees.
Solution is shown after 400 time-steps and the maximum CFL no. is 0.349.
The maximum value of the pressure is 8.63.
The minimum value of the pressure is 0.90.
C_L = 0.0000.
C_D = 0.0120.
First order method

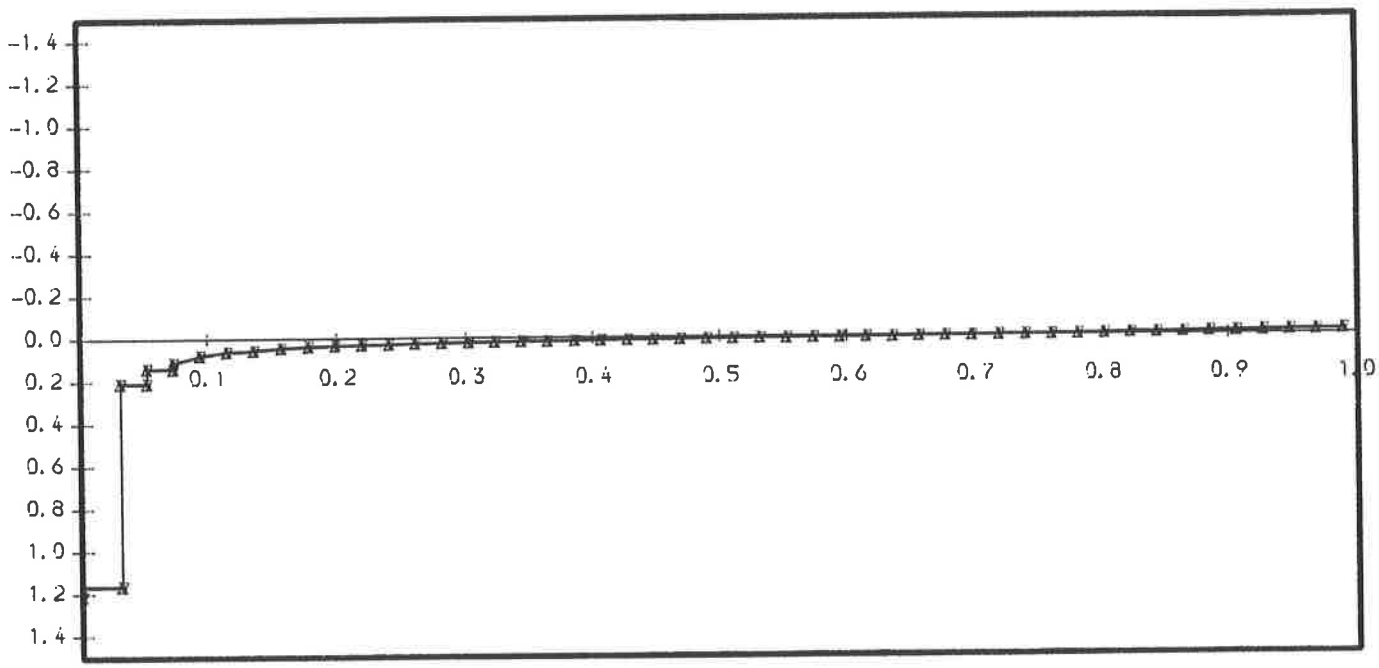

Figure 32

NACA0012 Aerofoil

Surface entropy deviation along NACA0012 aerofoil
in a Mach 3.00 flow. The angle of attack is 0.0 degrees.
Solution is shown after 400 time-steps and the maximum CFL no. is 0.349.
The maximum value of the entropy deviation is 1.01.
The minimum value of the entropy deviation is 0.62.
First order method

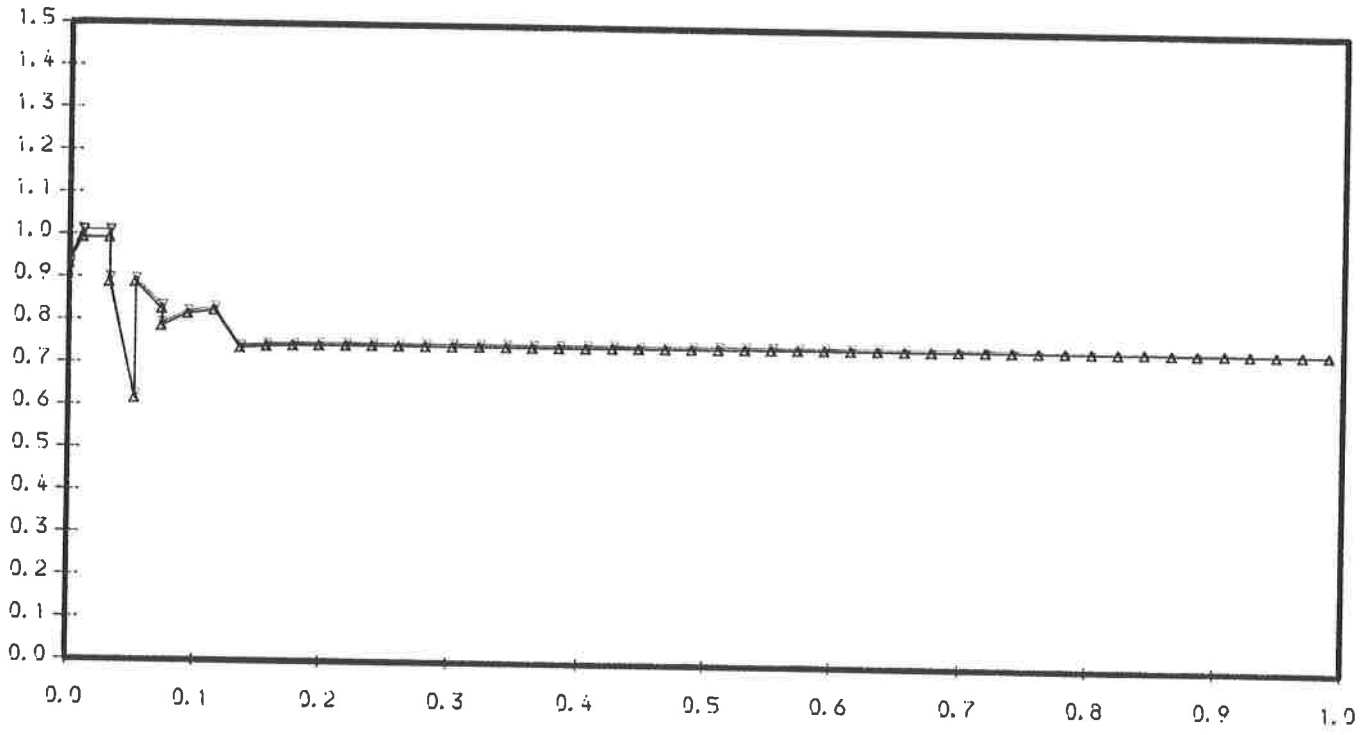

Figure 33

NACA0012 Aerofoil

Density contours for the NACA0012 aerofoil
in a Mach 3.00 flow. The angle of attack is 5.0 degrees.
Solution is shown after 400 time-steps and the maximum CFL no. is 0.365.
The maximum value of the density is 4.09.
The minimum value of the density is 0.64.
First order method

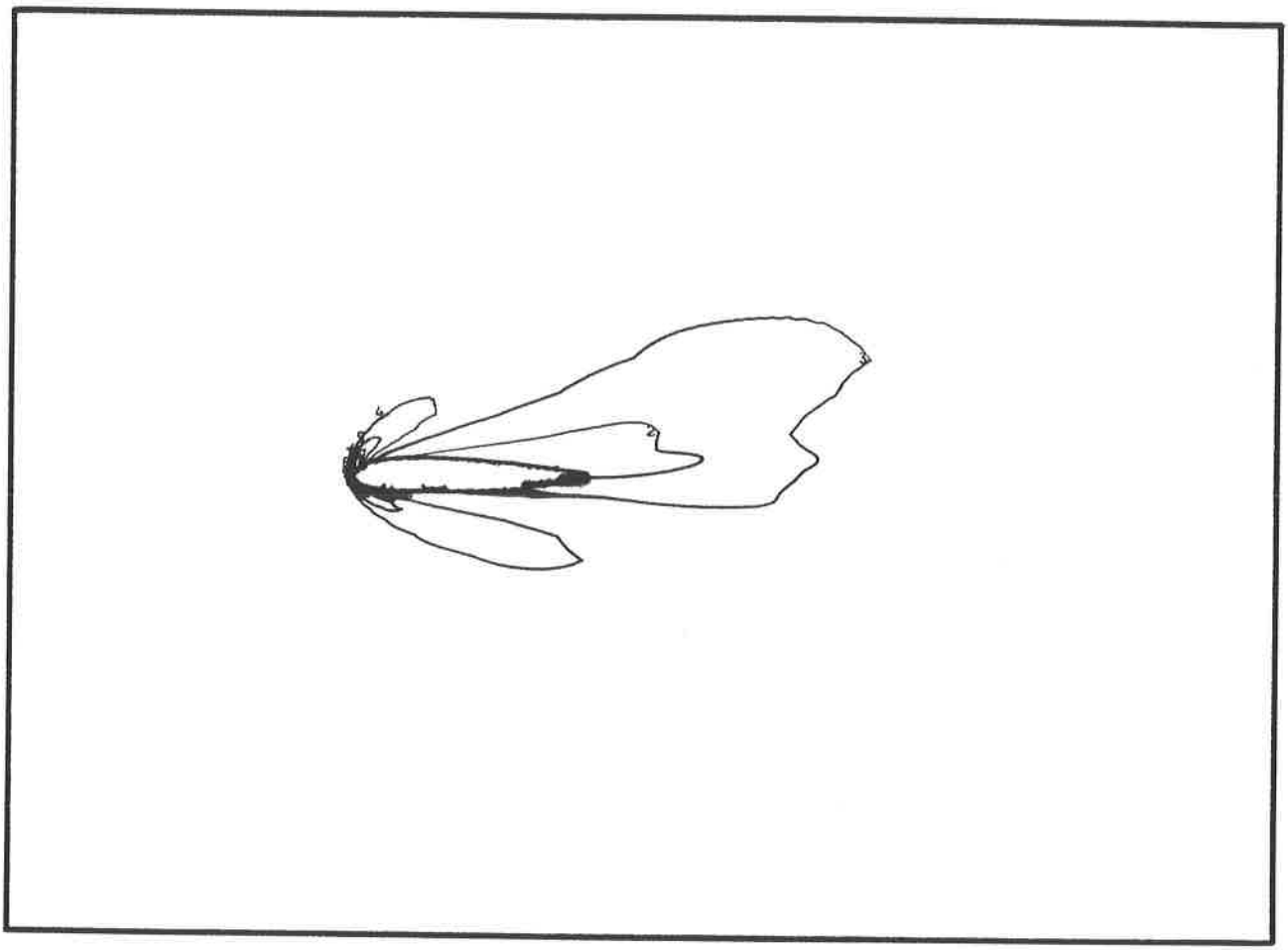

Figure 34

NACA0012 Aerofoil

Entropy deviation for the NACA0012 aerofoil
in a Mach 3.00 flow. The angle of attack is 5.0 degrees.
Solution is shown after 400 time-steps and the maximum CFL no. is 0.365.
The maximum value of the entropy deviation is 1.27.
The minimum value of the entropy deviation is 0.00.
First order method

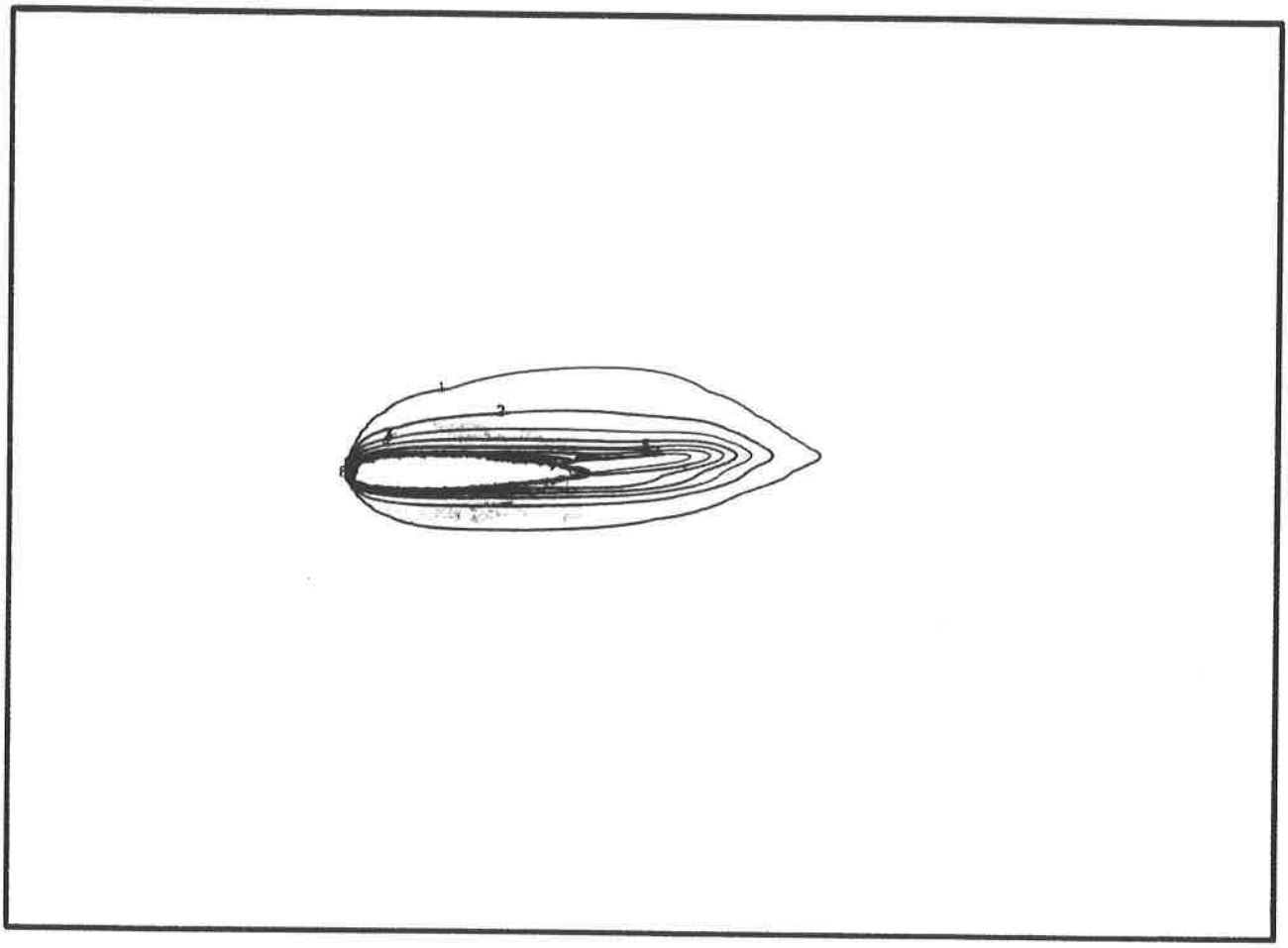

Figure 35

NACA0012 Aerofoil

Surface pressure deviation along NACA0012 aerofoil in a Mach 3.00 flow. The angle of attack is 5.0 degrees.

Solution is shown after 400 time-steps and the maximum CFL no. is 0.365.

The maximum value of the pressure is 8.53.

The minimum value of the pressure is 0.63.

C_L = 0.0954.

C_D = 0.0233.

First order method

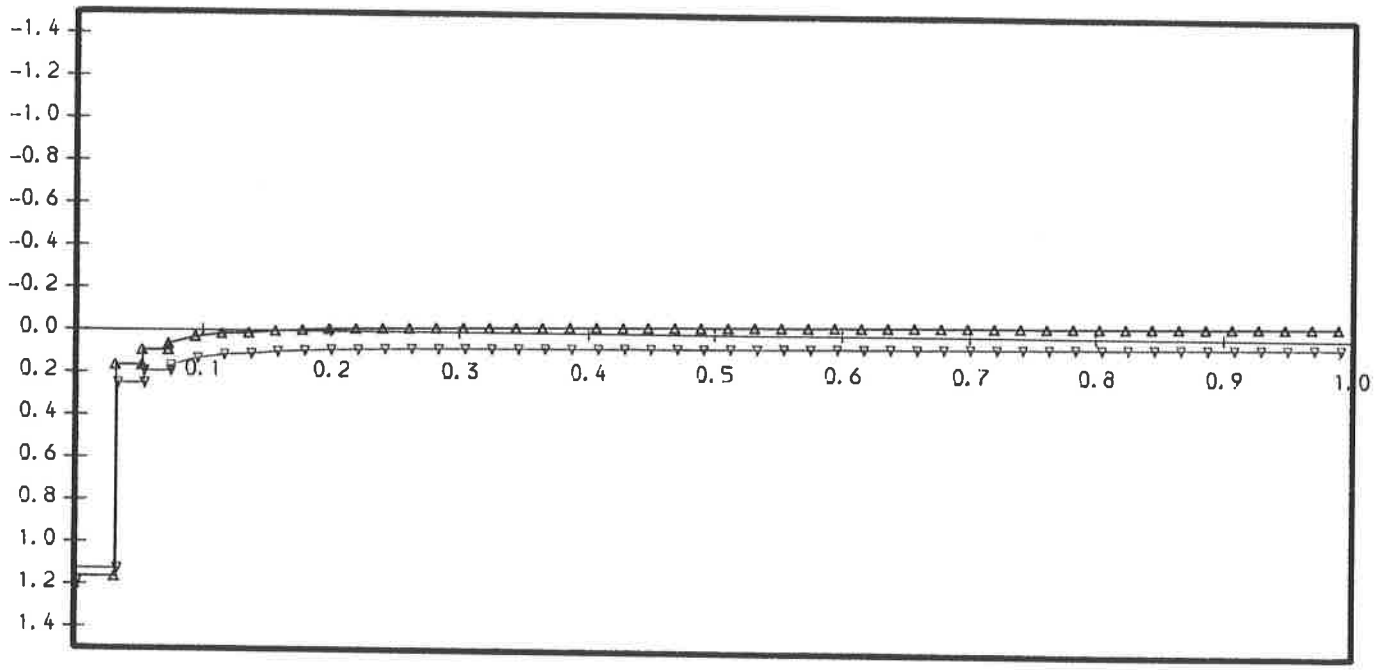

Figure 36

NACA0012 Aerofoil

Surface entropy deviation along NACA0012 aerofoil
in a Mach 3.00 flow. The angle of attack is 5.0 degrees.
Solution is shown after 400 time-steps and the maximum CFL no. is 0.365.
The maximum value of the entropy deviation is 1.08.
The minimum value of the entropy deviation is 0.59.
First order method

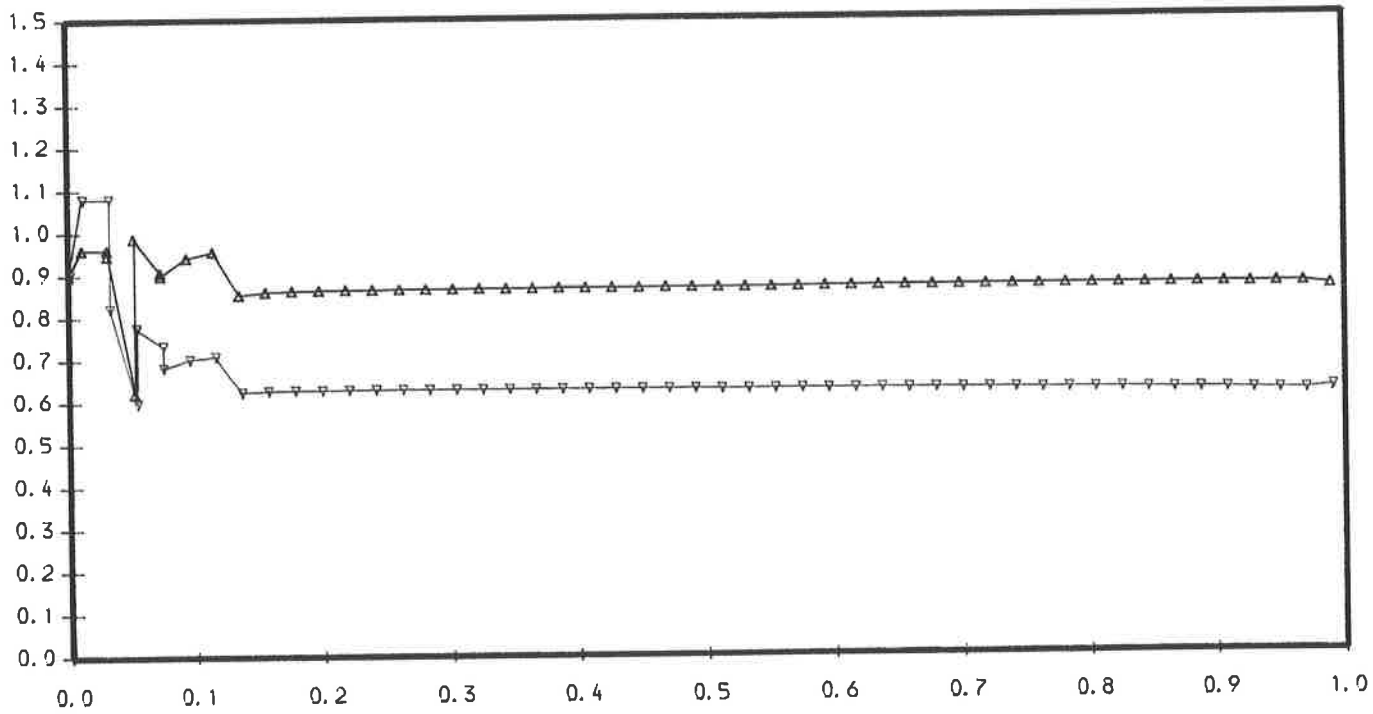

Figure 37

NACA0012 Aerofoil

Density contours for the NACA0012 aerofoil
in a Mach 3.00 flow. The angle of attack is 10.0 degrees.
Solution is shown after 400 time-steps and the maximum CFL no. is 0.380.
The maximum value of the density is 3.89.
The minimum value of the density is 0.47.
First order method

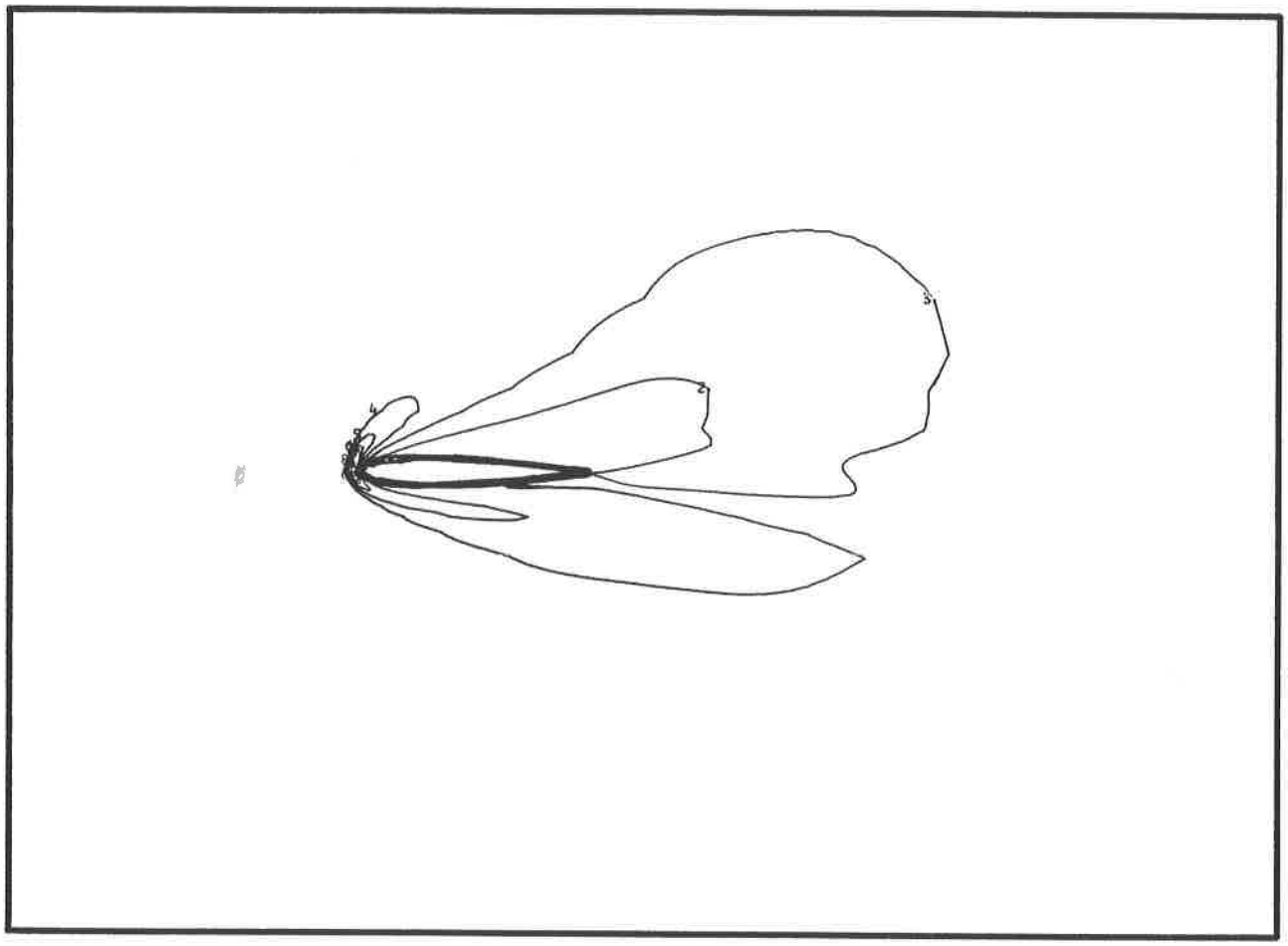

Figure 38

NACA0012 Aerofoil

Entropy deviation for the NACA0012 aerofoil
in a Mach 3.00 flow. The angle of attack is 10.0 degrees.
Solution is shown after 400 time-steps and the maximum CFL no. is 0.380.
The maximum value of the entropy deviation is 1.39.
The minimum value of the entropy deviation is 0.00.
First order method

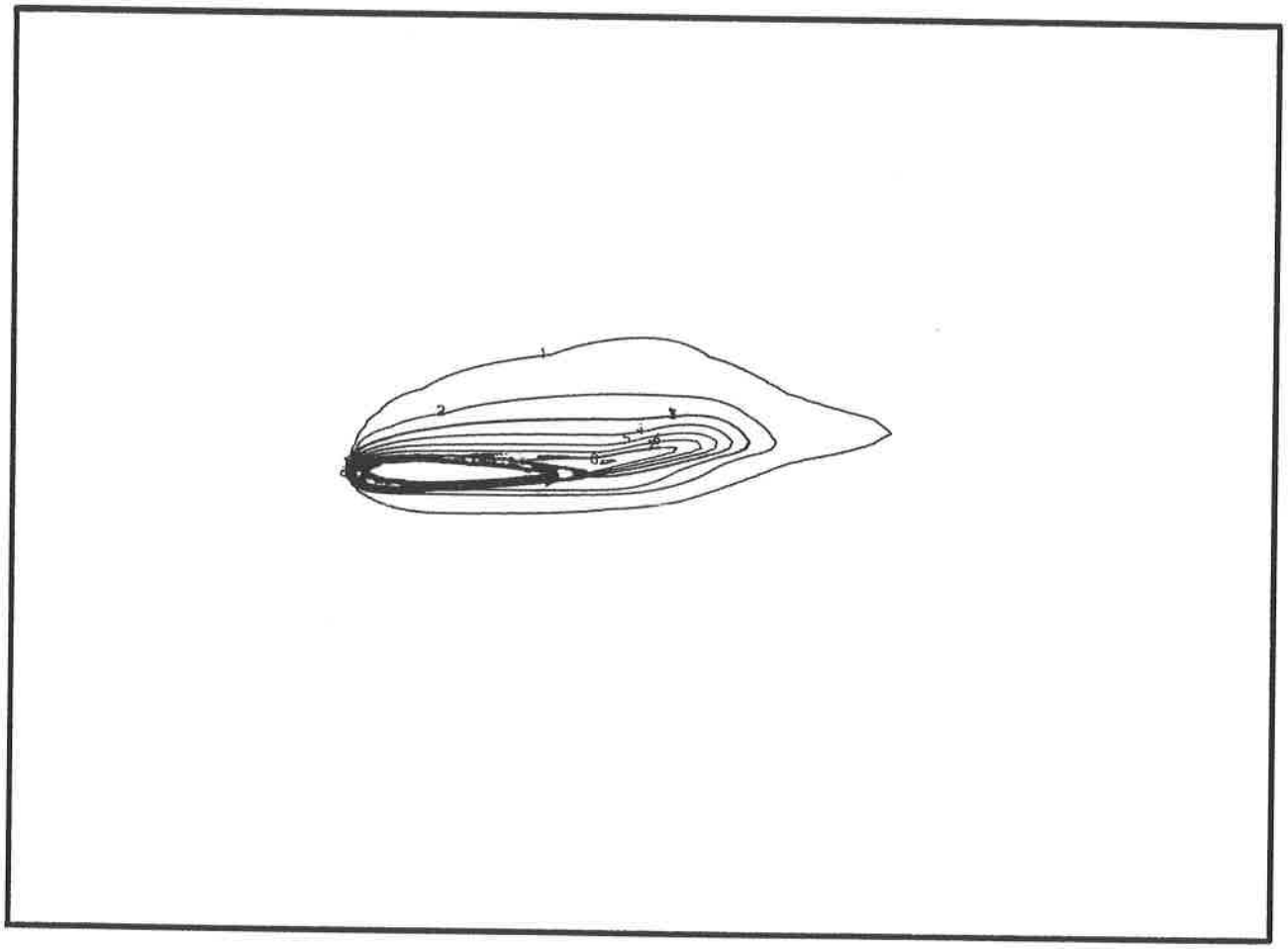

Figure 39

NACA0012 Aerofoil

Surface pressure deviation along NACA0012 aerofoil
in a Mach 3.00 flow. The angle of attack is 10.0 degrees.
Solution is shown after 400 time-steps and the maximum CFL no. is 0.380.
The maximum value of the pressure is 8.06.
The minimum value of the pressure is 0.44.
C_L = 0.1985.
C_D = 0.0531.
First order method

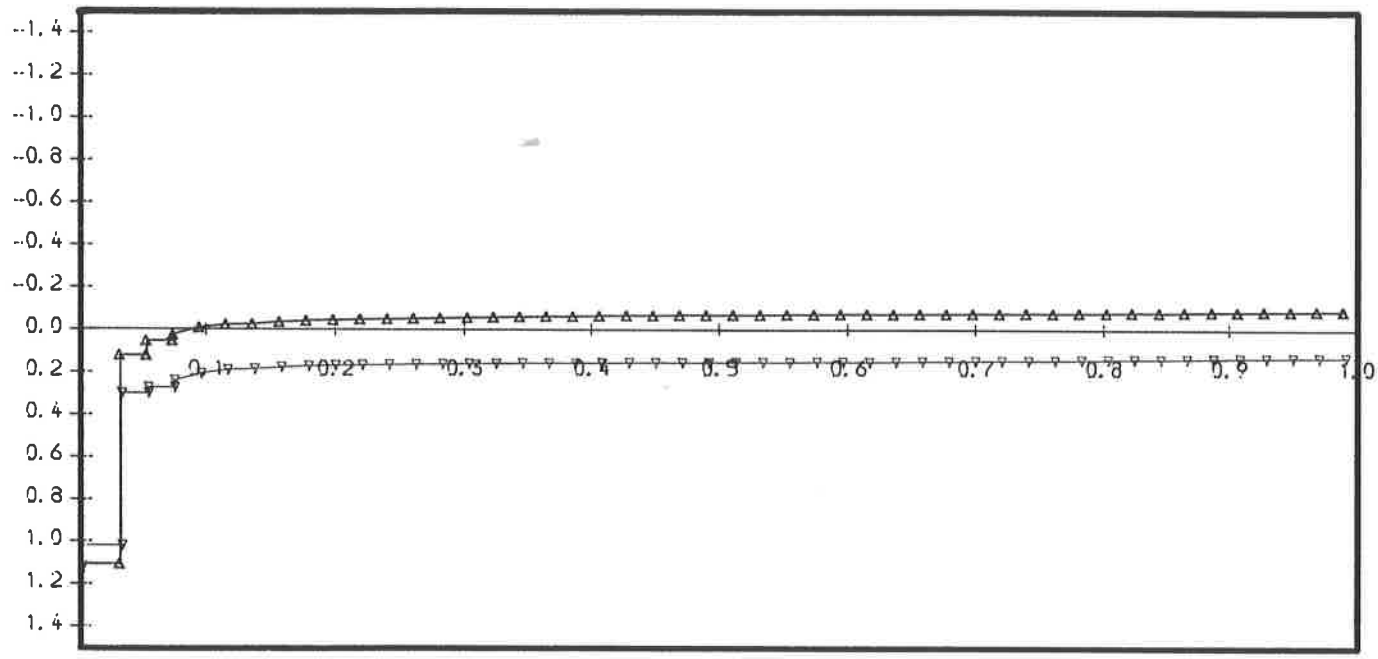

Figure 40

NACA0012 Aerofoil

Surfece entropy deviation along NACA0012 aerofoil
in a Mach 3.00 flow. The angle of attack is 10.0 degrees.
Solution is shown after 400 time-steps and the maximum CFL no. is 0.380.
The maximum value of the entropy deviation is 1.17.
The minimum value of the entropy deviation is 0.43.
First order method

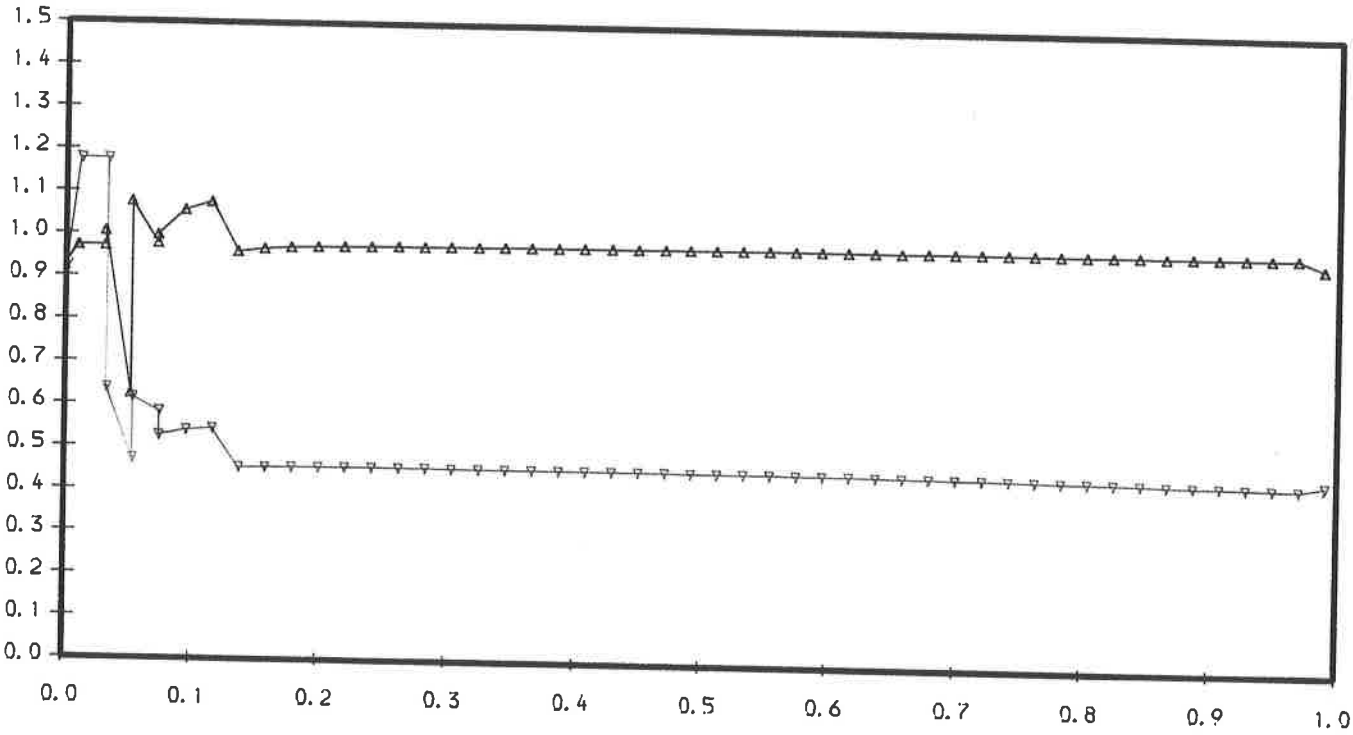

Figure 41

NACA0012 Aerofoil

Density contours for the NACA0012 aerofoil
in a Mach 3.00 flow. The angle of attack is 15.0 degrees.
Solution is shown after 400 time-steps and the maximum CFL no. is 0.401.
The maximum value of the density is 3.77.
The minimum value of the density is 0.34.
First order method

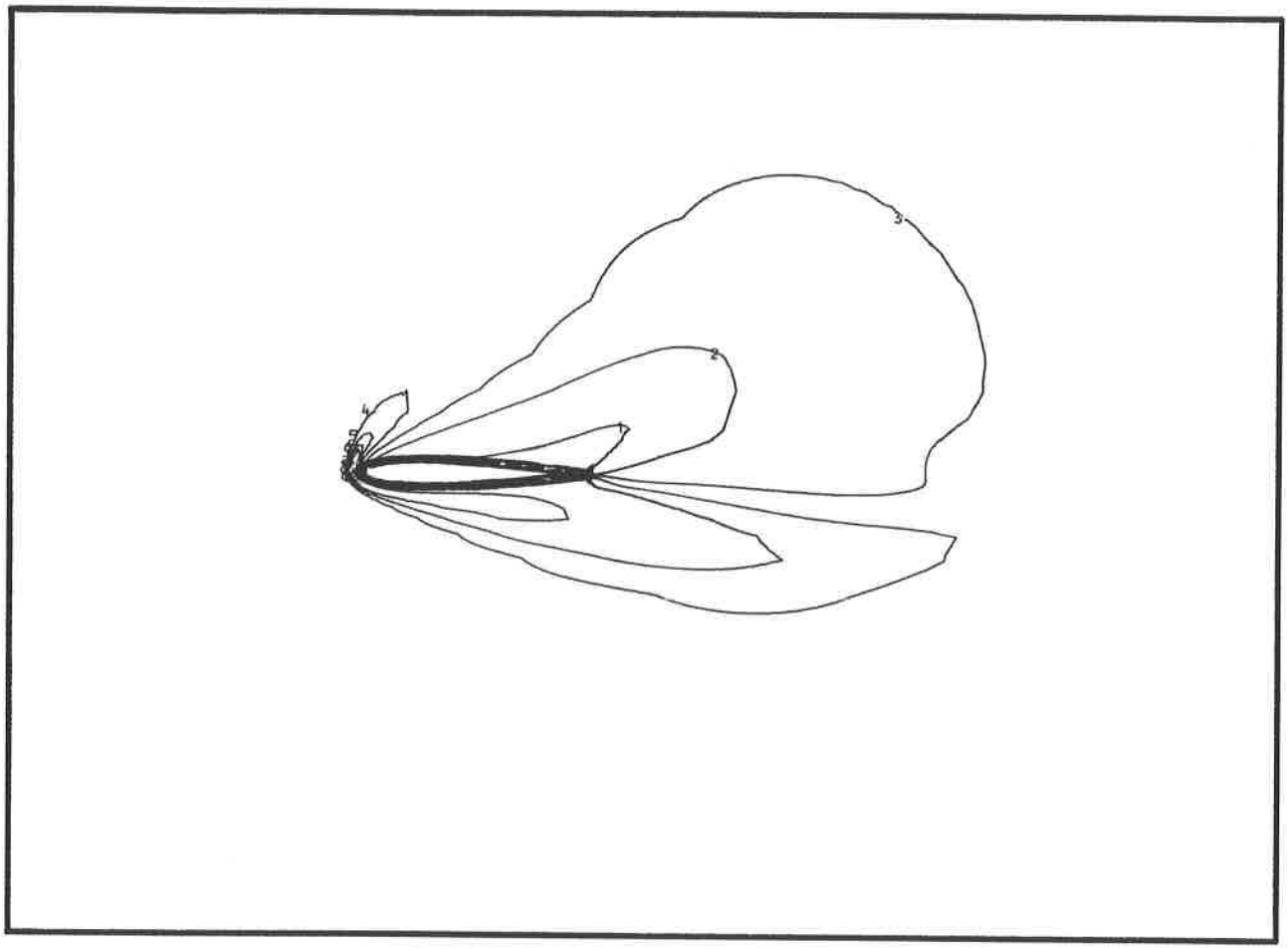

Figure 42

NACA0012 Aerofoil

Entropy deviation for the NACA0012 aerofoil
In a Mach 3.00 flow. The angle of attack is 15.0 degrees.
Solution is shown after 400 time-steps and the maximum CFL no. is 0.401.
The maximum value of the entropy deviation is 1.55.
The minimum value of the entropy deviation is 0.00.
First order method

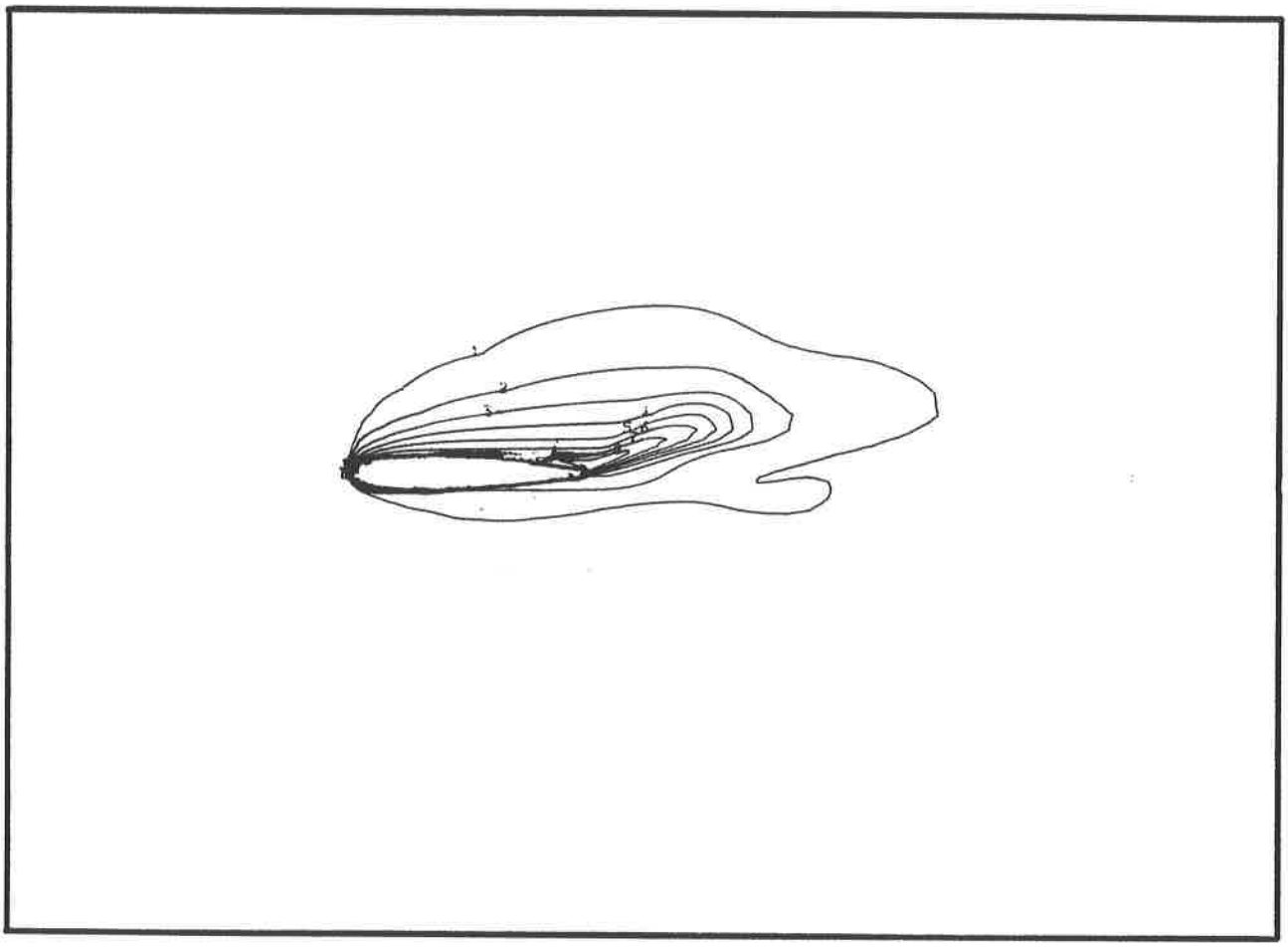

Figure 43

NACA0012 Aerofoil

Surface pressure deviation along NACA0012 aerofoil
in a Mach 3.00 flow. The angle of attack is 15.0 degrees.
Solution is shown after 400 time-steps and the maximum CFL no. is 0.401.
The maximum value of the pressure is 7.97.
The minimum value of the pressure is 0.30.
C_L = 0.3168.
C_D = 0.1063.
First order method

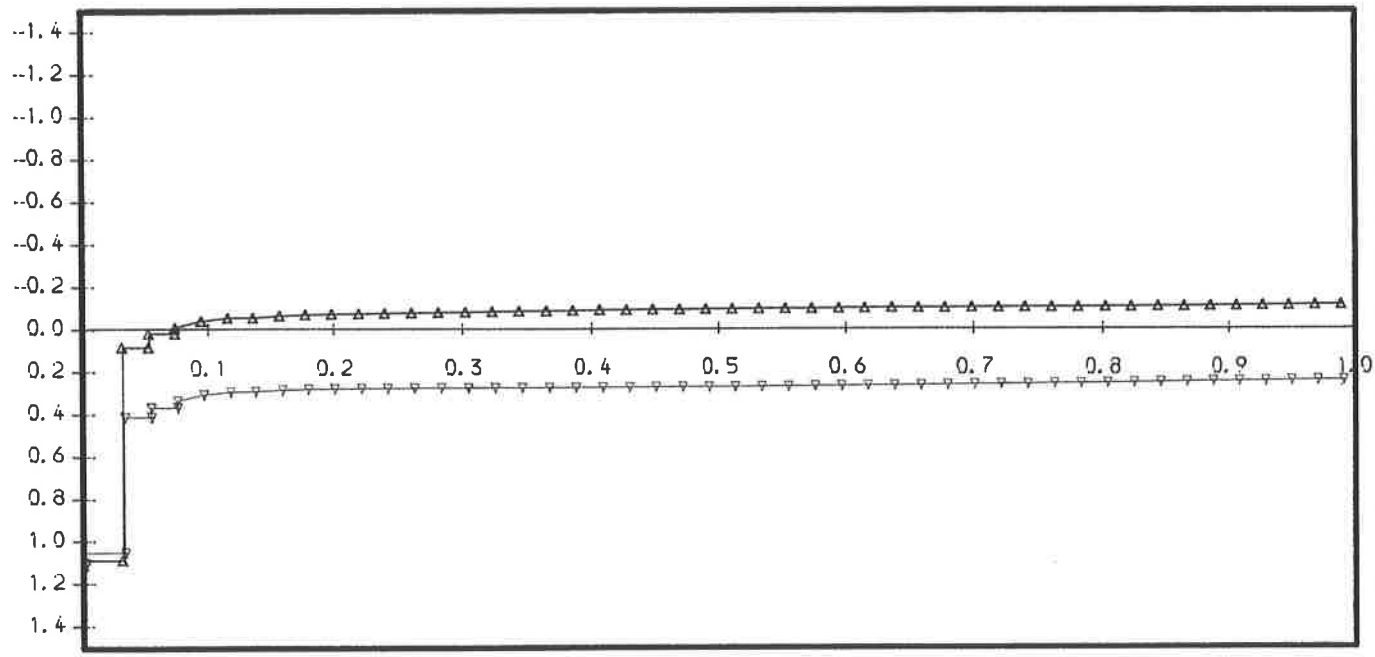

Figure 44

NACA0012 Aerofoil

Surfece entropy deviation along NACA0012 aerofoil
in a Mach 3.00 flow. The angle of attack is 15.0 degrees.
Solution is shown after 400 time-steps and the maximum CFL no. is 0.401.
The maximum value of the entropy deviation is 1.25.
The minimum value of the entropy deviation is 0.32.
First order method

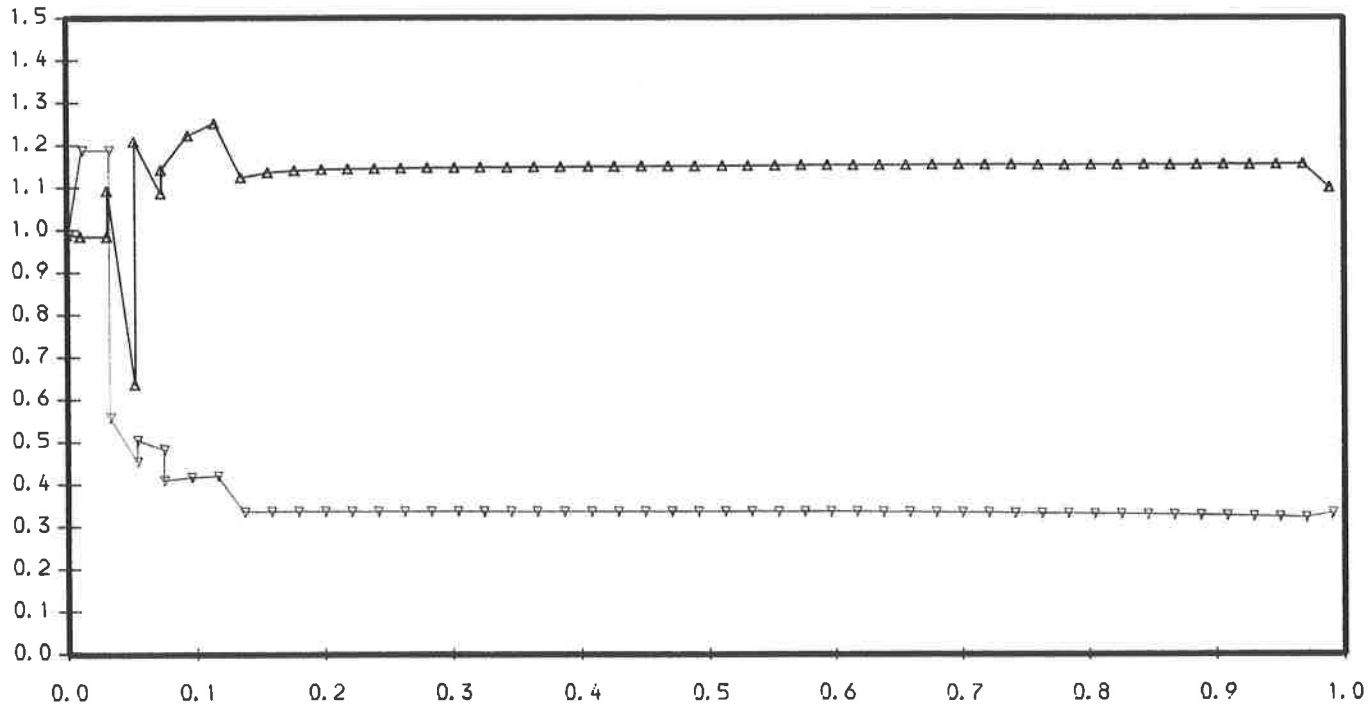

Figure 45

NACA0012 Aerofoil

Density contours for the NACA0012 aerofoil
in a Mach 3.00 flow. The angle of attack is 20.0 degrees.
Solution is shown after 400 time-steps and the maximum CFL no. is 0.420.
The maximum value of the density is 3.77.
The minimum value of the density is 0.25.
First order method

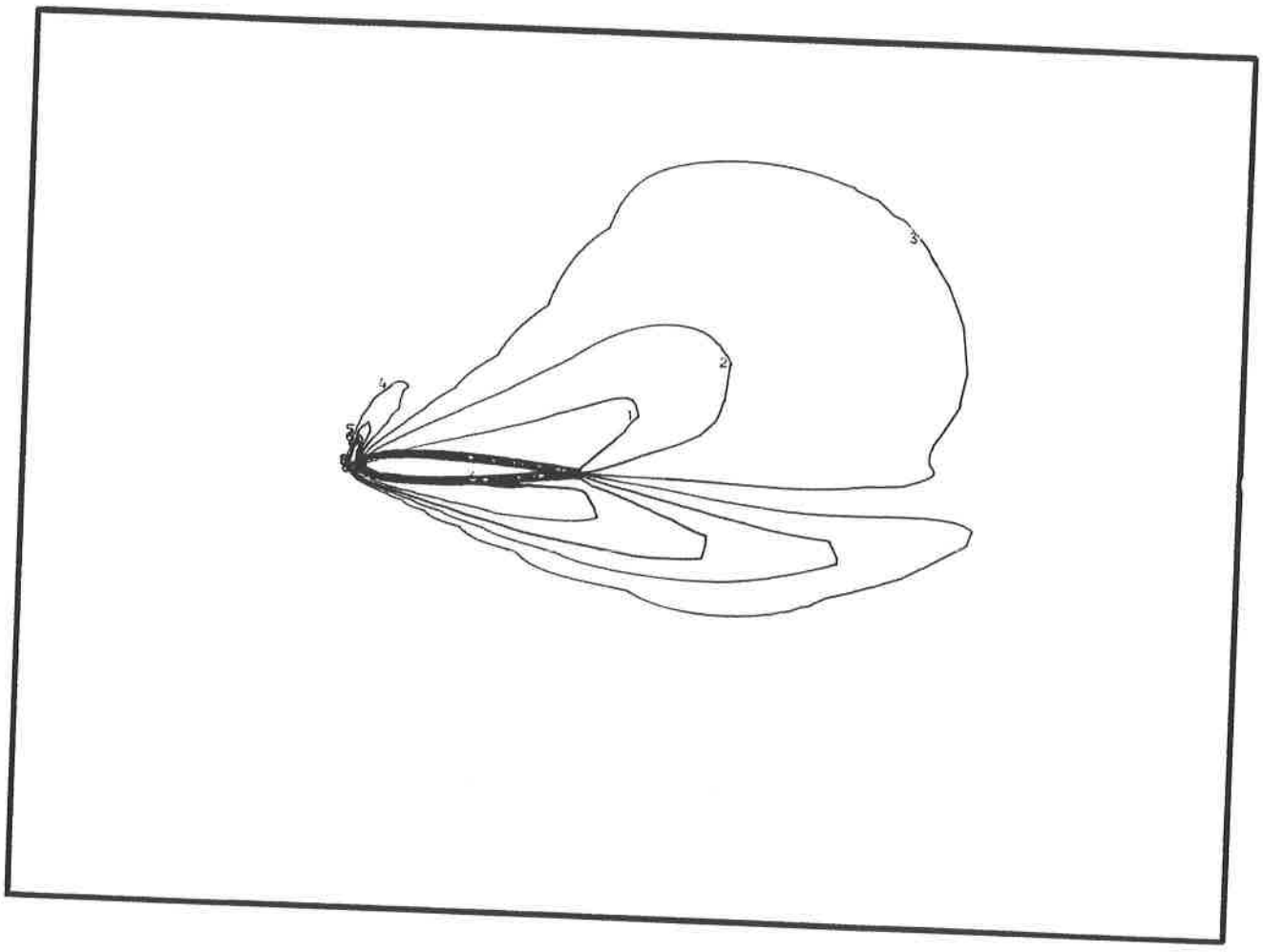

Figure 46

NACA0012 Aerofoil

Entropy deviation for the NACA0012 aerofoil
in a Mach 3.00 flow. The angle of attack is 20.0 degrees.
Solution is shown after 400 time-steps and the maximum CFL no. is 0.420.
The maximum value of the entropy deviation is 1.72.
The minimum value of the entropy deviation is 0.00.
First order method

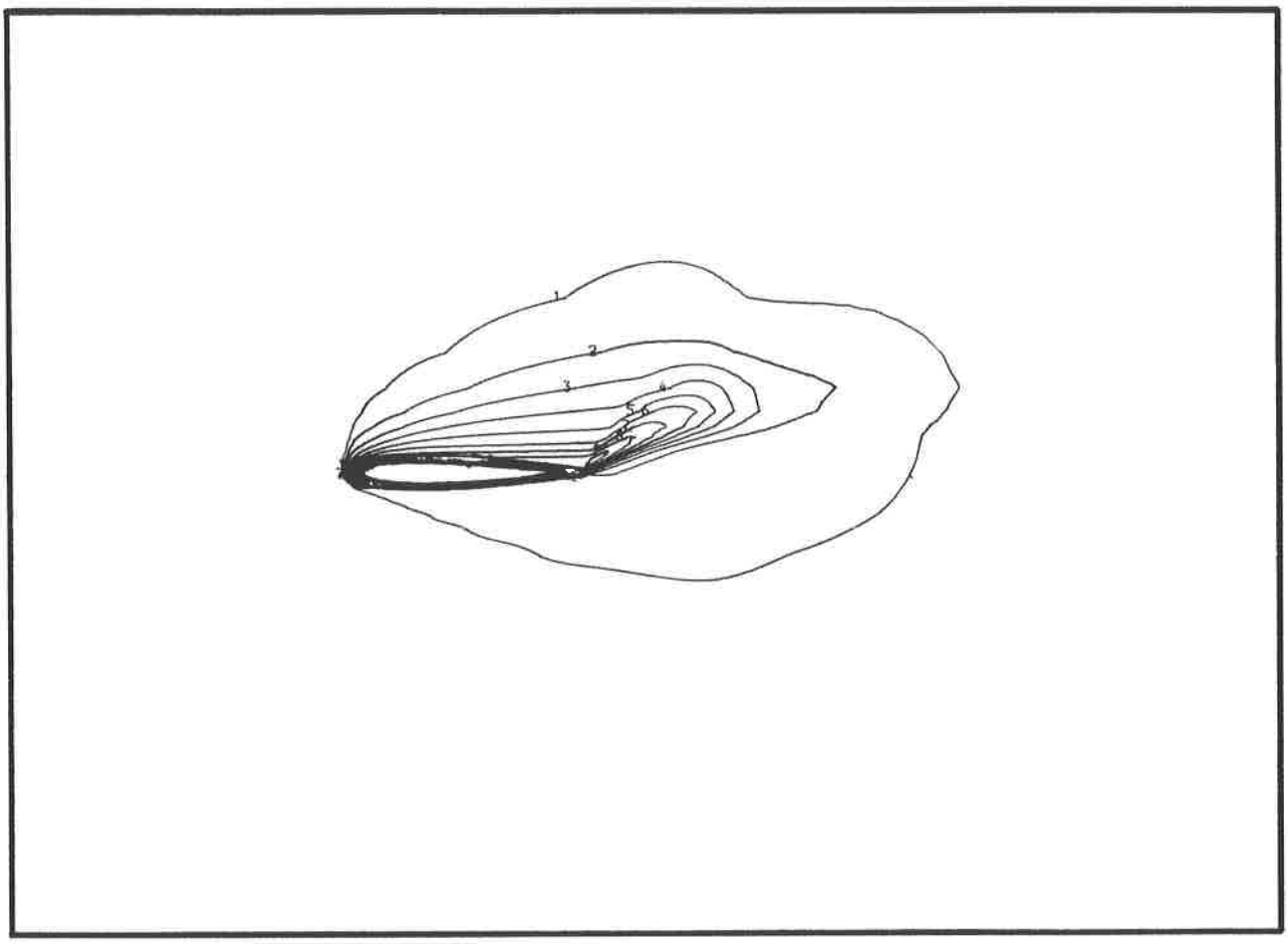

Figure 47

NACA0012 Aerofoil

Surface pressure deviation along NACA0012 aerofoil
in a Mach 3.00 flow. The angle of attack is 20.0 degrees.
Solution is shown after 400 time-steps and the maximum CFL no. is 0.420.
The maximum value of the pressure is 7.94.
The minimum value of the pressure is 0.21.
C_L = 0.4452.
C_D = 0.1879.
First order method

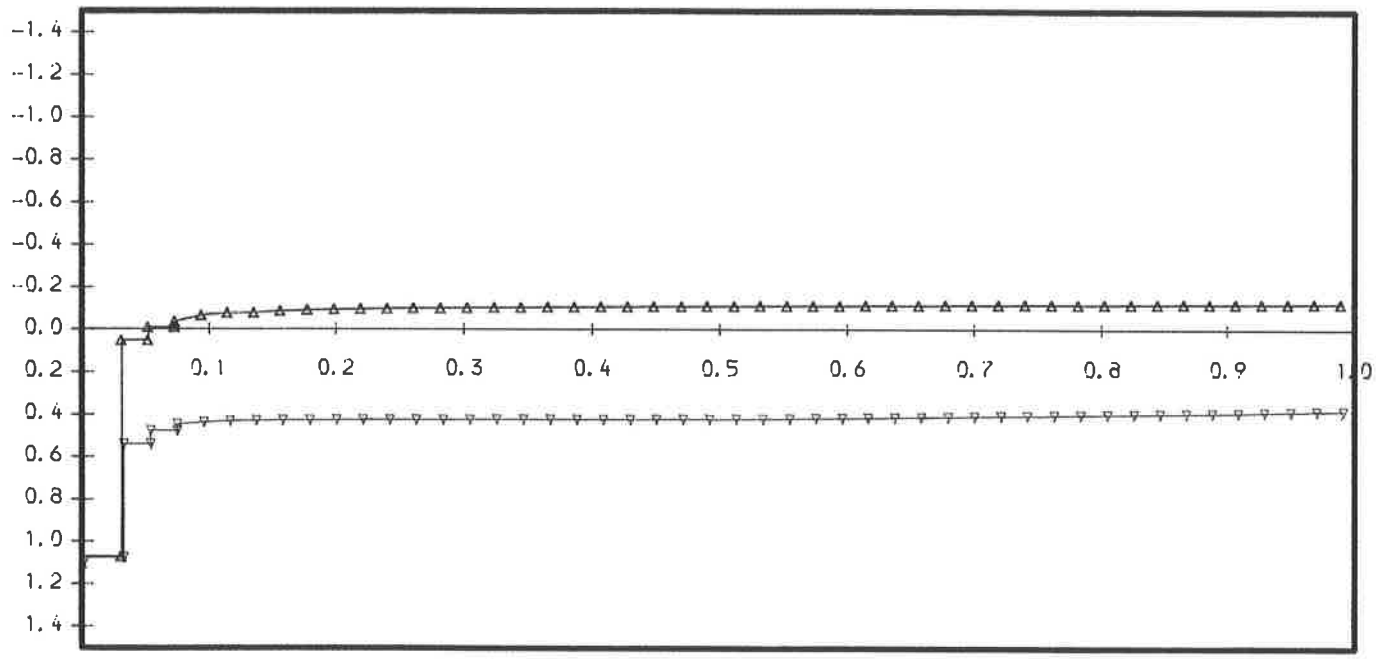

Figure 48

NACA0012 Aerofoil

Surface entropy deviation along NACA0012 aerofoil
in a Mach 3.00 flow. The angle of attack is 20.0 degrees.
Solution is shown after 400 time-steps and the maximum CFL no. is 0.420.
The maximum value of the entropy deviation is 1.45.
The minimum value of the entropy deviation is 0.20.
First order method

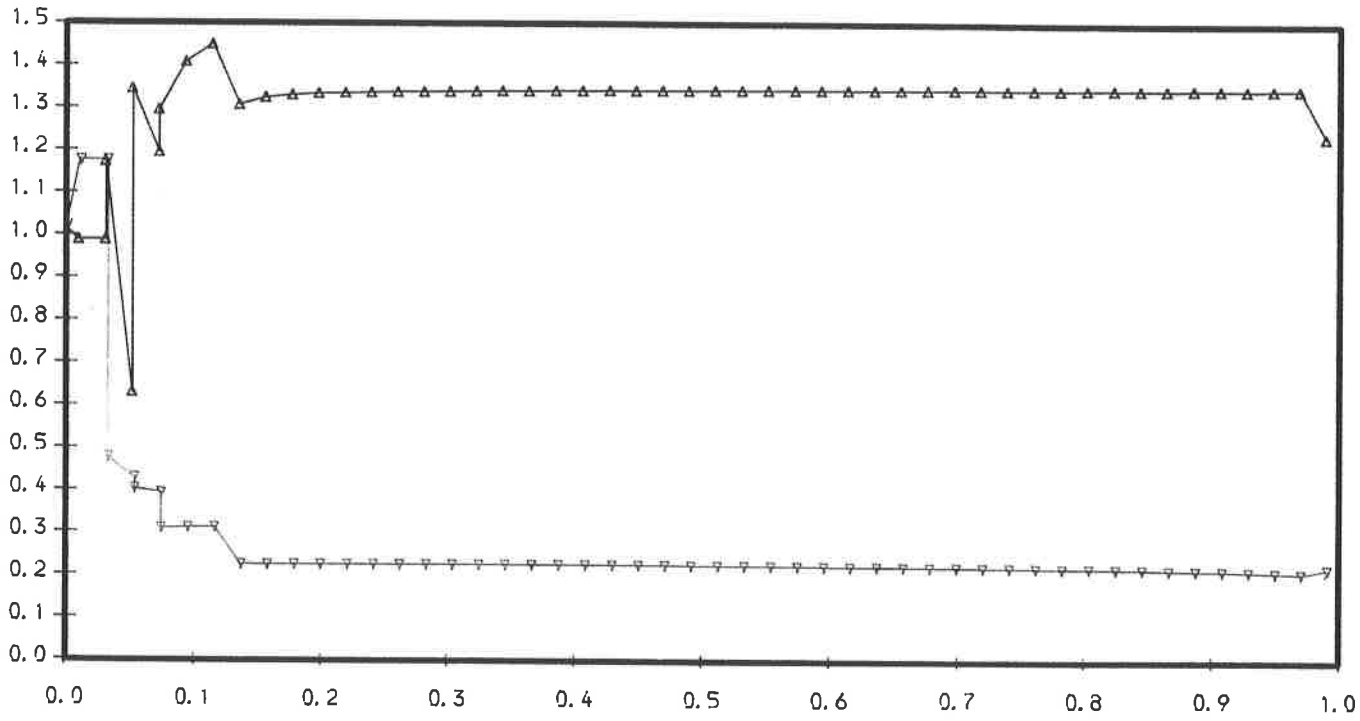

Figure 49

NACA0012 Aerofoil

Density contours for the NACA0012 aerofoil
in a Mach 3.00 flow. The angle of attack is 5.0 degrees.
Solution is shown after 100 time-steps and the maximum CFL no. is 0.855.
The maximum value of the density is 3.46.
The minimum value of the density is 0.67.
First order method

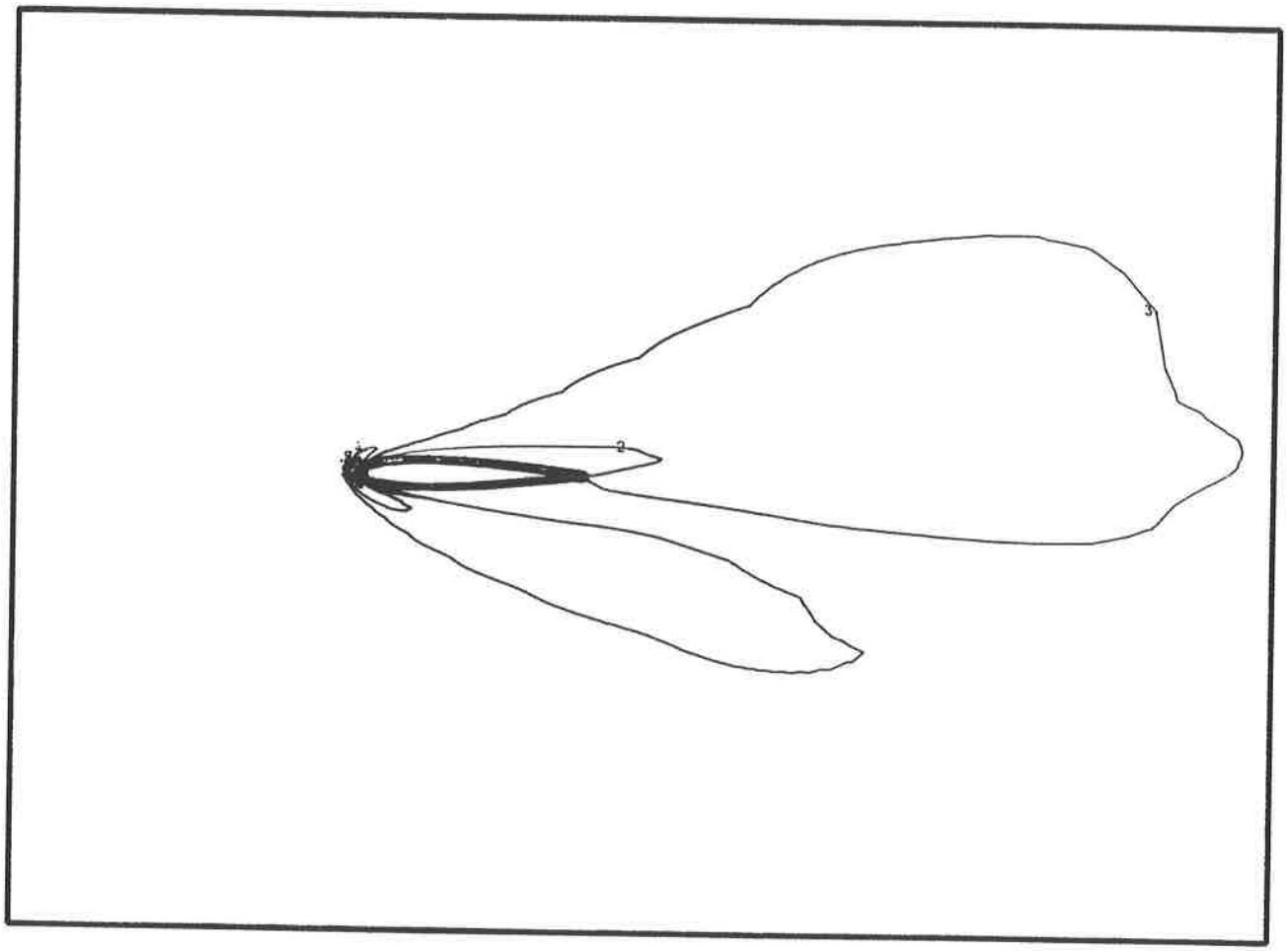

Figure 50

NACA0012 Aerofoil

Entropy deviation for the NACA0012 aerofoil
in a Mach 3.00 flow. The angle of attack is 5.0 degrees.
Solution is shown after 100 time-steps and the maximum CFL no. is 0.855.
The maximum value of the entropy deviation is 1.30.
The minimum value of the entropy deviation is 0.00.
First order method

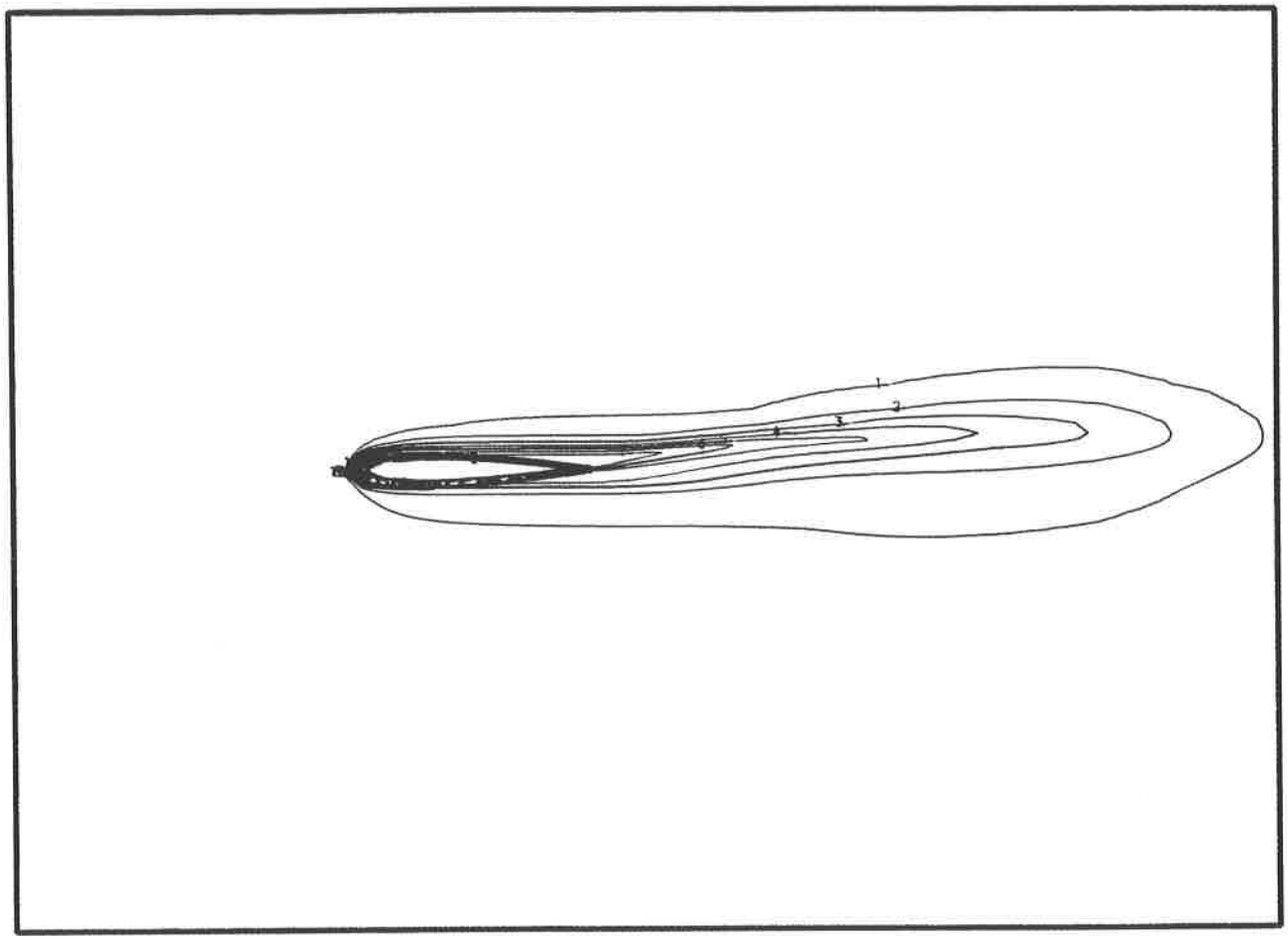

Figure 51

NACA0012 Aerofoil

Density contours for the NACA0012 aerofoil
in a Mach 3.00 flow. The angle of attack is 5.0 degrees.
Solution is shown after 200 time-steps and the maximum CFL no. is 0.852.
The maximum value of the density is 3.46.
The minimum value of the density is 0.67.
First order method

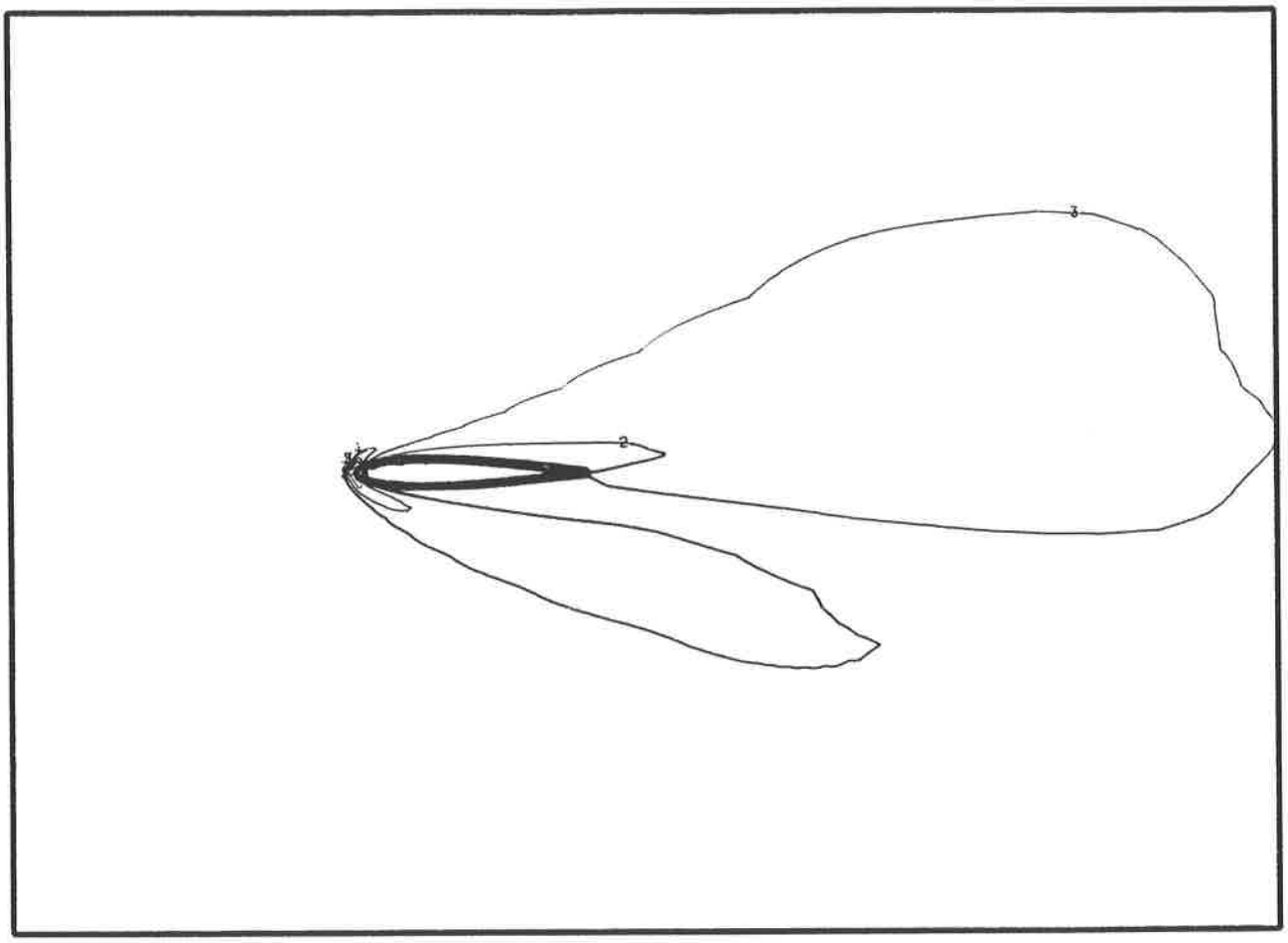

Figure 52

NACA0012 Aerofoil

Entropy deviation for the NACA0012 aerofoil
in a Mach 3.00 flow. The angle of attack is 5.0 degrees.
Solution is shown after 200 time-steps and the maximum CFL no. is 0.852.
The maximum value of the entropy deviation is 1.30.
The minimum value of the entropy deviation is 0.00.
First order method

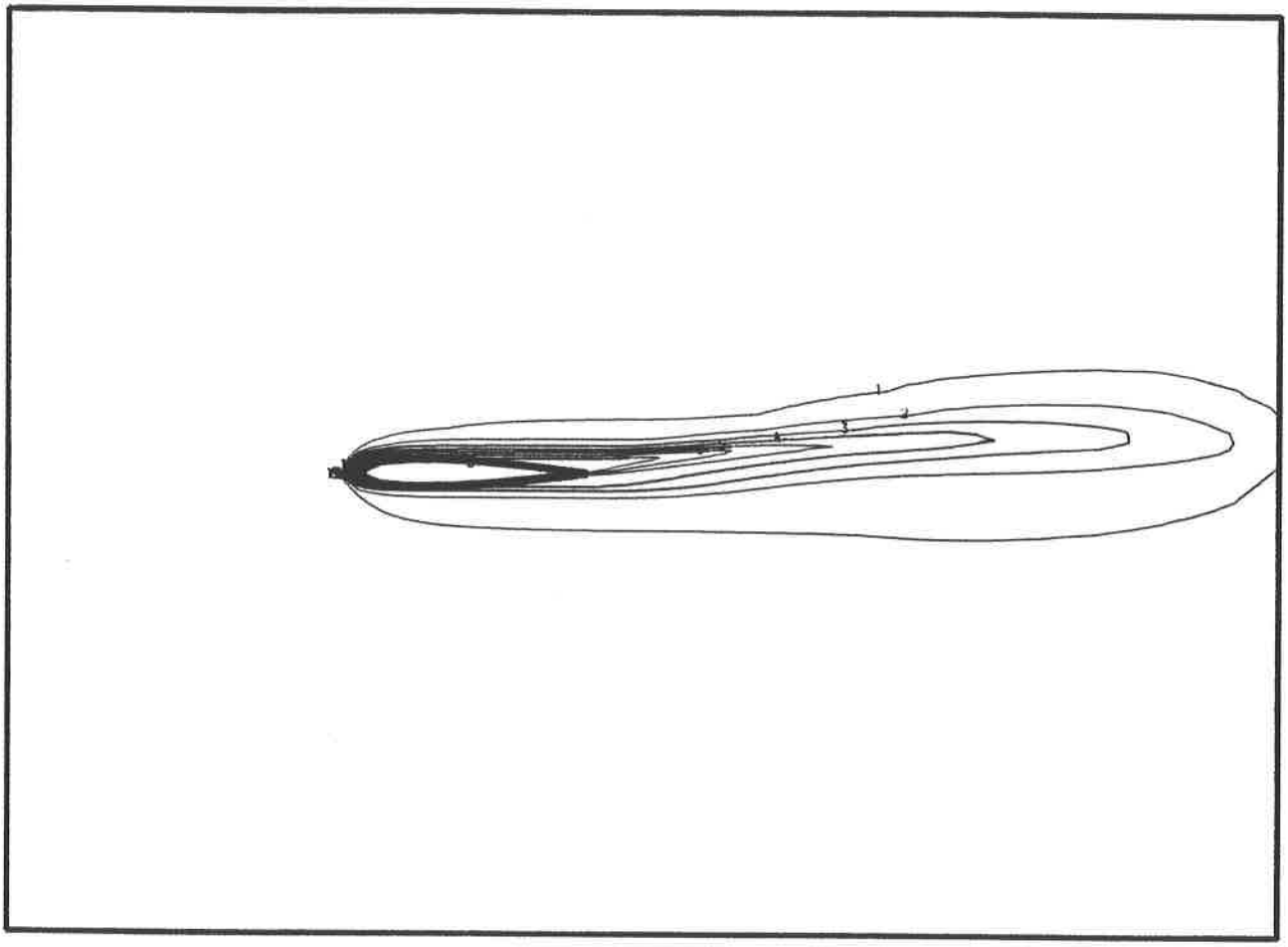

Figure 53

NACA0012 Aerofoil

Density contours for the NACA0012 aerofoil
in a Mach 3.00 flow. The angle of attack is 5.0 degrees.
Solution is shown after 300 time-steps and the maximum CFL no. is 0.852.
The maximum value of the density is 3.46.
The minimum value of the density is 0.67.
First order method

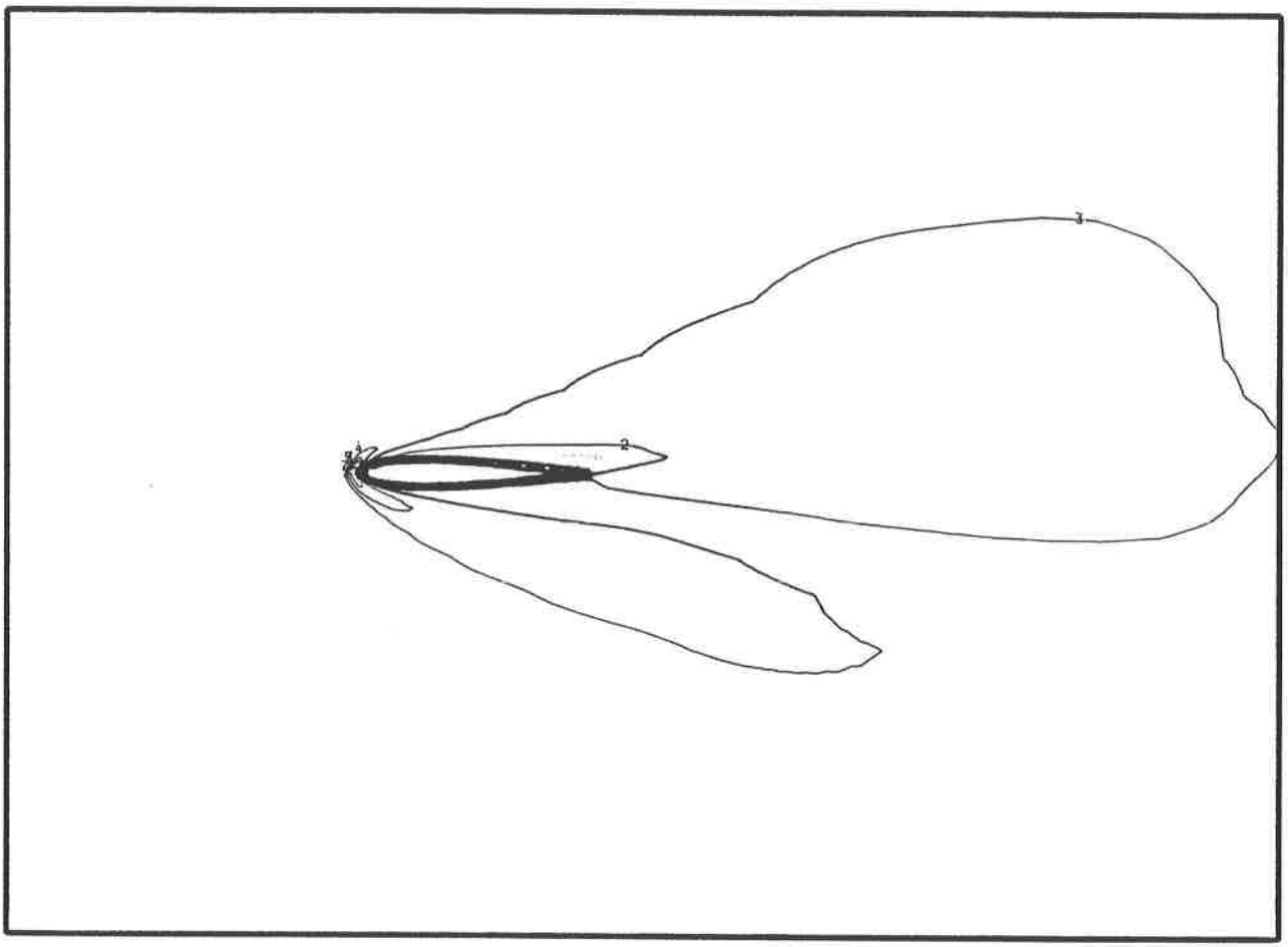

Figure 54

NACA0012 Aerofoil

Entropy deviation for the NACA0012 aerofoil
in a Mach 3.00 flow. The angle of attack is 5.0 degrees.
Solution is shown after 300 time-steps and the maximum CFL no. is 0.852.
The maximum value of the entropy deviation is 1.30.
The minimum value of the entropy deviation is 0.00.
First order method

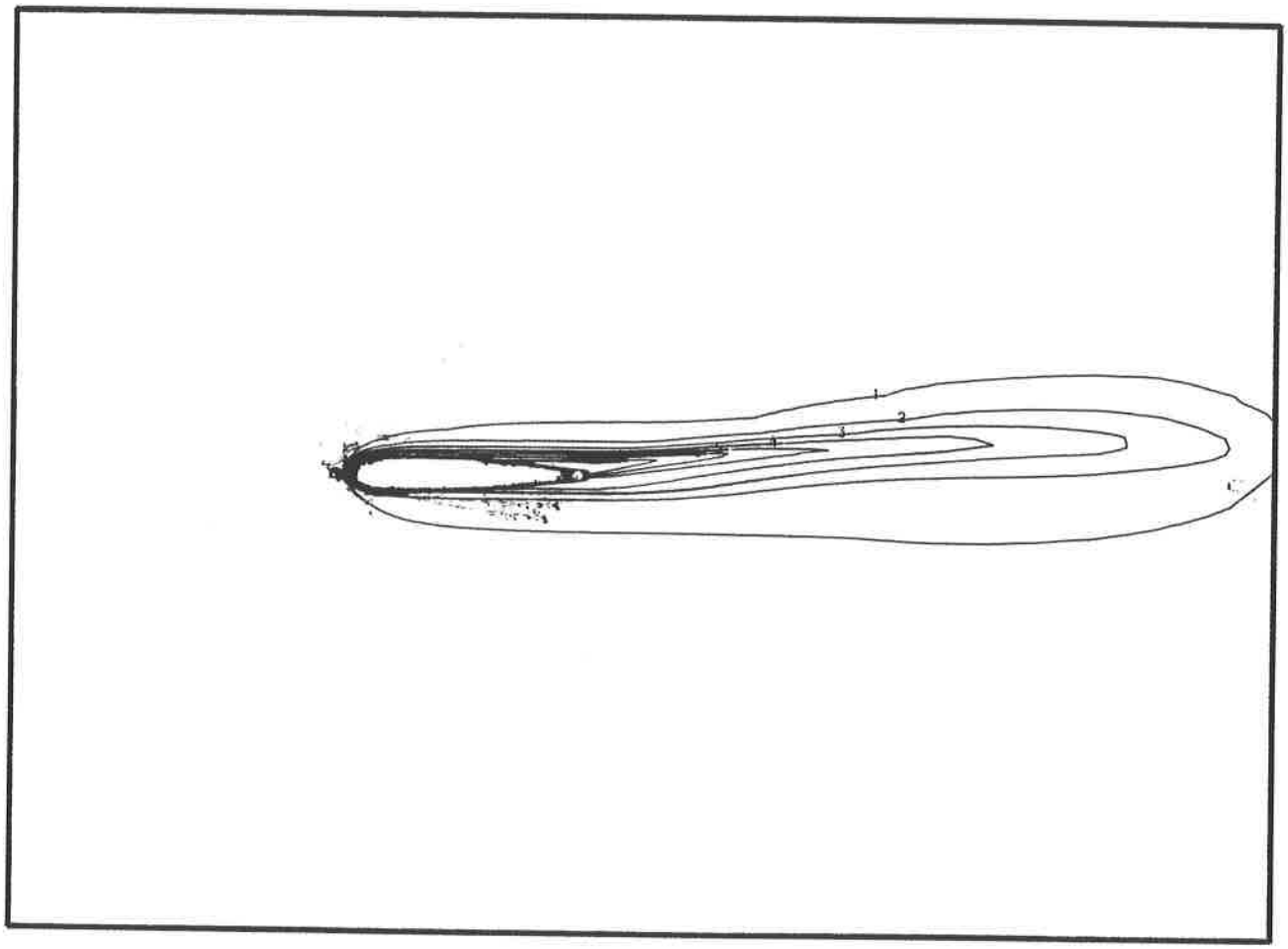

Figure 55

NACA0012 Aerofoil

Density contours for the NACA0012 aerofoil
in a Mach 3.00 flow. The angle of attack is 5.0 degrees.
Solution is shown after 400 time-steps and the maximum CFL no. is 0.852.
The maximum value of the density is 3.46.
The minimum value of the density is 0.67.
First order method

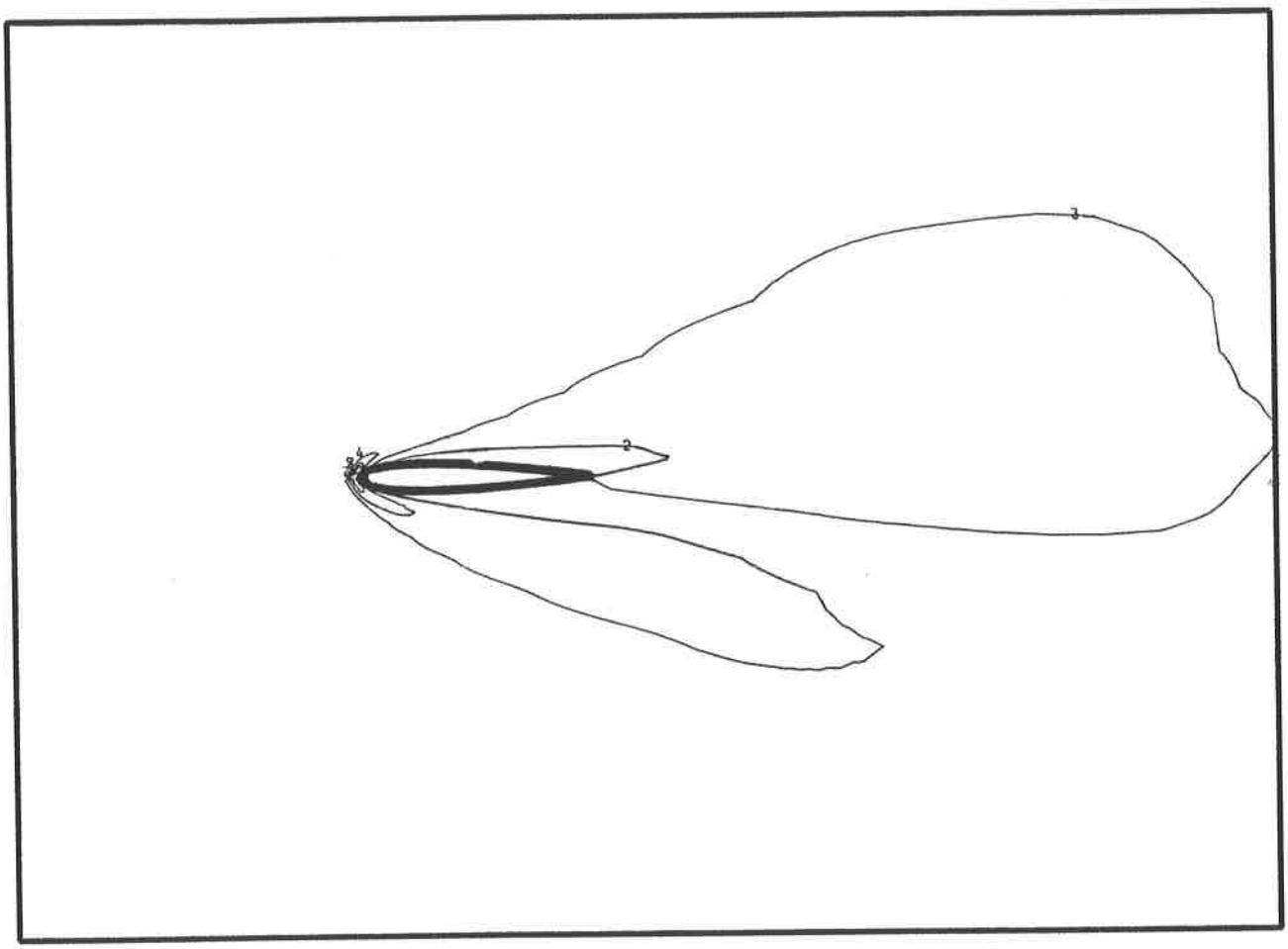

Figure 56

NACA0012 Aerofoil

Entropy deviation for the NACA0012 aerofoil
In a Mach 3.00 flow. The angle of attack is 5.0 degrees.
Solution is shown after 400 time-steps and the maximum CFL no. is 0.852.
The maximum value of the entropy deviation is 1.30.
The minimum value of the entropy deviation is 0.00.
First order method

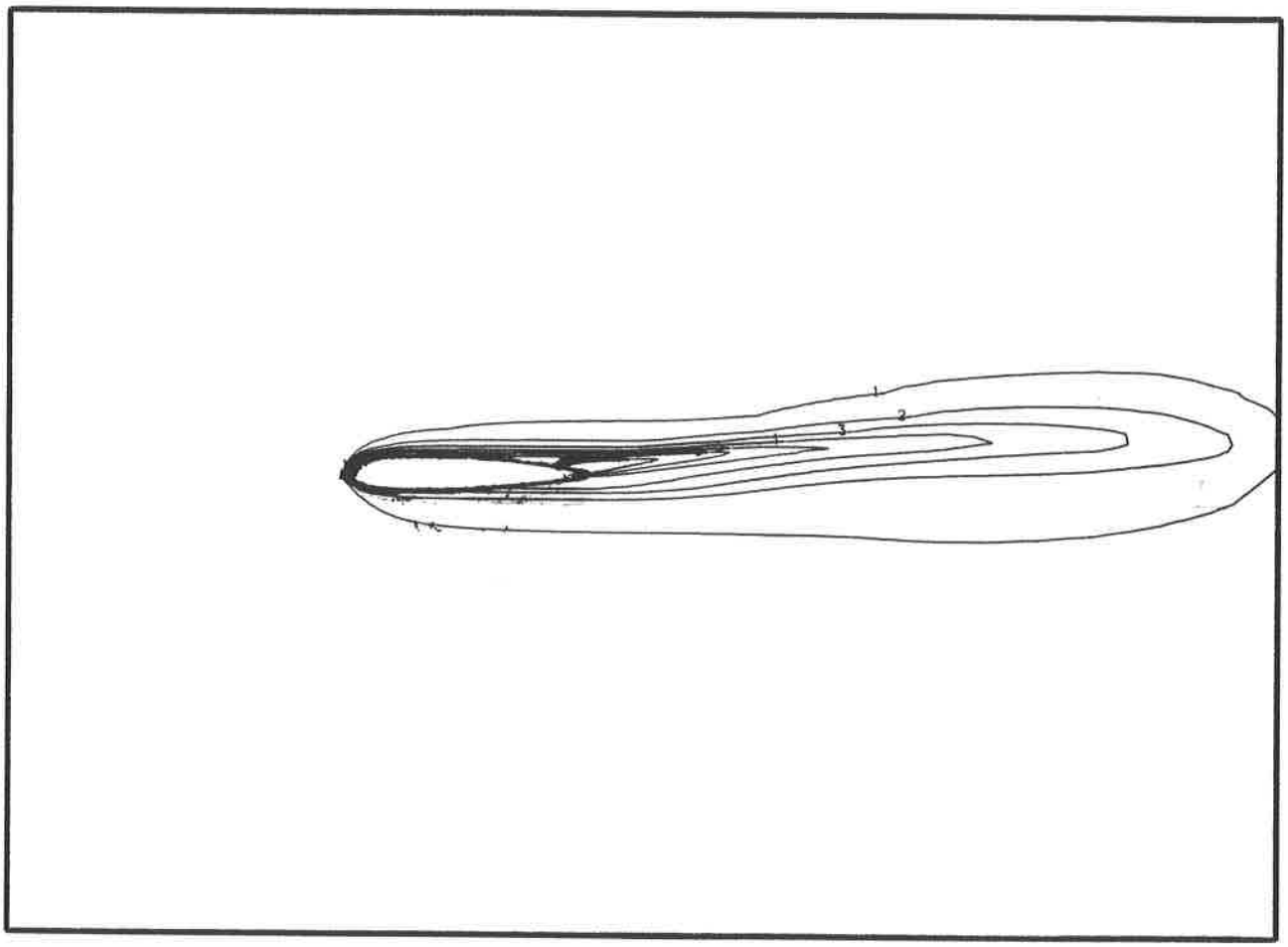

Figure 57

NACA0012 Aerofoil

Density contours for the NACA0012 aerofoil
in a Mach 3.00 flow. The angle of attack is 5.0 degrees.
Solution is shown after 500 time-steps and the maximum CFL no. is 0.852.
The maximum value of the density is 3.46.
The minimum value of the density is 0.67.
First order method

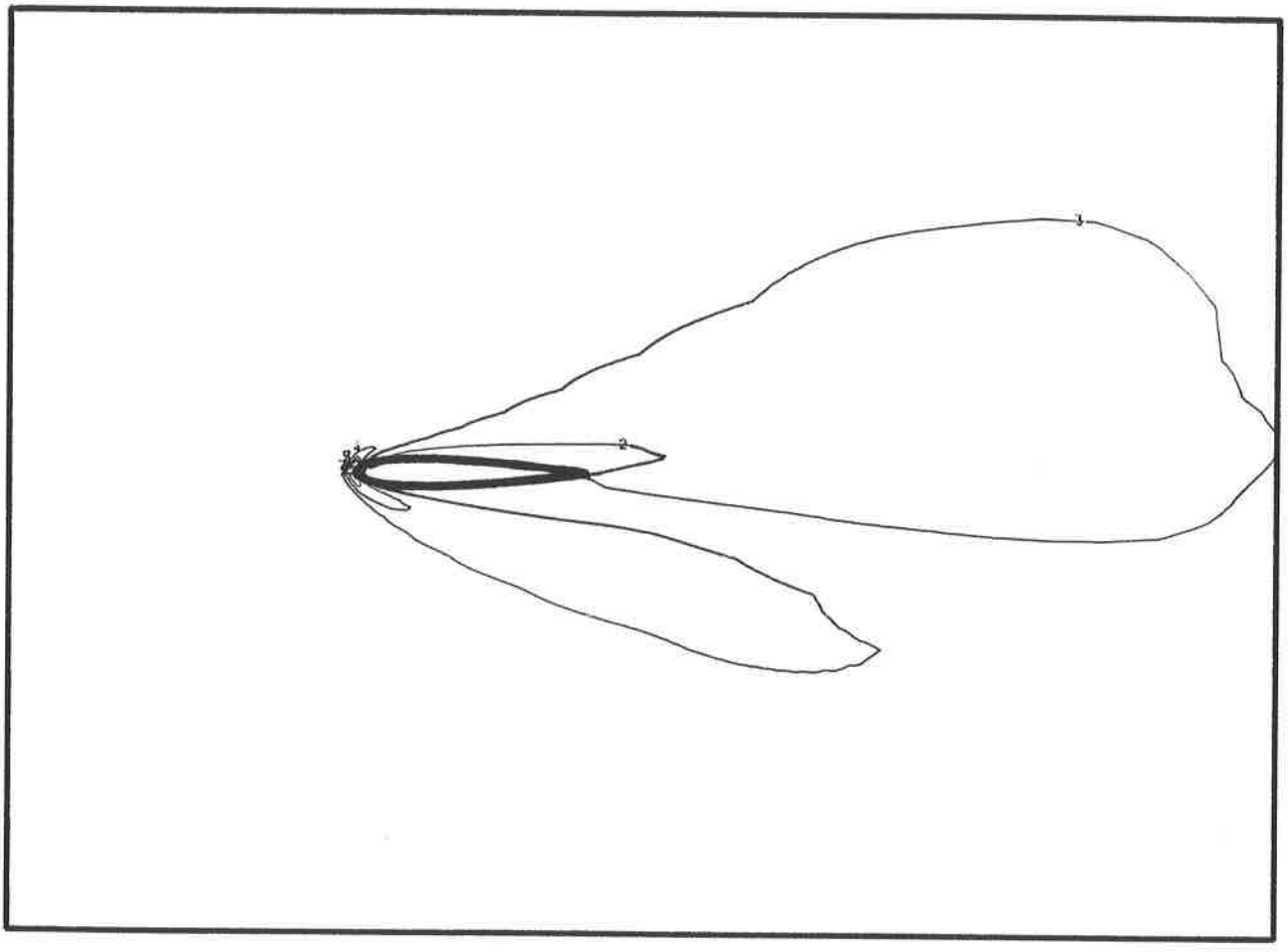

Figure 58

NACA0012 Aerofoil

Entropy deviation for the NACA0012 aerofoil
in a Mach 3.00 flow. The angle of attack is 5.0 degrees.
Solution is shown after 500 time-steps and the maximum CFL no. is 0.852.
The maximum value of the entropy deviation is 1.30.
The minimum value of the entropy deviation is 0.00.
First order method

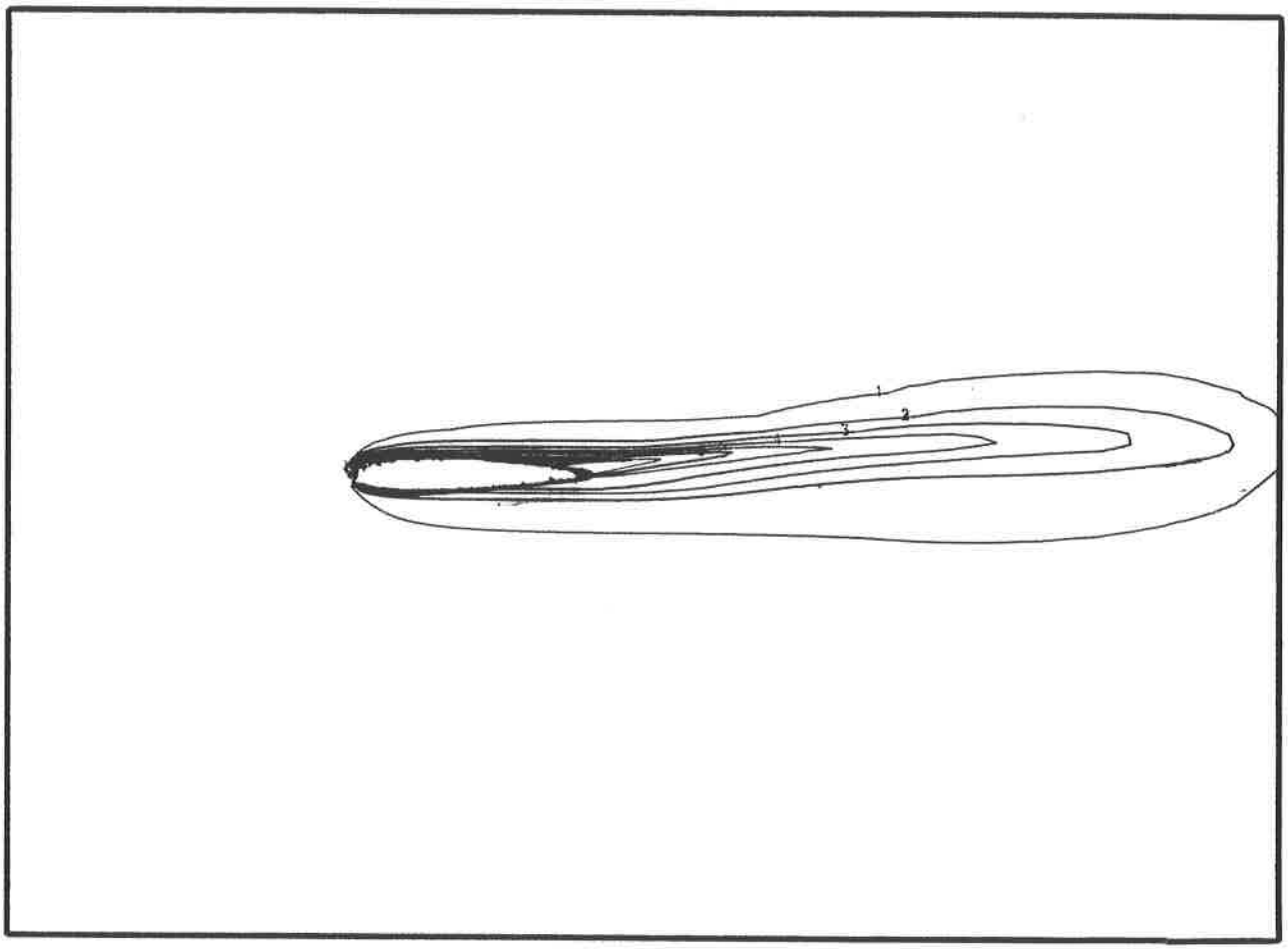

Figure 59

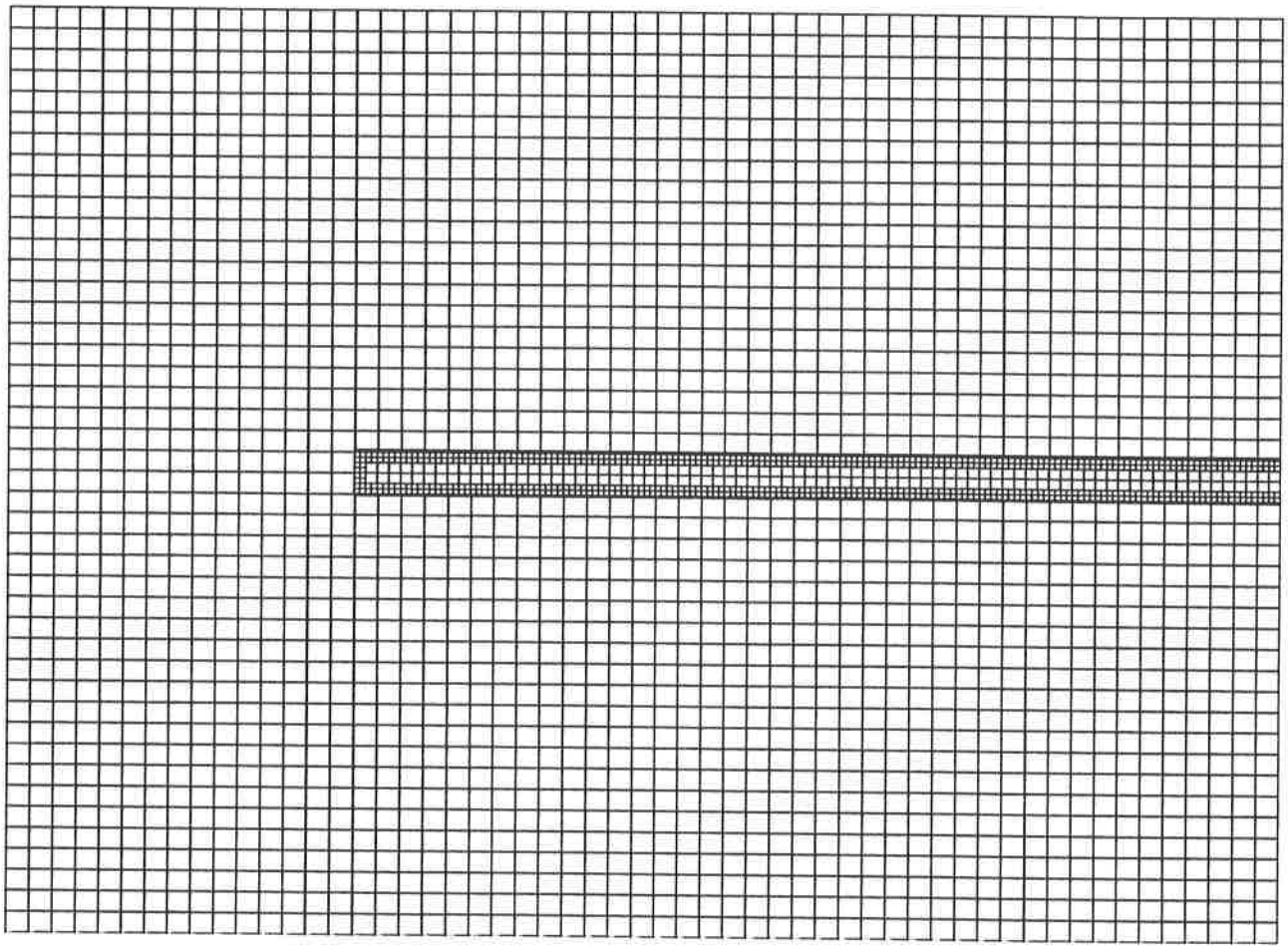

Figure 60

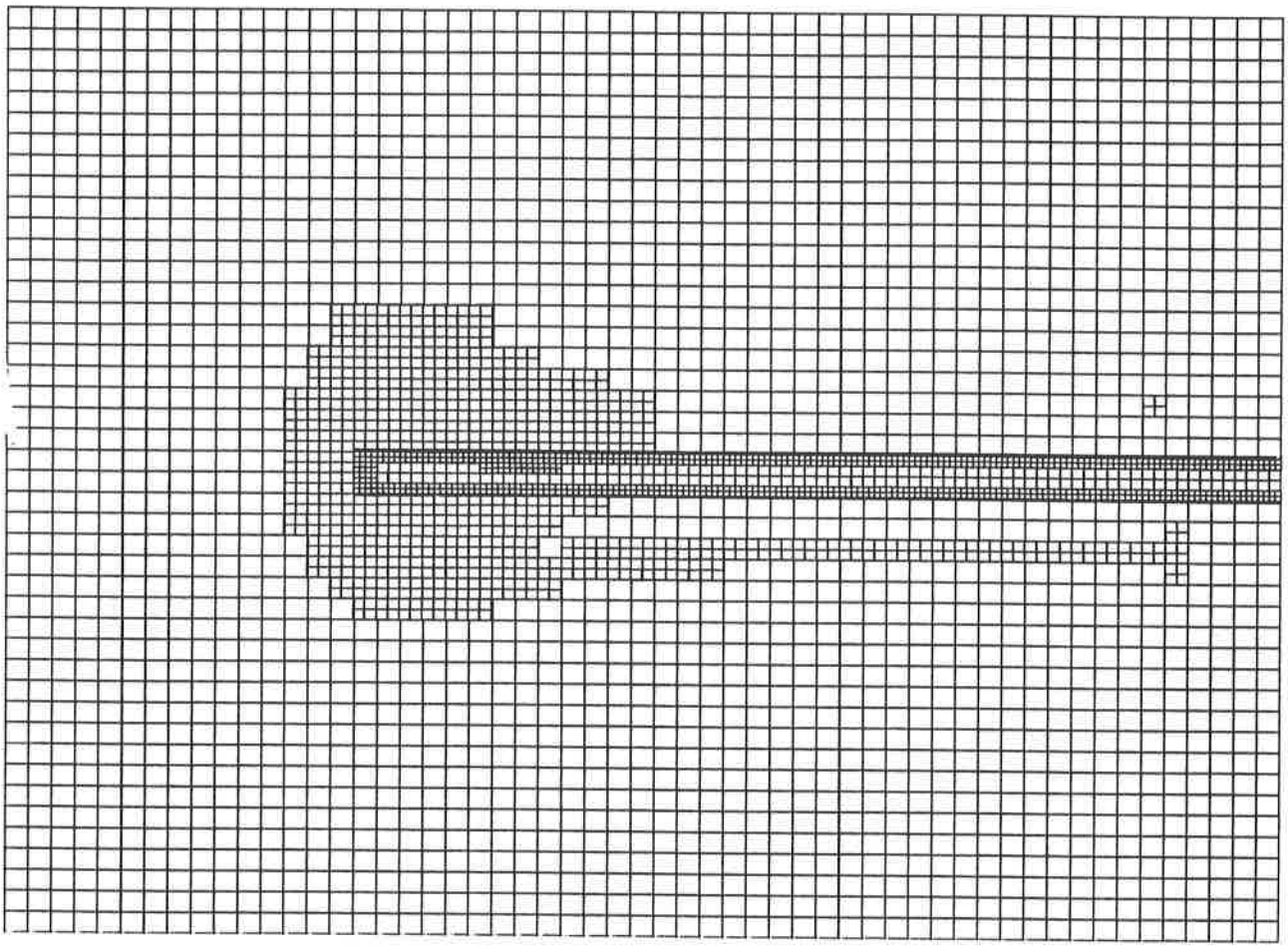

Figure 61

NACA0012 Aerofoil

Density contours for the NACA0012 aerofoil
In a Mach 3.00 flow. The angle of attack is 5.0 degrees.
Solution is shown after 101 time-steps and the maximum CFL no. is 0.213.
The maximum value of the density is 4.68.
The minimum value of the density is 0.58.
First order method
The number of cells in use is 3944.

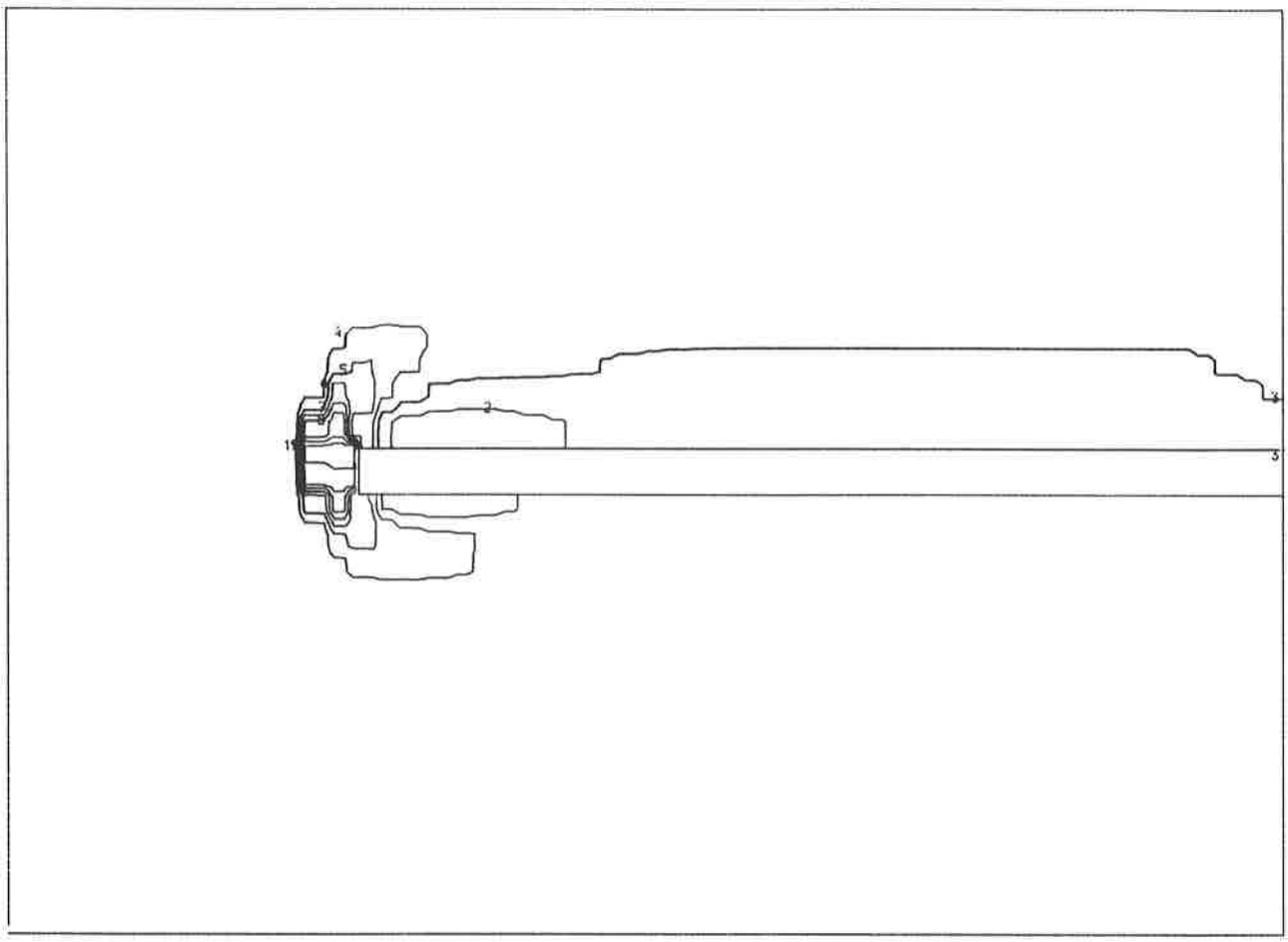

Figure 62

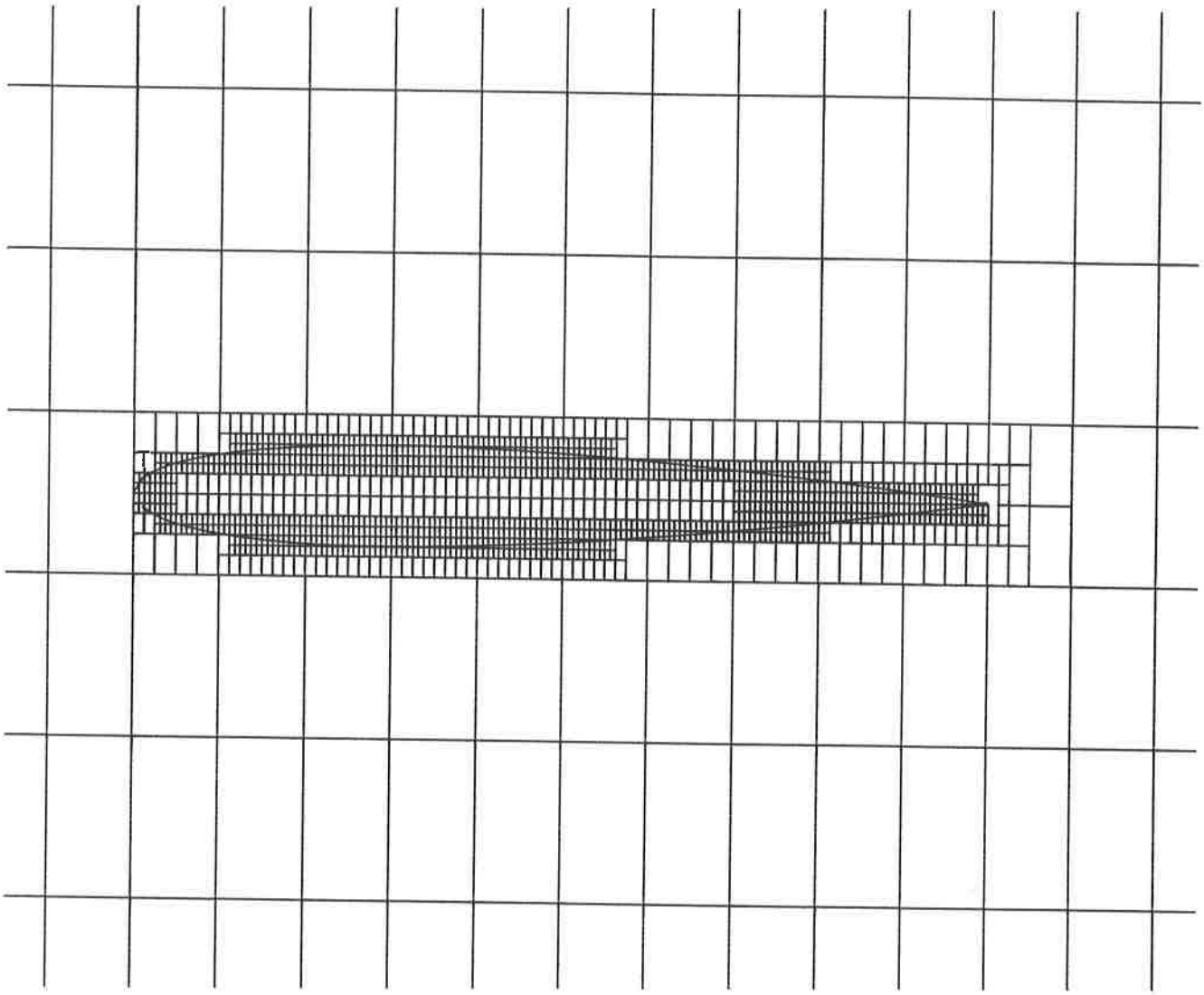

Figure 63